Methods for Optimal Charging of Large Fleets of Electric Vehicles

by

Caroline Le Floch

A dissertation submitted in partial satisfaction of the
requirements for the degree of
Doctor of Philosophy

in

Engineering - Civil and Environmental Engineering

in the

Graduate Division

of the

University of California, Berkeley

Committee in charge:

Professor Scott Moura, Chair
Professor Alexandre Bayen
Professor Laurent El Ghaoui

Summer 2017

Methods for Optimal Charging of Large Fleets of Electric Vehicles

Abstract

Methods for Optimal Charging of Large Fleets of Electric Vehicles

by

Caroline Le Floch

Doctor of Philosophy in Engineering - Civil and Environmental Engineering

University of California, Berkeley

Professor Scott Moura, Chair

Today's electric grid must be transformed to meet modern consumption behaviors and safely integrate renewable energy sources. This has led to major efforts to develop grid-scale energy management solutions and ensure safety and reliability of our modern power network. In particular, large penetrations of Plug-in Electric Vehicles (PEVs) are expected increase energy needs and peak consumption, which would bring new challenges for utilities and grid operators.

In this work, we develop optimization methods to coordinate the charging of large fleets of PEVs in distribution grids. We show that different methods should be applied, based on the infrastructure requirements and the objective of the controller.

The first Chapter *Optimal Charging of Fleets of Electric Vehicles with Discrete Charging rates: PDE Modeling and Control Techniques* presents a continuum modeling framework to coordinate PEV charging with discrete charging rates. We consider PEVs as loads, which diffuse along the State Of Energy (SOE) axis, and can be in three different categories: charging, discharging or idle. We use a discretized form of Partial Differential Equations (PDEs) to model the dynamics of the system and control the transitions between each category. The second Chapter *Dual Splitting Framework for Optimal Charging of Fleets of Electric Vehicles with Continuous Charging rates* proposes a tailored distributed optimization method to coordinate PEV charging for load shaping. Three iteration methods are presented and their convergence characteristics are detailed. The third Chapter *Electric Vehicle Charging in the Smart Grid: Plug-and-Play Model Predictive Control techniques* studies a voltage-regulation scenario for PEV charging. Power flow and distribution grid constraints are modeled, and PEV charging is controlled with Plug-and-Play Model Predictive Control. Finally, the final chapter *Behavioral study of Demand Response programs* studies the impact of non rational choices on energy consumption and on the success of Demand Response programs.

"If we knew what it was we were doing, it would not be called research, would it?"
Albert Einstein

Contents

List of Figures

List of Tables

Acknowledgments

I would like to gratefully thank my advisor Pr Scott Moura, who has transformed my doctorate study into a fascinating, elevating and life-changing experience. More than what is exposed in this dissertation, I learned great Chinese proverbs, as well as conference best-practices under his supervision. Thank you to all my committee members for their advise and support: Pr Claire Tomlin, Pr Joan Walker, Pr Laurent El Ghaoui and Pr Alexandre Bayen. I would like to acknowledge all my collaborators and colleagues who have been greatly inspiring and helpful: Eric Munsing, Dr Emre Can Kara, Pr Melanie Zeilinger, Dr Samveg Saxena, François Belletti, Jon Mather, Pr Florent Di Meglio and Somil Bansal.

My warm thoughts extend to my family and friends in Quimper, Paris and Mougins: François Rerolle for his exceptional lifestyle coaching, my close family and family-in-law for their support and numerous visits, with special mention to my parents who have always been extremely supportive. Special thanks to my graduation ceremony fan-club for their cheering and joyful presence. This dissertation is a small success compared to what others have accomplished during the time of its realisation: cheers to my brother, sister, and their great kids, Clara, Gabriel and Hugo. This experience would not have been possible without my friends, neighbors, running, tennis and yoga partners in Berkeley. Special thanks to Sreeta Gorripaty, with whom I have been lucky and glad to share all the milestones of Ph.D. and life during my doctorate studies.

Thank you to the institutions who supported me: the Siebel Scholarship and Women in Transportation Scholarship.

Chapter 1

Introduction

1.1 Background: traditional power network and Smart Grids

1.1.1 Power network: definition and challenges

The power network is one of the most complex, large and old infrastructure we have ever built in our modern societies. In the US, the electrical grid was built more than 80 years ago, with the idea that centralized energy sources would offer great economy of scale in order to produce electricity. As a result, our electrical grid has been built to transfer the electricity from vast and distant energy sources, to the end customers. It is traditionally composed of a transmission network that transfers the electricity long distances through high voltage lines, and a distribution system where the power is stepped down to the required service voltage, and the electricity transported to consumption nodes. The US power grid is composed of 420,000 miles of high voltage lines, which connect power plants and transformers. Its aging infrastructure has required extensive upgrade, and the 2009 American Recovery Act [2], enacted 4.5 Billion dollars investment for grid upgrade, in order to enhance grid reliability. On the other hand, a lot of efforts have been made to reduce CO2 emissions from electricity production, and increase penetration of renewable energy sources [130]. Renewable energy can, in theory, provide 3078 times the global energy needs at low economic and environmental costs [39], which provides great advantage compared to traditional sources. Figure 1.1 shows the share of US energy consumption from 1778 and 2016, and illustrates the modern trend of using more renewable energy. Figure 1.2 shows the portfolio of energy production sources in the US in 2015, when 10% was coming from renewable energy. Although this trends shows great promises for the environment, it comes with two main challenges [28, 80]:

- Renewable energy sources, such as solar and wind, are variable, intermittent, unlike traditional sources that provide a controllable, steady stream of power. This creates new needs to predict renewable energy production, and provide Demand Response (DR) services to adapt the demand to the uncontrollable source.
- More and more energy sources are distributed, i.e. generating power at the distribution level, requiring the electricity system to perform in ways for which it was not designed.

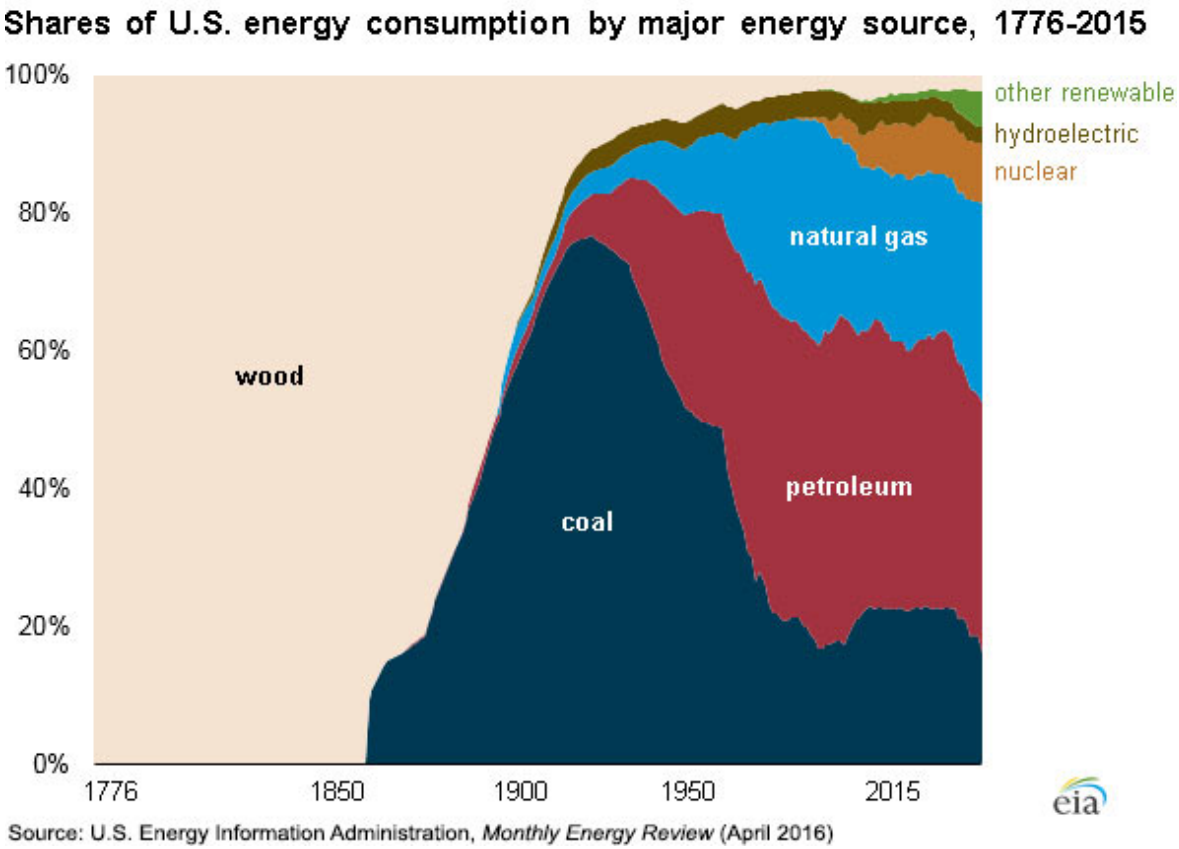

Figure 1.1: Share of US energy consumption from 1778 to 2016 (source: US energy information).

> Distribution generation can significantly impact the flow of power and voltage conditions at customers and utility equipments.

In this rapidly changing context, grid modernization has become a key factor to safely integrate new energy consumption and production habits.

1.1.2 Modernization of the power network: the "Smart grid"

For the past years, the concept of smart grid has emerged, revolutionizing the traditional vision of the electrical grid. According to the US Department Of Energy: "Smart grid generally refers to a class of technology people are using to bring utility electricity delivery systems into the 21st century, using computer-based remote control and automation. These systems are made possible by two-way communication technology and computer processing that has been used for decades in other industries" [1]. Figure 1.3 illustrates major goals, technologies and transformations associated with the modern smart grids, as the US Department Of Energy defines them in [31]. The smart grid is based on two-way communication between utilities and customers, which relies on advanced metering infrastructure. With more monitoring and control capabilities, the smart grid

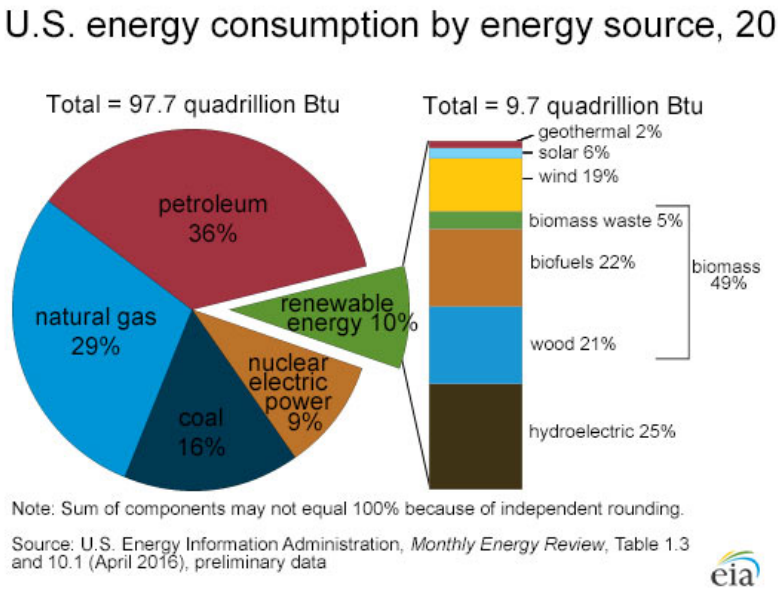

Figure 1.2: US energy consumption by energy source in 2015 (source: US Energy Information).

can be operated to safely integrate new technologies, such as distributed generation and electric vehicles. This opens opportunities and research questions to define novel grid management methods, that schedule loads and grid-control devices in order to improve network reliability, while avoiding major upgrades. In that context, Demand Response (DR) and Demand Side Management (DSM) programs are designed by utilities to influence or control energy demand. This can be achieved through price incentives and automated load control. With DR programs, loads become additional control variables to manage the power network.

1.2 The Vehicle Grid Integration Challenge

1.2.1 Challenge

Plug-in Electric vehicles (PEVs) are types of vehicles that are powered by electricity. They fall into two categories: plug-in hybrid electric vehicles (PHEVs), and battery electric vehicles (BEVs). As shown in Fig 1.4, their number has been growing for the past years. The two main electric car markets are China and the United States, and seven countries had reached over 1% EV market share in 2015 (Norway, the Netherlands, Sweden, Denmark, France, China and the United Kingdom). The electric vehicle is a form of clean transportation, which is expected to reduce the environmental impact of the transportation sector by shifting fuel consumption towards electricity consumption. However, as their number increases, aggregate PEV consumption rises and the risk to strain the grid becomes more and more serious. Past research has found that uncontrolled EV charging could result in 8% increase of electricity consumption and 11% increase of peak consumption in California by 2025 [49]. Following this observation, utilities are becoming more and more concerned

Characteristic	Today's Grid	Smart Grid
Enables active participation by consumers	Consumers are uninformed and non-participative with power system	Informed, involved, and active consumers - demand response and distributed energy resources.
Accommodates all generation and storage options	Dominated by central generation- many obstacles exist for distributed energy resources interconnection	Many distributed energy resources with plug-and-play convenience focus on renewables
Enables new products, services and markets	Limited wholesale markets, not well integrated - limited opportunities for consumers	Mature, well-integrated wholesale markets, growth of new electricity markets for consumers
Provides power quality for the digital economy	Focus on outages - slow response to power quality issues	Power quality is a priority with a variety of quality/price options - rapid resolution of issues
Optimizes assets & operates efficiently	Little integration of operational data with asset management - business process silos	Greatly expanded data acquisition of grid parameters - focus on prevention, minimizing impact to consumers
Anticipates and responds to system disturbances (self-heals)	Responds to prevent further damage- focus is on protecting assets following fault	Automatically detects and responds to problems - focus on prevention, minimizing impact to consumer
Operates resiliently against attack and natural disaster	Vulnerable to malicious acts of terror and natural disasters	Resilient to attack and natural disasters with rapid restoration capabilities

Figure 1.3: Today's grid versus tomorrow's grid, according to the US Department of Energy. Source: US Department Of Energy [31]

about the potential stresses and performance degradations that may occur in distribution systems with large penetrations of EVs. Uncontrolled and random EV charging can cause increased power losses, overloads and voltage fluctuations, which are all detrimental to the reliability and security of the power network [33, 74, 58]. On the contrary, PEVs can be integrated into the smart grid, communicate with other loads and utilities, and managed to charge at strategic times and places for the power network. In particular, PEV fleets provide a compelling opportunity for supplying demand-side management services in the smart grid. Namely, a vehicle-to-grid (V2G) capable PEV communicates with the grid, stores energy, and can return energy to the electric grid. If properly managed, PEVs can enhance energy infrastructure resilience, enable renewable integration, and reduce economic costs for consumers and energy providers [105]. In addition to these societal-level infrastructure and environmental benefits, V2G may provide additional revenue streams to PEV owners [62]. Underscoring this opportunity, U.S. personal vehicles are parked and

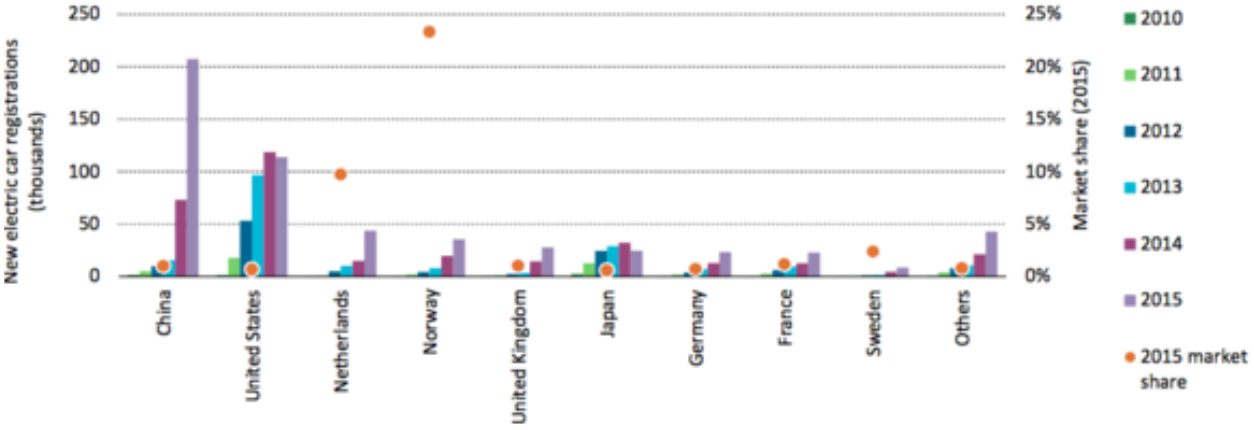

Figure 1.4: EV sales and market share in a selection of countries and regions, 2015. The penetration of PEVs is growing worldwide [101]

un-used 96% of time [69], which offers great flexibility for delaying and intelligently scheduling EV charging. Two main concepts have emerged to describe these smart charging opportunities [126]: Vehicle To Home (V2H) refers to power and communication exchange between one PEV and one home, and Vehicle To Grid (V2G) refers to power and communication exchange between PEVs and the electricity grid. A single PEV can generally provide 5-20 kW, which is insufficient to participate in power grid markets. However, populations of PEVs can be aggregated to collectively provide grid services [23], and V2G is most often considered in an aggregation scenario. Next sections give more details about V2H and V2G concepts.

In this dissertation, we consider the latter case of V2G and aggregation. The first goal of this dissertation is to schedule large fleets of PEVs, and maximize their benefits on the grid. Lots of parameters, including PEV characteristics, type of charging infrastructure and computation time must be considered before selecting a modeling and optimization framework. This manuscript studies three cases, namely a case with discrete charging rates, a case with continuous charging rates and a combined case. We develop case-specific methods that effectively solve the PEV scheduling problem in each scenario.

1.2.2 Vehicle To Home (V2H)

In a V2H framework, one vehicle is connected to one home or building, and a controller manages the combined home/PEV consumption through an Energy Management System (EMS). The EMS collects and analyzes data from various loads, appliances or energy sources, which may include photovoltaic generation, stationary storage, smart HVAC system and remotely controllable appliances. In most cases, the objective of the EMS is to minimize the energy consumption cost of the building. Specific applications include optimization with time varying electricity rates [24, 136, 137], demand-charge reduction [98] or participation in DR programs [102, 140].

1.2.3 Vehicle To Grid (V2G) and aggregation

In a V2G framework, PEVs can communicate with the electricity grid and provide different types of grid regulation services. Because one PEV cannot participate in electricity markets alone, it is necessary to consider aggregation and coordination of fleets of PEVs in that context [23]. A growing body of literature addresses design of smart charging algorithms for PEV aggregation and control. In that case, an aggregator gathers signals from all PEVs in the fleet and from the power network, and schedules PEV charging to achieve grid regulation objectives (see Fig 1.5). The main challenge is managing a large population of distributed PEV resources while ensuring (i) computational tractability, (ii) PEV drivers' mobility requirements, and (iii) power system constraints. Several models have been proposed to model and solve this problem. The proposed optimization and control techniques highly depend on assumptions about the charging infrastructure: either a continuous or discrete charging rate.

In the first case, the charging rate takes values in a continuous range. Because charging power is modeled as a continuous function, lots of researchers seek to define convex optimization programs, and leverage convex optimization methods to efficiently solve this PEV scheduling problem. Both centralized and decentralized methods have been proposed to address this question. Centralized algorithms [29], [119], utilize a central infrastructure to communicate with each agent, collect information, and compute the optimal load profile of the fleet. The challenges for centralized methods are scalability, with respect to communication, computation and privacy. Indeed, as the number of agents grows, these methods require heavy communication, high memory and computation time. In distributed optimization algorithms each PEV solves a local problem and communicates information to its neighbors and/or a coordinator [106]. Previous work has studied various aspects of load shaping and PEV smart-charging including filling the night valley of loads (valley filling) in [86, 47], more general driving behaviors in [127, 107], market bidding strategies and market uncertainty in [133, 52, 15] and grid constraints such as transformer overheating [115, 134] and local distribution grid constraints [26, 125, 84]. A wide range of distributed algorithms has been used including game theoretic approaches and Nash Equilibrium in [86], proximal methods in [47], Alternating Direction Method of Multipliers (ADMM) in [127, 107], regret minimization in [85] and stochastic protocols in [48].

However, in reality, the vast majority of electric vehicle supply equipments and charging standards only enables a discrete range of charging rates, which makes the above methods unsuitable. For example, the North American standard SAE J1772 defines two types of charging rates: AC Level 1 chargers provide charging through 120V AC plugs and AC Level 2 chargers provide charging through 240V or 208V AC plugs [122]. In practice, this leads to combinatorial optimization problems, where the aforementioned distributed methods are not applicable, and where direct centralized algorithms are intractable to study large systems. In this case, available methods include unit commitment [112], simulation-based algorithms [29], stochastic protocols [48] or dynamic programming [110]. However, for all these methods, the problem becomes harder to solve as the number of PEVs grows: either the convergence time increases or the optimality of the computed solution decreases.

The second goal of this dissertation is to to develop optimization techniques that ensure com-

putational feasibility of PEV scheduling methods. Namely, an aggregator may have limitation requirements for the computational memory or time it can allocate to the scheduling decision. These constraints need to be taken into account in the selection of the method. For the continuous charging rate scenario, we define a tailored method for the distributed PEV smart charging problem and analyze convergence to yield explicit linear rate-of-convergence bounds, providing precise guidance on the relationship between iterations, error and algorithm parameters. For the discrete charging rate, we develop a modeling framework that is computationally tractable for a large number of agents. We define novel continuum models that are based on Partial Differential Equations (PDE), and whose complexity does not depend on the number of PEVs in the fleet.

1.2.4 A more general approach: PEV aggregation within the smart grid context, technologies and behaviors

Although PEV fleets are expected to have a big impact, and exert strong influence in the future of power networks, their benefit will only be higher if considered in the broader context of the smart grid. First, PEV charging should be managed in coordination with other loads or control devices. Second, PEV charging should consider user choices, which often are non-rational in the case of energy consumption behaviors. In particular the effectiveness of price-based demand response programs is still under debate, and past trials have resulted in mixed conclusions [96]. Faruqui et al review 15 price-based experiments and find that time-of-use rates induce a drop in peak demand that ranges between 3 to 6 percent whereas critical-peak pricing tariffs induce a drop in peak demand that ranges between 13 to 20 percent [44]. Conversely, Jessoe et al [60] study a time-of-use experiment through a regression discontinuity framework, and shows that the impact is opposite from what was expected, i.e. households tend to reduce energy consumption when the price goes down. These findings suggest that PEV-based demand response and PEV aggregation models are likely to produce wrong results if they assume that PEV owners schedule their charging based on cost reduction only. Therefore, it is essential to consider more realistic user behaviors to understand and predict how drivers will respond to incentive signals sent by the aggregator.

The third goal of this dissertation is to propose advanced methods that improve our understanding of DR behaviors. Over the past 20 years, more than twenty DR trials have been conducted worldwide. These programs seek to reduce or shift household electricity consumption through various incentives or treatments, including time of use rates and information technologies. These trials have highlighted energy consumption behaviors, that can be extended to the case of PEV charging behaviors. These findings can be leveraged to effectively plan PEV-based DR programs, and better predict the impact of PEV aggregation. Our vision of PEV aggregation is illustrated in Fig 1.5, where we consider that the most important parameters are behavior choices and charging infrastructure (i.e. continuous versus discrete charging rates).

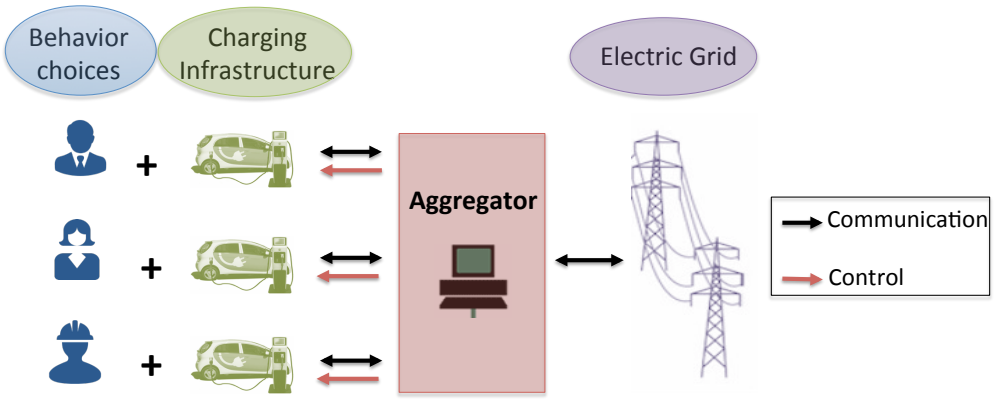

Figure 1.5: The PEV aggregator communicates with PEVs and the power network in order to schedule and control PEV charging

1.3 Technical challenges and summary of contributions

This dissertation addresses modeling techniques and mathematical methods to solve the optimal PEV charging problem in the case of large fleets of electric cars. The main challenge is to define models and techniques that incorporate all aspects of such a complex system, but remain solvable for large scale systems. The dissertation proposes four types of contribution to address this challenge:

- **A novel modeling technique for fleets of PEVs with discrete charging rates (Chap 2)**
  - We propose a novel state-space modeling framework for large fleets of PEVs, via aggregation and continuum modeling.
  - We formulate a Linear Quadratic Regulator (LQR), and use Model Predictive Control (MPC) techniques to track a power reference signal with PEVs. To the best of our knowledge, power and voltage signal tracking with MPC methods has been proposed for continuous charging rate [7, 76] or semi continuous charging rate [51], but this is new to the field of PEV control with discrete charging rate.
- **Dual splitting techniques with explicit convergence bounds (Chap 3)**
  - We derive a distributed dual-splitting optimization scheme that exploits the unique aggregate charging problem structure (i.e. a summed objective, strong convexity, and independent constraints). We additionally analyze convergence to yield explicit linear rate-of-convergence bounds, providing precise guidance on the relationship between iterations, error and algorithm parameters. To the best of our knowledge, this is the first comprehensive convergence analysis of the coordinated PEV charging problem.

  - We propose stochastic variations of the main dual-splitting algorithm. These variations provide communication and computation trade-offs, thus providing options for practitioners.

- **Plug & Play MPC methods for combined voltage regulation and load shaping services (Chap 4)**

  - We present a novel P&P MPC scheme that optimally schedule loads to be connected and shape current loads while satisfying power network constraints at all times. We model power flows in the distribution network using the Second Order Cone relaxation of the DistFlow equations (see [41]) and improve the accuracy of the model compared to the linear approximation used in [7].
  - The controller is applicable to different types of loads. In particular, we define two types of loads: deferrable loads that can be delayed but have a fixed profile, and shapeable loads that have a flexible profile but need a fixed amount of energy. The proposed algorithm satisfies users' requirements by ensuring that every flexible load reaches the desired energy level at the desired time and any deferrable load demand is met before its deadline.

- **Integrating Demand Response behavioral choices (Chap 5)**

  - We present a novel method to study DR program impacts. We segment households based on the energy product that is most likely to have a positive impact on their energy consumption behavior.
  - Previous work has considered energy segmentation for DR enrollment, but to the best of our knowledge, prior literature does not propose methods to predict both likelihood of a consumer enrolling in a DR program, and the resulting response to DR events. We add to previous literature by studying more comprehensive DR behaviors that describe how households react when presented with DR opportunities. For the first time, we study DR customer segments based on both enrollment choices and energy consumption, i.e. energy saving and peak shifting behaviors.

1.4 Organization of the dissertation

In this dissertation we develop methods for optimal charging of large fleets of electric vehicles. In Chapter 2 we develop Partial Differential Equation models to solve the PEV charging problem in the case of discrete rates. In Chapter 3 we design distributed protocols to solve the PEV scheduling problem in the case of continuous charging rates. We prove that the method converges to the optimal solution and provide convergence rate analysis, that can be used to adapt the method in case of limited computation capabilities. In Chapter 4, we combine the cases above, and develop Plug & Play Model Predictive Control (MPC) technique, which can be used for fleets with both continuous and discrete charging rates. This method enlarges the scope of the previous chapters

by jointly scheduling loads, battery banks and capacitors in a distribution grid. In Chapter 5, we address the question or electricity price sensitivity, with the goal of developing more realistic user behavior models. We analyze a Demand Response program in Australia, and provide customer segmentation techniques to target DR programs. We hope this can be used and extended to the case of PEV-based DR programs, and result in more efficient and realistic PEV aggregation models.

Chapter 2

Optimal Charging of Fleets of Electric Vehicles with Discrete Charging rates: PDE Modeling and Control Techniques

2.1 EV charging with discrete charging rates

Today, the majority of electric vehicle supply equipment and standards only enable a discrete range of charging rates. For example, the North American standard SAE J1772 defines two types of charging rates: AC Level 1 chargers provide charging through 120V AC plugs and AC Level 2 chargers provide charging through 240V or 208V AC plugs [122]. In practice, optimal PEV charging with discrete charging rates can be formulated as combinatorial optimization problems. In this case, available methods include unit commitment [112], simulation-based algorithms [29], stochastic protocols [48] or dynamic programming [110]. However, for all these methods, the problem becomes harder to solve as the number of PEVs grows: either the convergence time increases or the optimality of the computed solution decreases.

We adopt a significantly different approach for PEV charging with discrete charging rates that utilizes partial differential equations (PDEs). Rather than modeling each agent individually, we use aggregation methods to model and control the population dynamics [12, 71]. Continuum models have been largely applied to the case of Thermostatically Controlled Loads (TCLs) where PDEs represent the diffusion of air conditioning loads$'$ temperatures within the deadbands of their thermostats [11, 88, 92]. In this chapter we use a similar modeling framework and consider PEVs as loads, which diffuse along the State Of Energy (SOE) axis. We utilize a discretized form of PDEs and propose a novel state space model, where we can control flows between different discrete charging rates. Contrary to other methods, the complexity of our problem does not depend on the number of agents, and the accuracy of the model increases as the number of PEVs increases.

Table 2.1: PDE aggregation symbols

Symbol	Description
x	PEV battery SOE
t	Time
$u(x,t)$	Density of charging PEVs (nb of PEVs per SOE)
$v(x,t)$	Density of idle PEVs (nb of PEVs per SOE)
$w(x,t)$	Density of discharging PEVs (nb of PEVs per SOE)
$\sigma_{i\to c}(x,t)$	Flow of PEVs from Idle to Charge
$\sigma_{i\to d}(x,t)$	Flow of PEVs from Idle to Discharge
$\sigma_{i\to Or}(x,t)$	Net Flow of PEVs from Idle to On Road

2.2 Modeling aggregation of PEVs with PDE techniques

We seek to model a large homogeneous population of N discrete PEVs as a continuous representation, mathematically represented by three coupled PDEs. PEVs in the population fall into three discrete states:

- *Charging*: a PEV receives energy from the grid (Grid-to-Vehicle or G2V)
- *Idle*: a PEV is plugged-in but does not charge, nor discharge.
- *Discharging*: a PEV gives energy to the grid (Vehicle-to-Grid or V2G)

Each discrete state will be described by a transport PDE, i.e. a first order hyperbolic PDE. The aggregator controls how PEVs switch from one discrete state to another. This ultimately renders coupling terms and forms a system of three coupled transport PDEs.

2.2.1 PDE model

Consider a large homogeneous population of plugged-in PEVs over the State of Energy (SOE) interval $[0,1]$ at some fixed time, as visualized by Fig. 2.1. PEVs can be in three states: charge $u(x,t)$, idle $v(x,t)$, and discharge $w(x,t)$. The σ terms model PEVs moving between individual states $\sigma_{i\to c}, \sigma_{i\to d}$, and between states and the environment, i.e. checked-in or out by drivers on the road $\sigma_{i\to Or}$. The three states described above (i.e. charging, idle and discharging) only account for plugged-in PEVs. Hence, this framework does not model the dynamics of cars that are on the road (uncontrollable). Instead, the contribution coming from departures and arrivals is modeled by the uncontrollable flow $\sigma_{i\to Or}$.

To derive this aggregated PDE population model, we consider a simple PEV battery model. Denote the i'th PEV battery SOE and power by $x_i(t)$ and $P_i(t)$, respectively. Then a simple battery

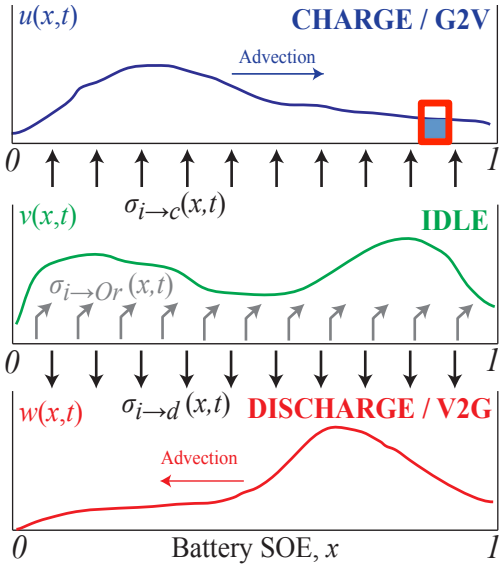

Figure 2.1: PEV population state dynamics (see zoom on Fig. 2.2)

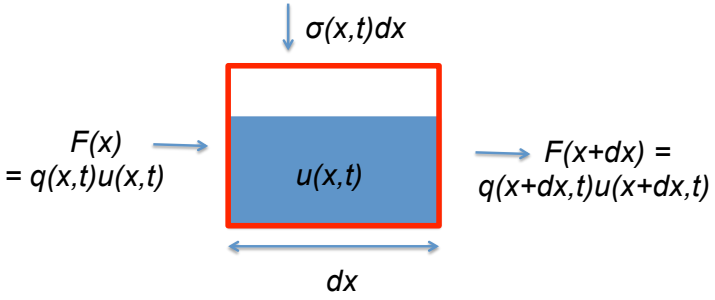

Figure 2.2: Zoom over an infinitesimal segment of charging PEVs: flows between x and $x+dx$

model is given by

$$\dot{x}_i(t) = \frac{\eta^m(x_i)}{E_{\max}} P_i(t), \qquad i = 1, \cdots, N, \tag{2.1}$$

$$m = \begin{cases} 1 & \text{if } P_i(t) \geq 0, \\ -1 & \text{if } P_i(t) < 0, \end{cases} \tag{2.2}$$

where $E_{\max}$, η, N are parameters that represent the battery energy capacity, power conversion efficiency, and PEV population size. Efficiency $\eta \in [0,1]$ is generally a function of SOE x_i. We assume $E_{\max}$ and η are homogeneous across the entire population. In this chapter we choose to express x in terms of SOE instead of SOC because dx/dt is linearly related to power. This provides a linear model (see Eq.2.1) that is amenable to the aggregation process we employ to derive a PDE. Note that unit-wise, dx/dt is normalized kWh. Furthermore, the cumulative power consumption from charging and power generation from discharging is given, respectively, by

$$P_c(t) = \sum_{i=1}^{N} P_i \cdot \mathbb{1}(P_i > 0), \quad P_d(t) = \sum_{i=1}^{N} P_i \cdot \mathbb{1}(P_i < 0), \tag{2.3}$$

where $\mathbb{1}(\cdot)$ is the indicator function. More complex battery models could be considered in future work.

Consider an infinitesimal segment of $u(x,t)$ as shown in Fig. 2.2. The number of charging PEVs at SOE level x at time t is denoted by $u(x,t)$ and charge at rate $q_c(x,t) = \eta(x)/E_{\max} \cdot P(t)$. We seek to model the evolution of the number of charging PEVs contained in the infinitesimal volume between x and $x+dx$. Let $F(x,t)$ denote the flow of PEVs at SOE x and time t, the entering flow and exiting flow are respectively:

$$F(x,t) = q_c(x,t)u(x,t), \tag{2.4}$$
$$F(x+dx,t) = q_c(x+dx,t)u(x+dx,t). \tag{2.5}$$

An additional flow of PEVs from the idle state to charging state are denoted $\sigma_{i\to c}(x,t)$ (see Fig. 2.1). As illustrated in Fig. 2.2, $u(x,t)dx$ is an approximate measure of the number of PEVs with SOE between x and x+dx at time t. Therefore, the conservation law during the infinitesimal time interval dt gives:

$$\begin{aligned}&[u(x,t+dt) - u(x,t)]dx = \\ &q_c(x,t)u(x,t)dt - q_c(x+dx,t)u(x+dx,t)dt + \sigma_{i\to c}(x,t)dt.\end{aligned} \tag{2.6}$$

In Eq. (2.6), PEVs should pass through the idle state to go from the G2V state to the V2G state. When $dt \to 0$ and $dx \to 0$, the relation becomes:

$$\frac{\partial u}{\partial t}(x,t) = -\frac{\partial}{\partial x}[q_c(x,t)u(x,t)] + \sigma_{i\to c}(x,t). \tag{2.7}$$

PDEs for the idle and discharging are similarly derived as:

$$\frac{\partial v}{\partial t}(x,t) = -\sigma_{i\to or}(x,t) - \sigma_{i\to c}(x,t) - \sigma_{i\to d}(x,t), \tag{2.8}$$
$$\frac{\partial w}{\partial t}(x,t) = \frac{\partial}{\partial x}[q_d(x,t)w(x,t)] + \sigma_{i\to d}(x,t). \tag{2.9}$$

2.2.2 Boundary Conditions

For the system to be well posed, we need to define boundary conditions at $x = 0$ for $u(x,t)$ and $x = 1$ for $w(x,t)$ [124]. We set the following Dirichlet conditions:

- $u(0,t) = 0$: no flow of charging PEVs from the SOE range $x \leq 0$.
- $w(1,t) = 0$: no flow of discharging PEVs from the SOE range $x \geq 1$.

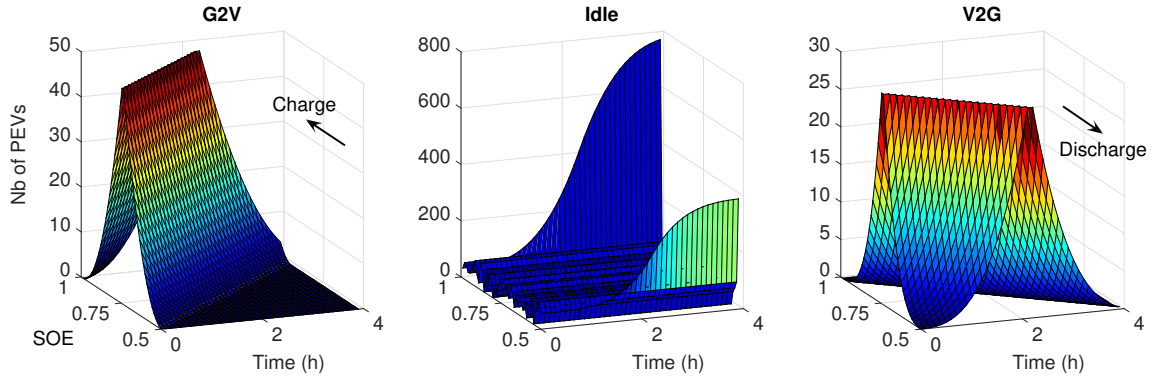

Figure 2.3: Evolution of the uncontrolled system of transport PDEs for SOE $\in [0.5,1]$. All G2V PEVs charge (transported towards high SOE values), and V2G PEVs discharge (transported towards low SOE values).

In addition, we must define boundary values for $q_c(x,t)$ and $q_d(x,t)$ to ensure physical meaning of the system:

- $q_c(1,t) = 0$: no charging at $x = 1$.
- $q_d(0,t) = 0$: no discharging at $x = 0$.

Figure 2.3 illustrates the PDE dynamics with the above boundary conditions. It shows the uncontrolled evolution of the PEV fleet during four hours when the boundaries of the system are $SOE \in [0.5,1]$. In this case $\sigma_{i\to c} = \sigma_{i\to or} = \sigma_{i\to d} = 0$. All G2V PEVs charge until they reach $SOE = 1$. Then they are transferred to the Idle category. Similarly, V2G PEVs discharge until $SOE = 0.5$. Then they are transferred to the Idle category. Figure 2.3 shows that PEVs tend to accumulate in the Idle category at the boundary points $SOE = 0.5$ and $SOE = 1$.

2.2.3 Dynamic System Properties

In this section we verify the conservation of mass (i.e. the conservation of PEVs in the system) when there is no external flow, $\sigma_{i\to Or} = 0$.

Proposition 1. *The system defined by the coupled dynamics (2.7), (2.8), (2.9) and the boundary conditions in Section 2.2.2 verifies the following property when* $\sigma_{i\to Or} = 0$*:*

$$\frac{\partial Nb_{PEVs}(t)}{\partial t} = 0$$
$$\text{where } Nb_{PEVs}(t) = \int_0^1 [u(x,t) + v(x,t) + w(x,t)]dx$$

Proof. When $\sigma_{i\to Or} = 0$, summing Eq (2.7), (2.8) and (2.9) leads to:

$$\frac{\partial}{\partial t}(u+v+w)(x,t) = \frac{\partial}{\partial x}(-q_c u + q_d w)(x,t) \tag{2.10}$$

By integrating each term of on $x \in [0,1]$, we obtain:

$$\begin{aligned} \frac{d}{dt}\mathrm{Nb}_{\mathrm{PEVs}}(t) &= \Big[(-q_c u + q_d w)(x,t)\Big]_{x=0}^{1} \\ &= 0 \end{aligned} \tag{2.11}$$

where Eq. (2.11) comes from the boundary conditions defined in Section 2.2.2. □

2.3 Discretization and validation

2.3.1 Discretization

In the following sections we will discretize the PDEs. The model is discretized using the high-resolution scheme with a Superbee flux limiter adapted to variable-coefficient linear transport equations from [75, Ch. 9, S. 4]. Practically, this is an upwind scheme with high-resolution corrections that makes it second-order in space.

2.3.2 V2G-Sim

We assess the aggregate PDE model's accuracy against the Vehicle-to-Grid Simulator (V2G-Sim) developed by the Grid Integration Group at Lawrence Berkeley National Laboratory [132]. V2G-Sim is an agent-based simulator that models the driving and charging behavior of individual PEVs and their grid impact. The necessary inputs for V2G-Sim are vehicle characteristics (e.g., battery capacity, battery charging model, powertrain parameters), driving schedules (e.g. duration of activities and drive cycles), and charging infrastructure (e.g. location of chargers, charging rate). The simulator is initialized with statistical data for trip length, departure times, and destination types derived from the 2009 National Household Travel Survey (NHTS) [131].

2.3.3 Validation method

The 2009 NHTS dataset includes trips from 17805 vehicles in California during a week-day. We study four cases, which differ with respect to charging rates and control algorithms. PEVs parameters are adopted from the Nissan Leaf with battery energy capacity 26.8 kWh.

The first control algorithm is the standard open-loop strategy: vehicles begin to charge as soon as they plug in, and stop when they are fully charged. The second control algorithm includes V2G services. We apply a rudimentary V2G control algorithm to validate the PDE model: every PEV discharges during peak hours (6pm to 9pm) if it has sufficient charge ($SOE > 0.6$) and PEVs stop charging if $SOE > 0.95$.

Table 2.2: Mean Normalized Error over Time

Case	Mean e(t) over time
L1 Open Loop	0.011
L1 V2G	0.023
L2 Open Loop	0.002
L2 V2G	0.028

We assume the charging/discharging power is constant with respect to SOE, which is valid for the low battery C-rates (normalized charge rates) considered here. We study two charging rates: Level 1 (1.44 kW) and Level 2 (6.6 kW).

2.3.4 Validation results

We test our model for a 24 hour period in four different cases: {L1 charger, L2 charger } $\times$ {open loop, V2G control}. In every case, we use a 0.01 SOE step. Since we need to satisfy the Courant Friedrichs Lewy (CFL) condition $\frac{qdt}{dx} \leq 1$ [75], time step sizes differ for L1 chargers and L2 chargers. Namely, we require a 11.4 minute interval for L1 chargers (120 time steps) and a 2.4 minute interval for L2 chargers (601 time steps).

We compute the L2 norm of the difference between the PDE model and the V2G-Sim distribution as

$$e(t) = \frac{||(u+v+w)_{PDE}(\cdot,t) - (u+v+w)_{V2Gsim}(\cdot,t)||_2}{||(u+v+w)_{V2Gsim}(\cdot,t)||_2}, \tag{2.12}$$

where f_{PDE} refers to the values from the aggregated PDE model and f_{V2Gsim} refers to V2G-Sim.

Table 2.2 provides the average normalized error over the 24 hour period. The PDE model approximates the SOE distributions with an average normalized error of less than 3% and is more accurate for the open loop cases. Figure 2.4 shows $e(t)$ for each time step. For both $L1$ cases and the open-loop $L2$ case, $e(t)$ is always smaller than 10%. For L2 chargers with V2G, Fig.2.4 shows that $e(t)$ has large values for some isolated time steps. These "spikes" only occur during the discharging period (from 6pm to 9pm) and have similar magnitudes. These errors are in fact a numerical artifact of the PDE discretization technique. Namely, at the end of the charging period (6pm), PEVs tend to be aggregated at the maximum allowable SOE. When PEVs discharge, then this peak transports toward 0% SOE. This is highlighted in Fig. 2.6, which show snapshots of the distributions immediately before, during, and immediately after the V2G period, for the PDE model and V2G-Sim. The numerical phenomenon occurs when there is a one SOE-step difference between the load peaks in V2G-Sim and the PDE model. This can be resolved via SOE smoothing. Figure 2.4 shows the smoothed error $e_{smooth}(t)$ (in green) after averaging the load distribution with

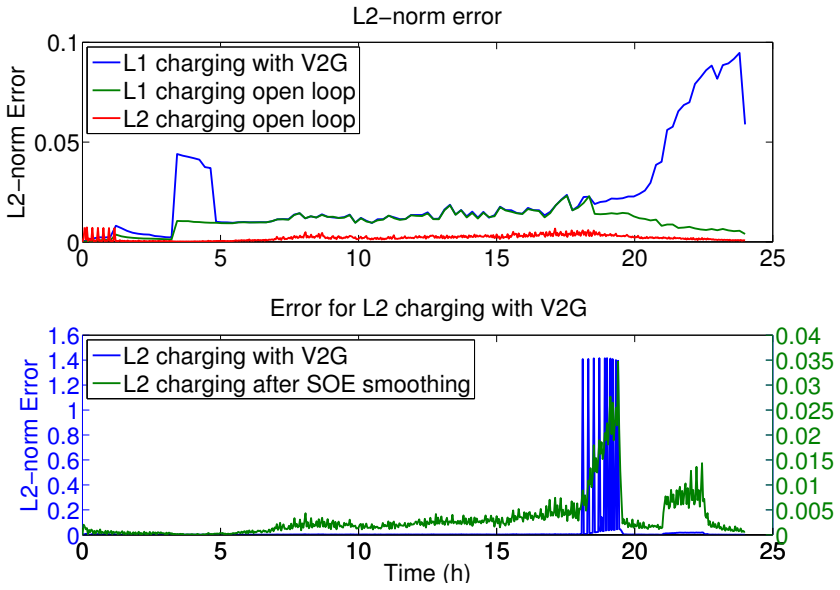

Figure 2.4: Error in the 4 different scenarios

the two closest SOE steps; the smoothed error $e_{smooth}(t)$ is smaller than 4% for every time step.

$$e_{smooth}(t) = \frac{||(u_a+v_a+w_a)_{PDE}(\cdot,t)-(u_a+v_a+w_a)_{V2Gsim}(\cdot,t)||_2}{||(u_a+v_a+w_a)_{V2Gsim}(\cdot,t)||_2}, \tag{2.13}$$

where $g_a(x,t) = \frac{g(x-dx,t)+g(x,t)+g(x+dx,t)}{3}$.

The aggregated charging and discharging power is provided in Fig. 2.5. The aggregated PDE provides excellent accuracy, even in the case of L2 charging with V2G control. Thus, the PDE model predicts aggregated fleet charge and discharge sufficiently well, despite small offsets in time or SOE due to numerical implementation. In the next section, we use this PDE formulation to design a control algorithm to optimally schedule PEV charging and discharging.

2.4 Optimal control in a load-following case

We use the symbols defined in Table 2.3. The control objective is to minimize the cost of charging PEVs, subject to supplying sufficient energy to the grid (for services contracted *a priori*) and providing sufficiently charged EVs to drivers. We make the following assumptions:

(A1) The cost of electricity $C_{elec}(t)$ is known in advance.

(A2) EVs must be provided to drivers with a minimum required State of Energy (SOE), X_{dep}.

(A3) The driver demand for vehicles is known in advance.

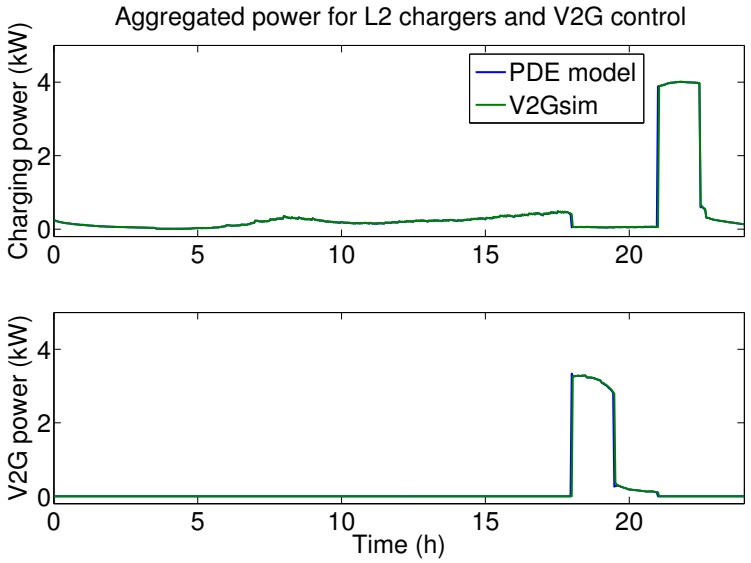

Figure 2.5: Aggregated Power for L2 charger and V2G control

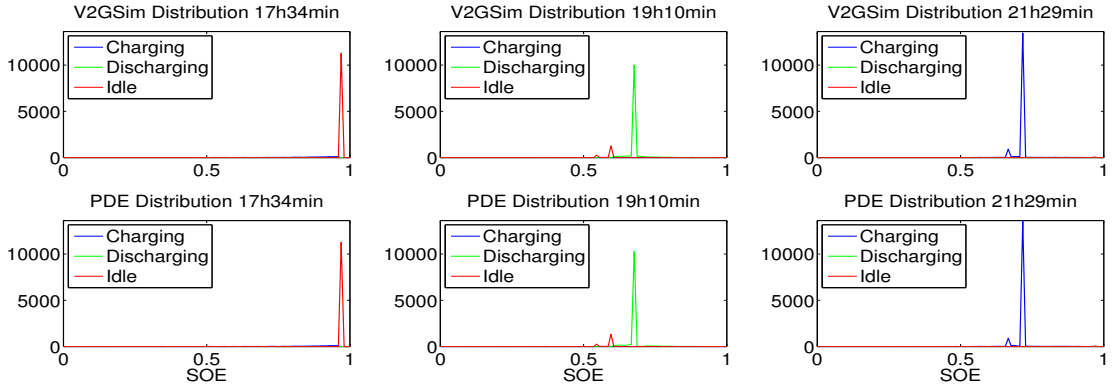

Figure 2.6: PEV distributions immediately before, during, and after V2G event for the PDE model and V2G-Sim. Large errors occur due to distribution peaks that are slightly offset in SOE (or time) between two models. This numerical error has relatively no impact for our control purposes.

(A4) The aggregator sells energy to the regulation market. It bids $P^{des}(t)$ one day in advance.

The real time regulation signal might be lower than $P^{des}(t)$. However, the optimization program seeks a robust control, which ensures that the aggregator has the available power capacity during the entire day.

Table 2.3: Nomenclature for PDE-based optimal charging model

Symbol	Description
$Arr(x,t)$	Flow of PEVs from On Road to Idle
$Dep(x,t)$	Flow of PEVs from Idle to On Road
$q_c(x)$	Instantaneous charging power
$q_d(x)$	Instantaneous discharging power
X_{dep}	Min allowed SOE for departing PEVs
X_{max}	Min SOE for discharging and idle PEVs
X_{min}	Max SOE for charging cars
N_{min}	Min number of departure-ready PEVs at T_{max}

2.4.1 Optimal problem

The aggregator minimizes the cost of charging vehicles over finite time period $t \in [0, T_{max}]$.

$$C = \int_0^{T_{max}} C_{elec}(t) \int_0^1 q_c(x,t)u(x,t)\, dx\, dt, \tag{2.14}$$

where only the charging state $u(x,t)$ appears explicitly. To ensure physical meaning of the system, we also impose boundaries on SOE values for each category. For $x > X_{max}$, cars are restricted from charging further and for $x < X_{min}$, cars are forced to charge:

$$u(x,t) = 0, \qquad \forall\, x \geq X_{max}, \tag{2.15}$$

$$v(x,t) = 0 = w(x,t), \qquad \forall\, x \leq X_{min}, \tag{2.16}$$

The system must also satisfy three additional constraints.

2.4.1.1 Power supply constraint

We consider a scenario where the PEV aggregator participates in a regulation market. We assume the bidding process has been completed and the system operator has assigned an available frequency up regulation capacity. Hence, the V2G aggregator commits to be able to supply $P^{des}(t)$:

$$\int_0^1 q_d(x)w(x,t)dx \geq P^{des}(t), \quad \forall\, t. \tag{2.17}$$

2.4.1.2 Drivers' demand constraint

We assume the demand and arrival of cars are known in advance. This could be true in a reservation-based system. This assumption is admittedly restrictive, and will be examined via a sensitivity analysis in Section 2.4.4. The arrival of cars $Arr(x,t)$ is known for all time and all SOE values.

Similarly the total demand of vehicles over time $Dem(t)$ is known one day in advance. The aggregator decides which PEVs are vended to the drivers, i.e. at what SOE. In addition, we require vended PEVs to have a minimum SOE level X_{dep} upon departure. Then, $Dep(x,t)$ becomes a controllable input, which satisfies the following constraint:

$$\int_{X_{dep}}^{1} Dep(x,t)\, dx = Dem(t), \quad \forall\, t. \tag{2.18}$$

2.4.1.3 Time horizon and final condition

Note that we consider a finite-time horizon optimization problem. To ensure continuity of the system after time period T_{max}, we require that the system contains a minimum number of PEVs N_{min} that are able to depart after T_{max}.

$$\int_{X_{dep}}^{1} (u+v+w)(x,T_{max})\, dx \geq N_{min}. \tag{2.19}$$

2.4.2 Formulation of the optimization problem

The optimization problem is summarized as

$$\min_{\sigma_{i\to d},\sigma_{i\to c},Dep} C = \int_0^{T_{max}} C_{elec}(t) \int_0^1 q_c(x,t)u(x,t)\, dx\, dt, \tag{2.20}$$

subject to

$(2.7), (2.8), (2.9)$

$$u(0,t) = 0,\ w(1,t) = 0, \tag{2.21}$$

$$u(x,0) = u_0(x),\ v(x,0) = v_0(x),\ w(x,0) = w_0(x), \tag{2.22}$$

$$-w(x,t) \leq \sigma_{i\to d}(x,t) \leq v(x,t), \tag{2.23}$$

$$-u(x,t) \leq \sigma_{i\to c}(x,t) \leq v(x,t), \tag{2.24}$$

$(2.15) - (2.19)$

Note all the functions and constraints are linear with respect to states u, v, w, rendering a linear program.

To generate a finite dimensional linear programming solution, we must discretize the PDEs. Denote $n \in [0,N]$ as the index for time with time step Δt, $T_{max} = N\Delta t$. Denote $j \in [0,J]$ as the index for SOE with step Δx. Spatio-temporally dependent variables are discretized into the form $f_j^n = f(j\Delta x, n\Delta t)$.

We denote M_c and M_d as the transition matrices derived from discretization of PDEs (see Section 2.3.1). The PDE dynamics are then approximated by:

$$u^{n+1} = M_c u^n + \sigma_{i\to c}^{n+1}, \tag{2.25}$$
$$v^{n+1} = v^n - [\sigma_{i\to c}^{n+1} + \sigma_{i\to d}^{n+1} + \sigma_{i\to Or}^{n+1}], \tag{2.26}$$
$$w^{n+1} = M_d w^n + \sigma_{i\to d}^{n+1}. \tag{2.27}$$

We arrive at an explicit linear formulation after eliminating the control variables $\sigma_{i\to d}$ and $\sigma_{i\to c}$ and expressing everything in terms of u, v, w. The optimization problem becomes

$$\min_{u,v,w,Dep} \Delta t\, \Delta x \sum_{n=0}^{N}\sum_{j=0}^{J} C_{elec}^n q_j^n w_j^n \tag{2.28}$$

subject to

$$[u+v+w]^{n+1} + \frac{Dep^{n+1}}{\Delta x} = M_c u^n + M_d w^n + \frac{Arr^{n+1}}{\Delta x} \tag{2.29}$$
$$u_0^n = 0, \quad v_J^n = 0, \tag{2.30}$$
$$u_j^0 = u_0(j\Delta x),\ v_j^0 = v_0(j\Delta x),\ w_j^0 = w_0(j\Delta x),\ \forall j, \tag{2.31}$$
$$u^n, v^n, w^n, Dep^n \geq 0, \tag{2.32}$$
$$u_j^n = 0\ \forall\ j \geq X_{max}\cdot J \tag{2.33}$$
$$v_j^n = 0 = w_j^n\ \forall\ j \leq X_{min}\cdot J \tag{2.34}$$
$$\Delta x \sum_{j=0}^{J} q_{d,j}^n w_j^n \geq P^{des,n} \tag{2.35}$$
$$\sum_{j=X_{dep}\cdot J}^{J} Dep_j^n = Dem^n \tag{2.36}$$
$$\Delta x \sum_{j=X_{dep}\cdot J}^{J} u_j^N + v_j^N + w_j^N \geq N_{min} \tag{2.37}$$

The program is linear in u, v, w, Dep and we use an off-the-shelf linear programming solver.

2.4.3 Results

2.4.3.1 Data

We extract data from the 2009 NHTS for 2300 California vehicles [131]. The data includes daily trips (departure and arrival time of vehicles). Figure 2.7 shows the total number of plugged-in cars over the day. Vehicles have a 28.6 kWh capacity and are charged with L1 chargers (1.9kW). A 30 minute time step is used. The price of electricity is taken from the California Independent System Operator website (CAISO [21]). We use the electricity price on the Day-Ahead market for an arbitrarily selected weekday (August 22nd 2014), from the local utility, PG&E (Fig. 2.8).

We also need to specify a sample regulation-up signal $P^{des}(t)$; generally, this is defined on a hourly basis. That is, the aggregator bids a Contracted Power Capacity (*CPC*) and the System

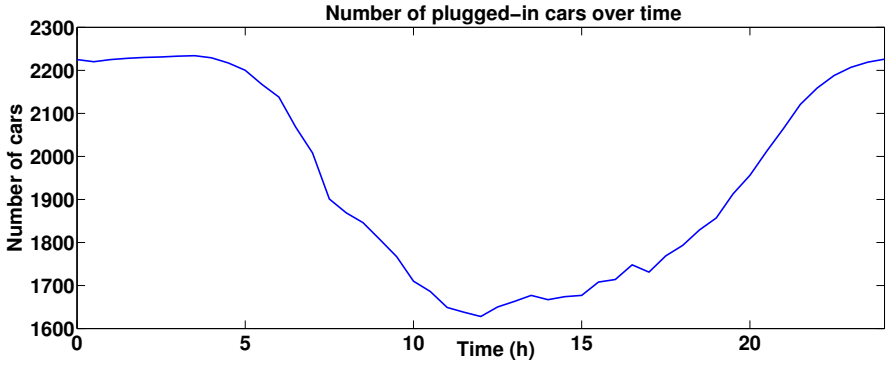

Figure 2.7: Number of Plugged-in cars

Operator provides orders for regulation up and down one day in advance. Due to uncertainties in the number of plugged-in cars and the required energy to satisfy drivers, determining a V2G *CPC* is a difficult question [64, 54]. One idea is to determine the Achievable Power Capacity (APC) from the number of plugged-in vehicles [54]. That is, $APC(t)$ is defined by the number of plugged-in PEVs (Fig. 2.7) and their discharging rate $q_d = 1.9kW$. $APC(t)$ provides the instantaneously available capacity and gives an upper bound for the fleet discharge power. Then a simple energy management method is to bid for a percentage $\alpha \in [0,1]$ of the APC,

$$CPC(t) = \alpha \cdot APC(t). \tag{2.38}$$

In the remainder of the section we define $P^{des}(t) = \alpha \cdot APC(t)$ for different values of α. Remaining simulation parameters include: $X_{dep} = 0.75$, $X_{max} = 0.95$, $X_{min} = 0.2$, $N_{min} = 800$, $u(x,0) = 2225$, $v(x,0) = w(x,0) = 0$.

2.4.3.2 Optimal Charging

The control algorithm ultimately provides the distributions of PEVs between the three categories: Charging, Idle, and Discharging. Figure 2.8(a) presents the resulting distribution for $\alpha = 0.25$. Figure 2.8(b) shows V2G power and requested power during the day.

The controller ensures enough PEVs exist in the discharging category to meet the power supply demand (Fig. 2.8(b)). Then the remaining PEVs are managed between Charge and Idle in order to meet demand from drivers and to minimize overall cost (Fig. 2.8(a)). In this case study, PEVs mainly charge from 1am to 3pm, when the price of electricity is low. After 4pm large flows occur from Charge to Idle to avoid charging during peak hours.

A second aspect of the controller is to optimize the distribution of cars along SOE values. Figure 2.9(a) shows how the controller tends to aggregate cars around particular SOE values. At the end of the optimization period, PEVs are mostly in the idle category and are charged at the minimum required value $X_{min} = 0.2$. A second peak occurs at $X_{dep} = 0.75$, which corresponds to the final constraint of having a minimum number of cars $N_{min} = 800$ at T_{max}. The controller also optimizes at which SOE level cars depart with respect to the condition $x \geq X_{dep}$. Figure 2.9(b) shows that almost all cars depart with the minimum required charge value, X_{dep}.

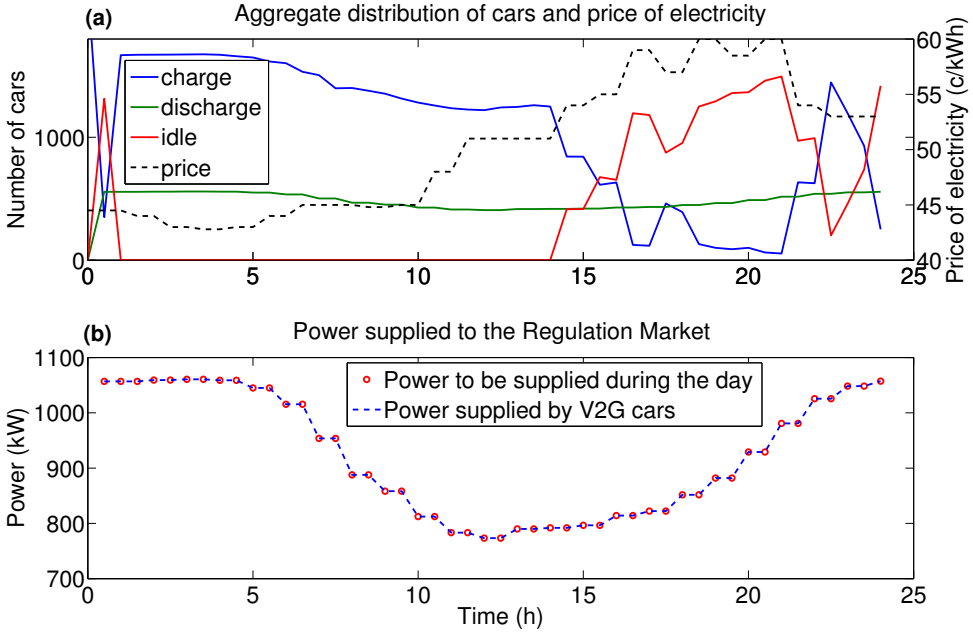

Figure 2.8: Resulting distribution of vehicles and V2G power for $\alpha = 0.25$

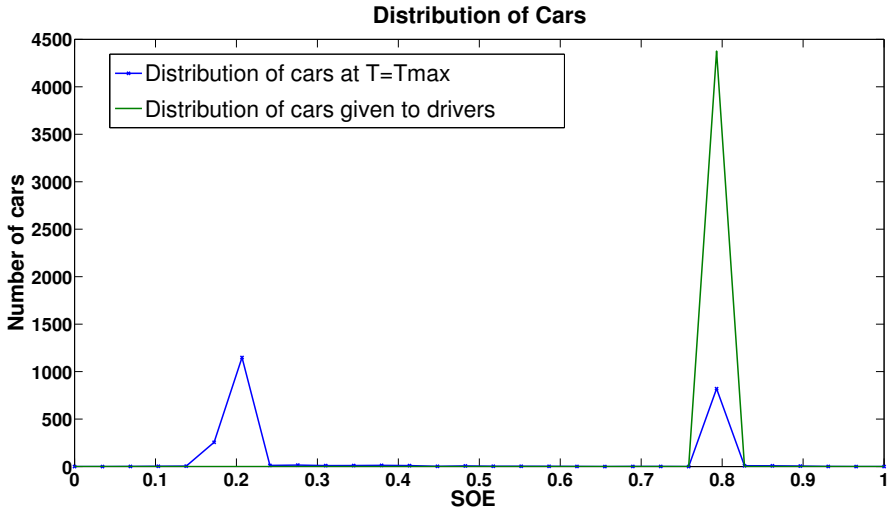

Figure 2.9: Distribution of cars along SOE values

2.4.4 Sensitivity Analysis and Feasibility

A major assumption is that PEV arrivals and departures are known in advance. Even if statistical studies or reservation-based systems provide very good estimates of driver behavior, it is impossible to have an exact prediction. Therefore, we investigate how the program reacts to uncertainties in driving schedules. I n the optimization program detailed above, the demand for cars (*Dem* and *Arr*) impacts the constraints and does not impact the cost function. Therefore, if the actual de-

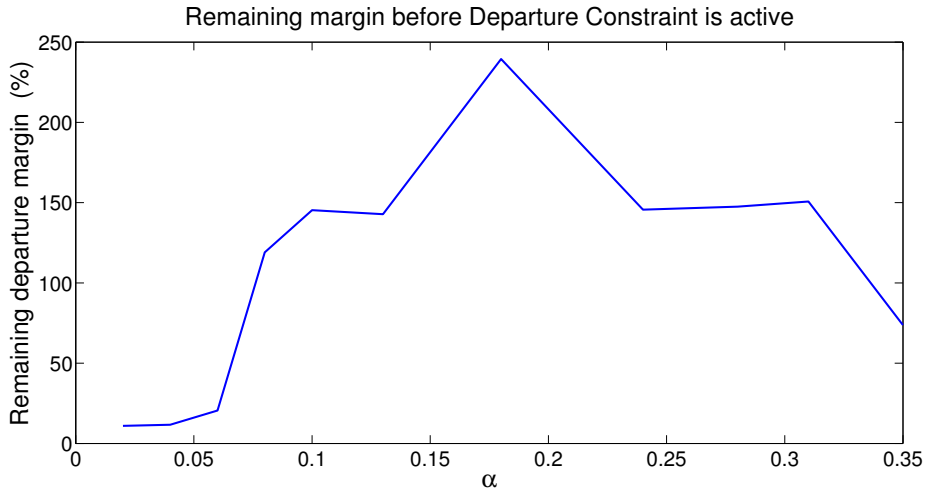

Figure 2.10: Sensitivity analysis to higher demands

mand is different from the expected one, then the cost will remain the same but constraints may be violated.

2.4.4.1 Higher demand than expected

We run the optimization with several parameters and various values for the expected demand. Then, we apply the resulting control signal with a higher demand than the expected one and examine the impact on the constraints. The simulations demonstrate the following:

- The final constraint (2.19) is almost always violated. If the overall demand for cars is $D+\Delta D$ instead of D, the constraint will be violated and the available number of cars at T_{max} will be $N_{min}-\Delta D$ instead of N_{min}.
- The demand departure constraint $x \geq X_{dep}$ is never active in our simulations. Figure 2.10 shows how much the demand can increase before the departure constraint becomes active, for different values of α. Except for small values of α, the demand can double (more than 100% margin) without violating $x \geq X_{dep}$, thus demonstrating robustness to this particular constraint.

2.4.4.2 Lower demand than expected

In this case, every constraint is satisfied but the solution is suboptimal. Since the aggregator overestimates the demand the resulting cost is higher. Figure 2.11 shows how the realized cost relates to the optimal cost for lower demands than expected.

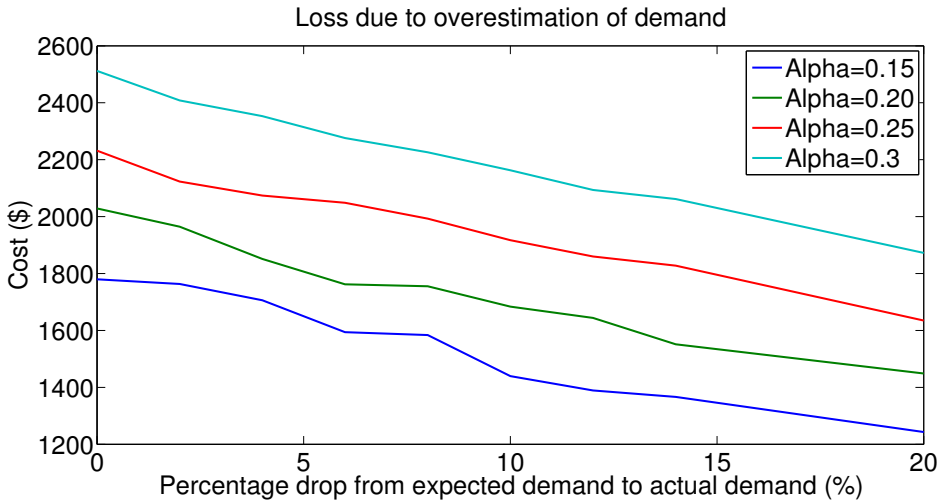

Figure 2.11: Impact of lower than expected demand on cost.

2.4.4.3 Impact of control parameters on cost and feasibility

We examine two sets of parameters for the aggregator:

- α is a grid-related parameter. If α increases, the aggregator bids more power and V2G power increases
- N_{min}, X_{dep} are driver-related parameters. If their values increase, SOE capacity offered to drivers increases.

Figure 2.12 shows the variability of cost with respect to variations in these three parameters and Fig. 2.13 shows the variability of cost per unit of V2G power ($\$/kWh$). The graphs show how the parameters impact cost and feasibility of the system, and the tradeoffs in selecting these values.

- If α increases, then more power is necessary for the regulation up and the cost of PEV charging increases.
- If α, X_{dep} and N_{min} simultaneously take sufficiently high values, then the constraints are too restrictive and the problem becomes infeasible. High values of α imply less flexibility to keep energy for drivers.
- Figure 2.13 shows that the optimization program leads to economies of scale. Cost per kW decreases with increasing α. That is, the aggregator is more aggressive in utilizing excess PEV SOE for V2G services.

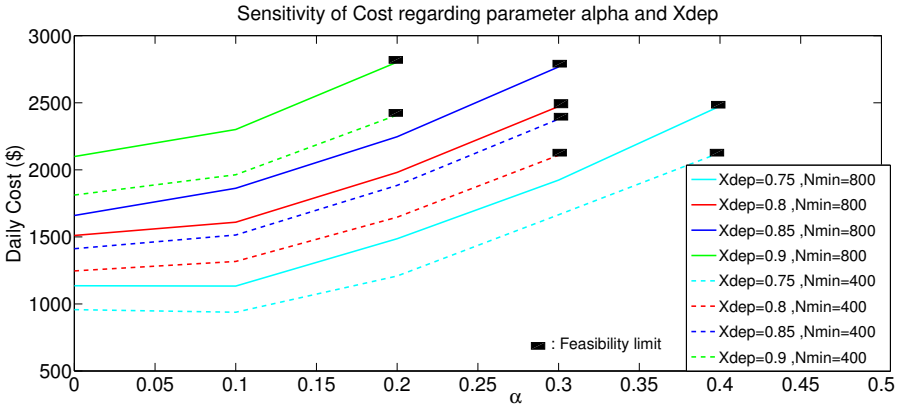

Figure 2.12: Sensitivity analysis regarding α , X_{dep} and N_{min}

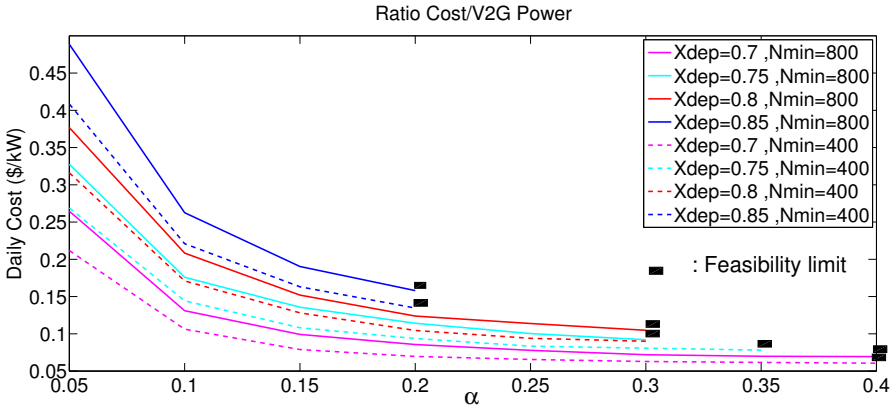

Figure 2.13: Sensitivity analysis regarding α and X_{dep} and N_{min}

2.4.4.4 Impact of charging rate on cost and feasibility

The optimization program depends on the available charging infrastructure and especially charge/discharge rates $q_c(x,t), q_d(x,t)$. Figure 2.14 presents the results for different rate values); fast charging allows more flexibility and higher instantaneous power. Cost per generated power is therefore lower with fast chargers and more stringent constraints can be satisfied.

2.5 State Space representation

In this section, we use the same discretization technique, we represent the dynamics in state space form, and we formulate a model predictive controller to track a power signal. The control problem is formulated as a Linear Quadratic Regulator, which is a particularly efficient method for tracking a signal.

We assume that the aggregator is free to control vehicles in a specific SOE range $[\underline{SOE}, \overline{SOE}] \subset [0,1]$ as shown in Fig. 2.15. In practice, drivers agree to receive their PEV with any $SOE \in$

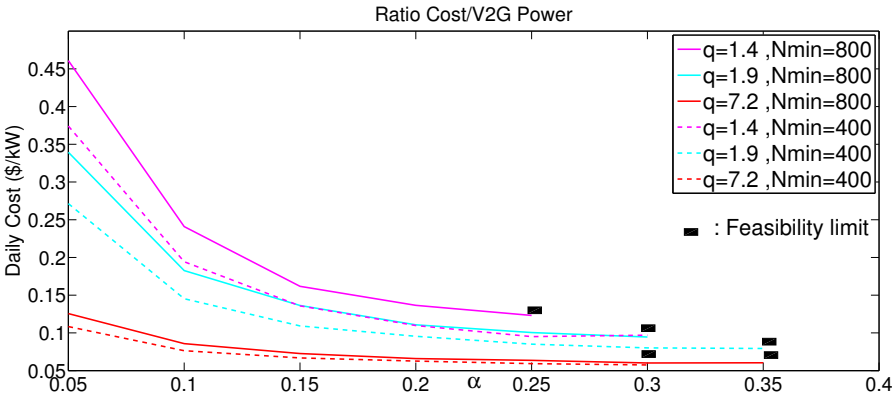

Figure 2.14: Sensitivity analysis regarding α, q and N_{min}

Table 2.4: State Space symbols

Symbol	Description
k	Discrete time index
$X(k)$	State: number of PEVs in bins
$U(k)$	Control input (flow Idle-G2V and Idle-V2G)
$Y(k)$	Output vector (eg: total power)
$S(k)$	Uncontrollable input (flow from drivers and $SOE < \underline{SOE}$)

$[\underline{SOE}, \overline{SOE}]$ upon departure (i.e. $\underline{\text{SOE}}$ is the minimum SOE when PEVs depart). In exchange, the aggregator manages the charging and discharging of PEVs between these bounds and bids this aggregated storage capacity for load following applications. Figure 2.15 shows the boundaries of the system: the grey part is not modeled in this framework, and any contribution from this part is considered as an uncontrollable input.

2.5.1 State Space model

We divide the space $[\underline{SOE}, \overline{SOE}]$ into N_b bins and discretize the system in time and SOE as shown in Fig. 3. The variables u_j^k, v_j^k and w_j^k denote the number of charging, idle and discharging PEVs in bin j at time k, respectively. The flows between bins are due to transportation dynamics (charging and discharging), controllable flows ($\sigma_{i\to c}$ and $\sigma_{i\to d}$), and uncontrollable flows due to driving ($\sigma_{i\to or}$). We discretize the system as presented in Section 2.3.1. Because the numerical scheme is explicit in time, we are able to represent the discretized dynamics of the system with the following state-space model:

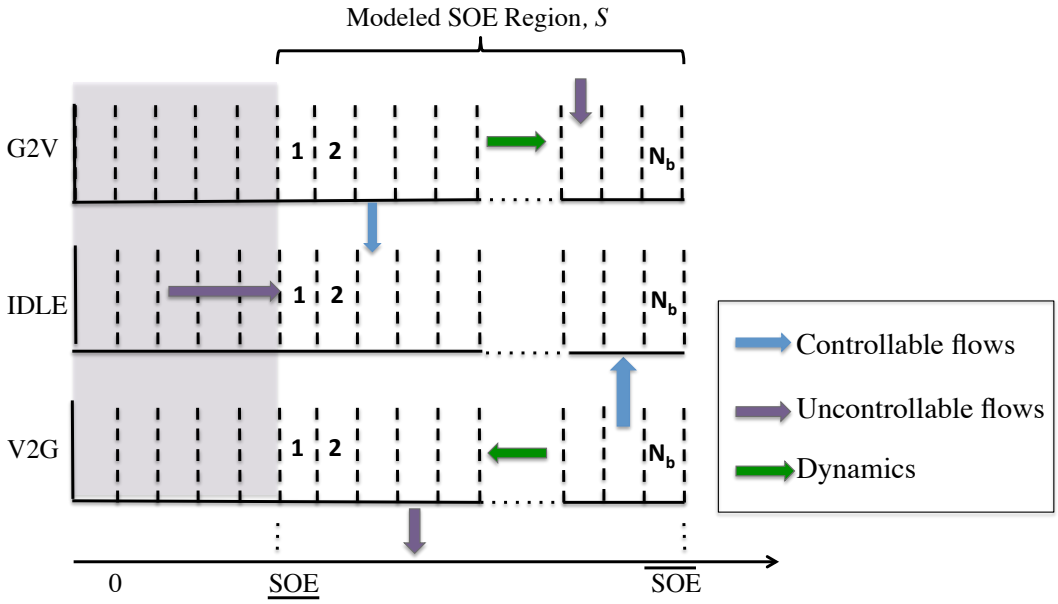

Figure 2.15: State transition model

$$X(k+1) = \mathbf{A}X(k) + \mathbf{B_u}U(k) + \mathbf{B_s}S(k) \tag{2.39}$$

$$Y(k) = \mathbf{C}X(k) \tag{2.40}$$

The variable X represents the state of the system, which is the number of PEVs in each category: ($G2V$, idle, and $V2G$). The variable U is the control input, which controls the flows of PEVs between the three categories. Finally, the variable S is the uncontrollable input, which comes from arrivals and departures of PEVs. This relates to the PDE model described in Section 2.2 as follows:

$$X(k) = \begin{bmatrix} u(\cdot, k\Delta t) \\ v(\cdot, k\Delta t) \\ w(\cdot, k\Delta t) \end{bmatrix}, U(k) = \begin{bmatrix} \sigma_{i\to c}(\cdot, k\Delta t) \\ \sigma_{i\to d}(\cdot, k\Delta t) \end{bmatrix}, S(k) = \sigma_{i\to or}(\cdot, k\Delta t)$$

Matrix $\mathbf{A}$ is the dynamic transition matrix, which includes boundary conditions and results from the Lax Wendroff discretization scheme. The output $Y(k) = \mathbf{C}X(k)$ gives the power consumed or supplied by the fleet of PEVs. We assume a uniform power rate p such that:

$$\mathbf{C} = \begin{bmatrix} -p \cdots -p & 0 \cdots 0 & p \cdots p \end{bmatrix} \tag{2.41}$$

In practice, U gives the SOE distribution of PEVs that are shifted from one charging category to another. In the proposed aggregate model, all the PEVs with the same SOE x at time k are indistinguishable. Thus, to implement the optimal control signal on the real system at time k, the controller chooses $\lfloor \max(0, \sigma_{i\to c}(x, k\Delta t)) \rfloor$ PEVs at random in the idle category and shifts them

to the charging category. Similarly, it selects $\lfloor \max(0, -\sigma_{i\to c}(x, k\Delta t)) \rfloor$ PEVs at random in the charging category and shifts them to the idle category. The implementation of $\sigma_{i\to d}$ follows the same control rule. Note that the control signal needs to be rounded before it is implemented.

2.5.2 Uncontrollable input and modified State Space model

As specified previously, the contribution from drivers and PEVs with $SOE < \underline{SOE}$ is incorporated into the uncontrollable input $\sigma_{i\to Or}(x,t)$ in the PDE model, and $S(k) \in \mathbb{R}^{N_b}$ in the state space model. The uncontrollable flow $S(k)$ only impacts idle cars and can be divided into negative contributions due to arrivals $Arr(k)$, and positive contributions due to departures $Dep(k)$ such that: $S(k) = Arr(k) + Dep(k)$ and a corresponding $\mathbf{B_s} = [0, -I, 0]^T$.

Arrivals into the system comes from drivers who plug-in with $SOE \in [\underline{SOE}, \overline{SOE}]$ and from PEVs reaching $SOE = \underline{SOE}$; this input is completely uncontrollable. In contrary, departures occur at any $SOE \in [\underline{SOE}, \overline{SOE}]$, and depends on the state dynamics and the previous control signals. Consider two distinct control inputs $[U_1(0), ..., U_1(k)]$ and $[U_2(0), ..., U_2(k)]$, which result respectively in the state values $X_1(k+1)$ and $X_2(k+1)$ at time $k+1$. The distribution of PEVs at time $k+1$ in scenario 1 and scenario 2 are distinct, which implies that $Dep_1(k+1)$ and $Dep_2(k+1)$ may be distinct (i.e. drivers don't get their cars with the same amount of energy). However, the total number of departures, calculated by the sum of departures from each bin as $1^T Dep_1(k+1) = 1^T Dep_2(k+1)$, remains the same in both scenarios We incorporate this characteristic by modeling $Dep \in \mathbb{R}^{N_b}$ by a controllable input with equality constraint $1^T Dep(k) = d(k)$, where $d(k)$ is the expected number of departures at time k. In contrary Arr is modeled as an uncontrollable input. Thus, we augment the state space model as follows:

$$X(k+1) = \mathbf{A}X(k) + \mathbf{B_u}U(k) + \mathbf{B_s}Dep(k) + \mathbf{B_s}Arr(k) \tag{2.42}$$

$$Y(k) = \mathbf{C}X(k) \tag{2.43}$$

We will use the state space model (2.42), (2.43) in the remainder of this chapter.

2.5.3 Linear Quadratic Regulator for Signal Tracking

Regulation and load following are ancillary services provided to balance the short term mismatch between generation and demand. Their main difference is their time horizons: while regulation occurs on the second-to-second basis, load following addresses longer-term changes in demand [94, 38]. Regulation and load following are particularly interesting for storage and PEV smart charging because they require fast response and are high price energy markets (see [63, 62]), Since we propose a single discrete charging rate for PEVs that is managed by hysteresis type actions, we choose a longer time horizon and assume that the aggregator provides load following reserves and is located in a unique balancing area.

2.5.3.1 Objective

The problem is formulated as a tracking problem where the reference $P_{des}(t)$ is updated every 15 minutes. The controller penalizes three items: deviation from the reference signal, battery degradation and large controllable flows. Experimental aging studies [100] have shown aging is highly correlated to the integral of power transferred through the battery. Therefore, degradation at time l is measured using $D_g(l) = C_g X(l)$ where C_g is defined as follows:

$$C_g(l) = \begin{bmatrix} p \cdots p & 0 \cdots 0 & p \cdots p \end{bmatrix} \tag{2.44}$$

The objective function then becomes:

$$\begin{aligned} J_k(X,U,Y) = & \sum_{l=k}^{N+k} \mathbf{Q_{track}}[Y(l) - P_{des}(l)]^2 + U(l)^T \mathbf{R} U(l) \\ & + \mathbf{Q_{degrad}}[C_g X(l)]^2 \end{aligned} \tag{2.45}$$

In this formulation R penalizes large control values and thus limits flows between the three states $G2V$, Idle and $V2G$. The relative value of $\mathbf{Q_{track}}$ and $\mathbf{Q_{degrad}}$ shows how much the aggregator prioritizes the compliance to balancing services, versus battery degradation.

2.5.3.2 Linear Quadratic Regulator

The optimal smart charging control comes from the solution of the following LQR - MPC scheme:

$$\min_{U,Dep} J_k = \sum_{l=k}^{N+k} \mathbf{Q_{track}}[Y(l) - P_{des}(l)]^2 + U(l)^T \mathbf{R} U(l) + \mathbf{Q_{degrad}}[C_g X(l)]^2 \tag{2.46a}$$

$$\text{st } X(l+1) = \mathbf{A}X(l) + \mathbf{B_u}U(l) + \mathbf{B_s}(Dep(l) + Arr(l)) \tag{2.46b}$$

$$Y(l) = \mathbf{C}X(l) \tag{2.46c}$$

$$X(l) \geq 0 \tag{2.46d}$$

$$1^T Dep(l) = d(l),\ Dep(l) \geq 0 \tag{2.46e}$$

$$X(k) = X_k \text{ measured at time k} \tag{2.46f}$$

$$X(N+k+1) \geq 0 \tag{2.46g}$$

$$l \in \{k, ..., k+N\}$$

In this MPC formulation, the control horizon is $T_{LQR} = N\Delta t$, the full horizon is $T_f = L\Delta t$ and the MPC is computed for $k \in \{0, ...L-N\}$. At each time step, we consider the control horizon T_{LQR} but implement only the first control action. The MPC stops when we reach the full horizon T_f. We assume P_{des} and d are known or forecasted a priori.

Assumption 1. *We assume that the number of departures is always smaller than the number of PEVs in the system, i.e.*

$$\sum_{k=0}^{l} [d(k) - 1^T |Arr(k)|] < 1^T [A^l X(0)] \ \ \forall l \in \{0, ..., L\}. \tag{2.47}$$

Proposition 2. *Under Assumption 1, the LQR (2.46) is recursively feasible: for all initially feasible points, X_0, and for all optimal sequences of control inputs, the MPC optimization problem remains feasible at all times.*

Proof. In practice, this comes directly from the PDE aggregation model, where we formulate boundary and initial conditions to ensure that the problem is well posed (Section 2.2.2). In the case of convection PDEs, this guaranties the conservation of loads. We denote $U_{idle}(l)$ the control sequence that transfers all the PEVs in the Idle category Then, under Assumption 1, we can show that the following control sequence is feasible:

$$U_{idle}(l) = \begin{bmatrix} -I_{N_b} & 0 & 0 \\ 0 & 0 & -I_{N_b} \end{bmatrix} \mathbf{A}X(l) \tag{2.48}$$

$$Dep(l) = d(l)\frac{\mathbf{A}X(l) + \mathbf{B_u}U(l) + \mathbf{B_s}Arr(l)}{1^T[\mathbf{A}X(l) + \mathbf{B_u}U(l) + \mathbf{B_s}Arr(l)]} \tag{2.49}$$

The detailed derivation is presented in the Appendix A. □

2.5.4 Simulations with real-world mobility data

In this section, we demonstrate how the proposed LQR framework applies to a particular case study, and provide general intuition for other cases. We use data presented in reference [61], which comes from more than 2000 non residential charging equipments in Northern California for the year of 2013. Figure 2.16 shows the maximum capacity of PEVs in the modeled aggregate system (see Fig 2.15) for a typical weekday. Thus, we derive the time-dependent forecasted maximum capacity based on the forecasted number of PEVs

$$\overline{Cap} = p \times \mathrm{Nb}_{\mathrm{PEVs}} \tag{2.50}$$

where p is the power rate of the charging stations and $\mathrm{Nb}_{\mathrm{PEVs}}$ the number of PEVs in the system.

Most Independent System Operators (ISO) have not developed a regulated market for load following yet. Because load following and regulation applications share a lot of similarities (see NERC operating manual [94]), we use existing attributes for regulation markets to base our performance analysis. In particular, if the aggregator bids the available capacity Cap, we assume that the load following signal $P_{des} \in [-Cap, Cap]$ has a zero average over the horizon time. In the following cases studies, we draw a signal uniformly in $[-Cap, Cap]$ and subtract the average to simulate realistic balancing signals.

We measure the performance of the aggregator with the Pennsylvania - New Jersey - Maryland Interconnection (PJM) precision score for regulation services. Specifically, the precision score

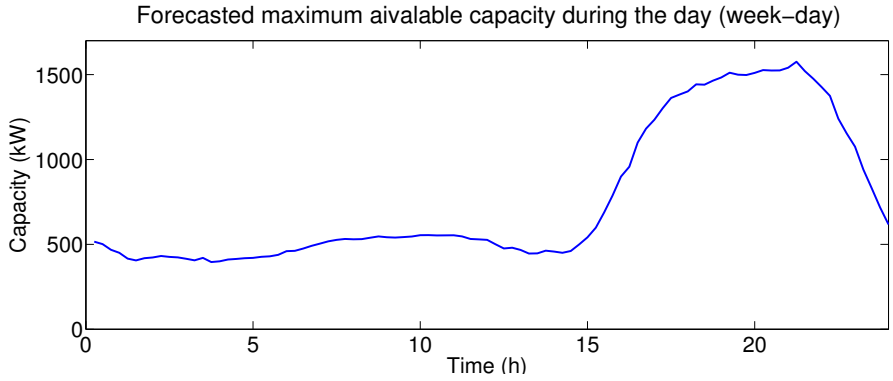

Figure 2.16: Maximum power capacity

is defined as follows [103]:

$$\text{Error}(i) = \left| \frac{Y(i) - P_{des}(i)}{P_{des}(i)} \right|, \tag{2.51}$$

$$\text{Precision score} = 1 - \frac{1}{N} \sum_{i=1}^{N} \text{Error}(i). \tag{2.52}$$

PJM sets a resource compliance score that includes the precision score defined in (2.52). In their market eligibility rules, PJM requires that the compliance score be higher than 0.75 [103]. For the purposes of this chapter, we use a 0.75 precision score as a metric to represent acceptable performance.

We define the time step $\Delta t = 15$min, the time horizon T_f =24h and the control horizon T_{LQR} =4h. Every 15 minutes, the values of P_{des} and d are updated for the next four following hours, a new control sequence is computed based on the LQR (2.46) for the next four following hours, and only the first control response is executed. This MPC algorithm is iterated until it reaches the time horizon T_f =24h. In the next section, we show how to tune the controller parameters to satisfy the minimum 0.75 precision score condition.

2.5.4.1 Impact of the LQR parameters

In the LQR (2.46), the parameters $\mathbf{R}$, $\mathbf{Q_{track}}$ and $\mathbf{Q_{degrad}}$ penalize, respectively, large control values, large deviations from the reference signal and large numbers of non-idle cars. These parameters must be tuned to meet the aggregator's objectives. Figure 2.17 depicts a signal P_{des} between $[-\overline{\text{Cap}}, \overline{\text{Cap}}]$. The signal is zero-mean over the entire horizon, it is updated every 15 minutes and sent to the aggregator. We assume $\underline{SOE} = 0.8$, $\overline{SOE} = 0.95$. Figure 2.18a shows the precision score for different ratios $\frac{||\mathbf{R}||}{||\mathbf{Q_{track}}||}$ and $\mathbf{Q_{degrad}} = 0$. As expected, the tracking improves when the ratio $\frac{||\mathbf{R}||}{||\mathbf{Q_{track}}||}$ decreases and in this specific case study, the aggregator meets the acceptable performance requirement for $\frac{||\mathbf{R}||}{||\mathbf{Q_{track}}||} \leq 10$. Figure 2.18b shows the number of PEVs during the day in each category G2V, V2G or Idle and Table 2.5 shows the precision score for four different ratios.

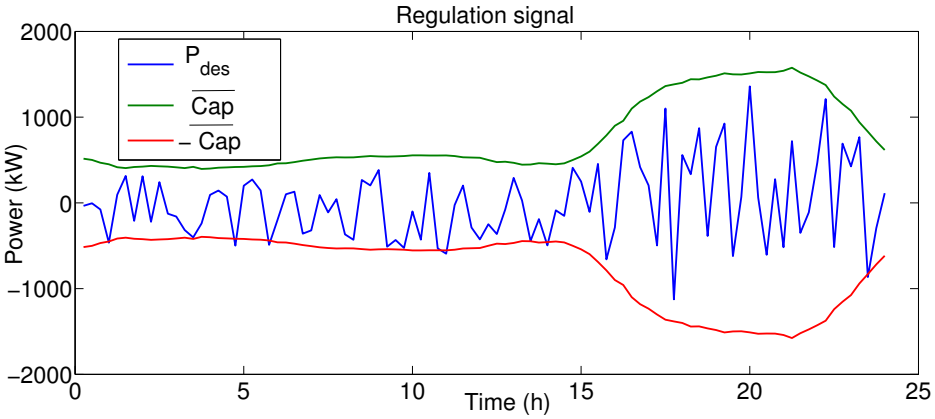

Figure 2.17: Load Following signal (every 15min)

Table 2.5: Precision scores

$\|\|R\|\|/\|\|\mathbf{Q_{track}}\|\|$	1	10	100	200
Precision Score	0.91	0.77	0.40	0.26

The number of idle PEVs tends to increase when less importance is given to tracking, however this has an impact on the aggregator performance and Table 2.5 shows that only $\frac{||\mathbf{R}||}{||\mathbf{Q_{track}}||} \leq 10$ satisfies the acceptable performance requirement.

Figure 2.19a shows the precision score for different ratios of $\frac{||\mathbf{Q_{degrad}}||}{||\mathbf{Q_{track}}||}$ and $R = 0$, Fig 2.19b visualizes the distribution of PEVs. As before, the tracking improves when the ratio $\frac{||\mathbf{Q_{degrad}}||}{||\mathbf{Q_{track}}||}$ decreases. The effect of $||\mathbf{Q_{degrad}}|| > 0$ is to limit the number of PEVs in the G2V and V2G categories. Figure 2.19b shows that when $||\mathbf{Q_{degrad}}|| > 0$, one of the G2V or V2G categories is empty at each time step: a positive reference signal is attained with only V2G PEVs and a negative reference signal is attained with only G2V categories, which is the minimum-degradation solution to attain this signal.

2.5.4.2 Impact of the SOE range $[\underline{SOE}, \overline{SOE}]$

As stated in Section 2.5, $[\underline{SOE}, \overline{SOE}]$ defines the boundaries of the system. The lower bound $\underline{SOE}$ comes from a tradeoff between flexibility in driver mobility and flexibility in storage capacity for the aggregator. Figure 2.20 shows the performance of the aggregator for different values of $\underline{SOE}$, when $\overline{SOE} = 0.95$ is fixed. The green curve illustrates a pessimistic case, where the reference signal is always positive $P_{des} = 0.7\overline{\text{Cap}}$ (i.e. not zero mean) and shows that the aggregator is not able to meet the requirements for $\underline{SOE} \geq 0.5$. The aggregator looses flexibility as the interval $[\underline{SOE}, \overline{SOE}]$ becomes narrower. Let T_{V2G}^{max} denote the longest time period a PEVcan stay in the V2G

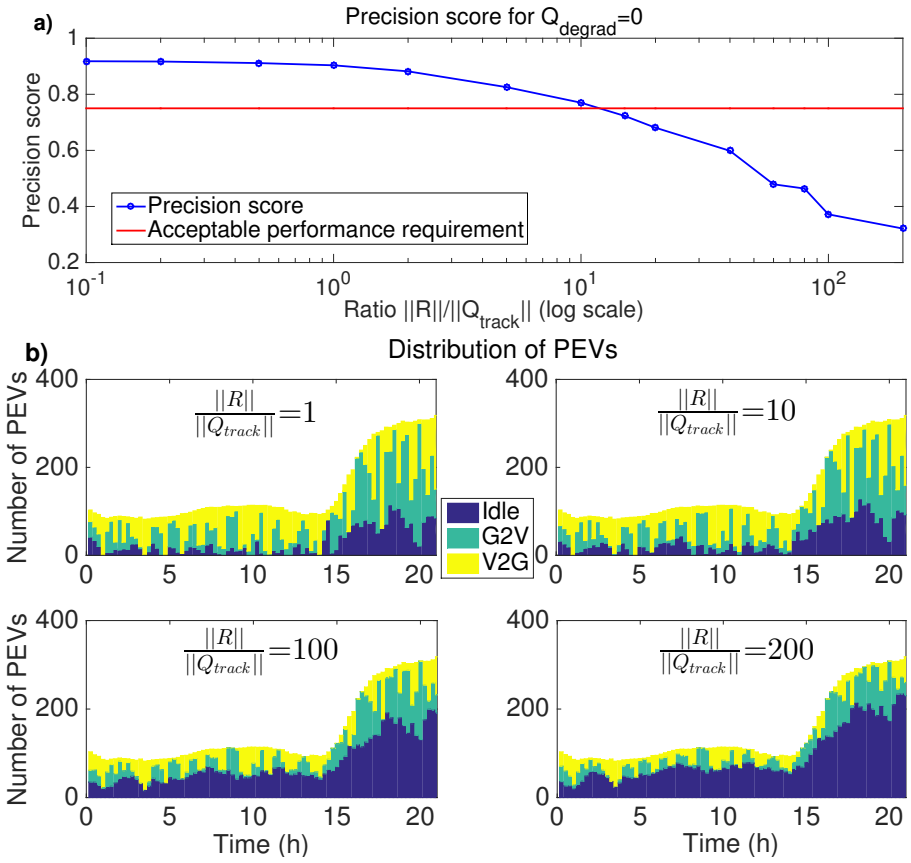

Figure 2.18: (a) Precision score and (b) number of PEVs in each charging category for $\mathbf{Q_{degrad}} = 0$ and varying $\frac{||\mathbf{R}||}{||\mathbf{Q_{track}}||}$

category, i.e. can produce a positive balancing signal. According to Equations (2.1) and (2.2), for a constant power p:

$$T_{V2G}^{max}(\underline{SOE}) = [\overline{SOE} - \underline{SOE}]\frac{\eta E_{max}}{p}. \tag{2.53}$$

Thus, for high values of $\underline{\text{SOE}}$, the aggregator is unable to track an all positive reference signal, which results in low precision scores when $P_{des} = 0.7\overline{\text{Cap}}$.

The blue curve shows the average and the interquartile range (IQR) error bars of the precision score after 50 simulations of zero-mean reference signals. In this case, simulated reference signals fluctuate between positive and negative values, and a small *SOE* range suffices to create short charge and discharge cycles to track the load following signal. However, IQR error bars show that the statistical dispersion increases as the *SOE* range narrows, and the risk to violate the acceptable performance requirement increases. In particular, the aggregator is unable to meet the acceptable performance requirement in more than 25% of cases when $\underline{SOE} \geq 0.85$.

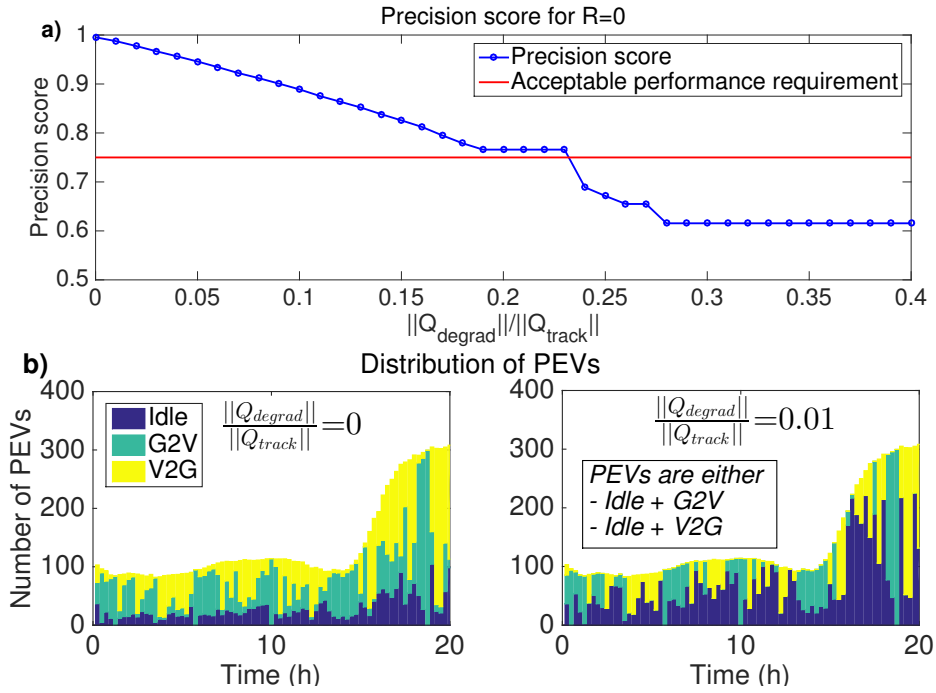

Figure 2.19: (a) Precision score and (b) number of PEVs in each charging category for $R = 0$ and varying $\frac{||\mathbf{Q_{degrad}}||}{||\mathbf{Q_{track}}||}$

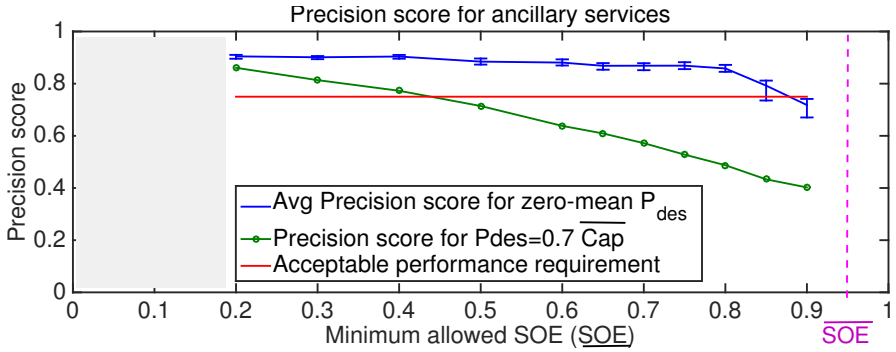

Figure 2.20: Average precision score and IQR error bars for different values of $\underline{SOE}$

2.5.4.3 Analysis on capacity bidding

In this section we are interested in finding the best capacity to bid C_{bid}. We assume the aggregator bids a percentage α of its available capacity $\overline{\text{Cap}}$:

$$C_{bid}(\alpha) = \alpha\overline{\text{Cap}} \tag{2.54}$$

We seek to examine the impact of conservative bidding strategies $\alpha < 1$ versus aggressive bidding strategies $\alpha > 1$.

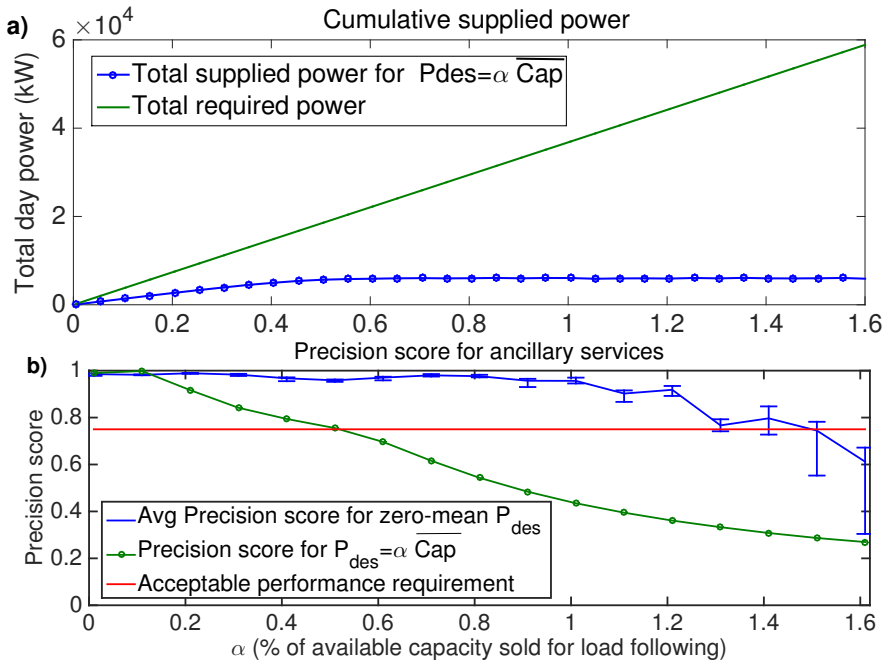

Figure 2.21: Average precision score and IQR error bars for different values of α

Figure 2.21 shows simulation results for $\alpha \in [0, 1.5]$, $\underline{SOE} = 0.75$, $||\mathbf{Q_{track}}|| = ||R||$, and $\mathbf{Q_{degrad}} = 0$. For each α, we simulate 400 reference signals $P_{des} \in [-C_{bid}(\alpha), C_{bid}(\alpha)]$, and we compute the average precision score and the interquartile range. We compare this result with the precision score obtained for the worst-case scenario where $P_{des} = C_{bid}(\alpha) = \alpha\overline{Cap}$. Figure 2.21b shows that the reference signal generally does not attain the maximum bid capacity, and the average performance of the aggregator is higher than 75% for $\alpha \in [0, 1.5]$. The statistical dispersion tends to increase when α increases, and the aggregator is able to meet the acceptable performance requirement in more than 75% of cases, only when $\alpha \in [0, 1.2]$. This shows that the aggregator could bid more than its actual capacity, and still reach the necessary precision score with a high probability.

However in the worst case scenario, the aggregator cannot bid more that 50% of its capacity. Figure 2.21a shows the cumulative power during the day when $P_{des} = C_{bid}(\alpha) = \alpha\overline{\text{Cap}}$. The total supplied power increases when α increases, until it attains a maximum reachable power around 1MW: the aggregator is not able to provide an all-positive or all-negative signal during the day. This example justifies that it is essential that the aggregator participates in a market with zero average signals and it confirms the relevance of balancing markets.

2.6 Optimal capacity bidding

Previous sections have explored sensitivity with bidden capacity. In this section we push this question further and seek to determine the optimal capacity to bid in a regulation market.

2.6.0.1 Feasibility analysis

Let X_0 denote the initial condition and N_t the time horizon. In this section, we seek to describe the set of reachable output trajectories $R(X_0) = [Y_1, Y_2, ..., X_{Y+1}]$ as a polyhedron.
Let $U = [U_0, U_1, ..., U_N]$ and $D_{ep} = [D_{ep0}, D_{ep1}, ..., D_{epN}]$, a feasible control trajectory. The feasible set $P_{\widetilde{U}}$ is a polyhedron defined as follows:

$$\begin{aligned} P_{\widetilde{U}} = \{\widetilde{U} = [U, D_{ep} \in \mathbb{R}^{3\times N_{bin}\times(N_t+1)}] \text{ st } -Dep \leq 0, \\ H_u U + H_d D_{ep} \leq -H_d A_{rr} + H_{X_0} X_0,\ M_{dep} D_{ep} = b_{dep}\} \end{aligned} \tag{2.55}$$

where

$$H_u = \begin{bmatrix} -B_u & 0 & \cdots & 0 \\ -AB_u & -B_u & \cdots & 0 \\ \vdots & \vdots & \ddots & \vdots \\ -A^{N-1}B_u & -A^{N-2}B_u & \cdots & -B_u \end{bmatrix},$$

$$H_d = \begin{bmatrix} -B_s & 0 & \cdots & 0 \\ -AB_s & -B_s & \cdots & 0 \\ \vdots & \vdots & \ddots & \vdots \\ -A^{N-1}B_s & -A^{N-2}B_s & \cdots & -B_s \end{bmatrix}, H_{x_0} = \begin{bmatrix} A \\ A^2 \\ \vdots \\ A^N \end{bmatrix},$$

$$M_{dep} = \begin{bmatrix} 1^T & 0 & \cdots & 0 \\ 0 & 1^T & \cdots & 0 \\ \vdots & \vdots & \ddots & \vdots \\ 0 & 0 & \cdots & 1^T \end{bmatrix}, b_{dep} = \begin{bmatrix} d_0 \\ d_1 \\ \vdots \\ d_N \end{bmatrix}$$

We note f and g the following affine maps:

$$f(\widetilde{U}) = [-H_u, -H_d]\widetilde{U} + (H_{X_0}X_0 - H_d A_{rr}) \tag{2.56}$$

$$g(X) = CX \tag{2.57}$$

Then the reachable output time trajectories is the following polyhedron, which can be written i-as a $H-polyhedra$.

$$R(X_0) = g \circ f \circ P_{\widetilde{U}} \tag{2.58}$$

$$= \left\{Y \in \mathbb{R}^{N_t} | H_y Y \leq b_y\right\} \tag{2.59}$$

2.6.0.2 Capacity bidding for a random signal

We assume that the regulator bids an absolute capacity $C_{bid} \in \mathbb{R}^{N_t}$. Then, any signal $-C_{bid} \leq y \leq C_{bid}$, can be asked by the utility, and has to be reachable. Therefore the bidden reserve capacity

with initial condition X_0 has to satisfy the following property:

$$P_c = \left\{ y \in \mathbb{R}^{N_t} \mid [I_{N_t}, -I_{N_t}]^T y \leq [C_{bid}, C_{bid}]^T \right\} \subset R(X_0) \tag{2.60}$$

Equation (2.60) can be reformulated :

$$\sum_j |h_{ij}| c_j \leq b_i \; \forall i \in \mathbb{R}^N \tag{2.61}$$

where $H_y = (h_{ij}) \in \mathbb{R}^{N \times N_t}$, $b_y = (b_i)$, $C_{bid} = (c_i)$
Proof:

$$H_y y \leq b_y \;\; \forall y \text{ st } -c \leq y \leq c \tag{2.62a}$$
$$\Leftrightarrow \max_{-c \leq y \leq c} \sum_j h_{ij} y_j \leq b_i \; \forall i \in \{1, ..., N\} \tag{2.62b}$$
$$\Leftrightarrow \sum_j |h_{ij}| c_j \leq b_i \quad \forall i \in \{1, ..., N\} \tag{2.62c}$$

Now, let $\lambda \in \mathbb{R}^{N_t}$ denote the capacity price. The optimal capacity problem is given by the following linear program:

$$\max_C \quad \lambda^T C \tag{2.63a}$$
$$\text{st} \quad \sum_j |h_{ij}| c_j \leq b_i \quad \forall i \in \{1, ..., N\} \tag{2.63b}$$

$$\min_{C,y} \quad -\lambda^T C + \mathrm{P} \max_{\substack{-c \leq s \leq c \\ -\varepsilon \leq 1^T s \leq \varepsilon}} |s - y| \tag{2.64a}$$
$$\text{st} \quad y \in R(X_0) \tag{2.64b}$$

2.6.0.3 Capacity bidding for a zero-average signal

Some utilities ensure that the overall average of the regulation signal is close to zero. In this case, condition (2.62) is modified as follows:

$$H_y y \leq b_y \;\; \forall y \text{ st } \{-c \leq y \leq c \; ; \; -\varepsilon \leq 1^T y \leq \varepsilon\} \tag{2.65a}$$
$$\Leftrightarrow \max_{\substack{-c \leq y \leq c \\ -\varepsilon \leq 1^T y \leq \varepsilon}} \sum_j h_{ij} y_j \leq b_i \; \forall i \in \{1, ..., N\} \tag{2.65b}$$

where ε is a small number provided by the utility. The overall problem 2.66 is a Linear Program with Complementary Constraints (LPCC), which is a special case of bilevel programming [83, 56]:

$$\max_{c,y_1,\dots,y_{Nt}} \quad \lambda^T c \tag{2.66a}$$
$$\text{st} \quad H_y y_i^* \leq b_y \ \forall i \in \{1,\dots,N\} \tag{2.66b}$$
$$c \geq 0 \tag{2.66c}$$
$$\text{where } y_i^* \text{ is solution of:}$$
$$\max \ \overline{h_i}^T y_i \tag{2.66d}$$
$$\text{st} \ -c \leq y \leq c \tag{2.66e}$$
$$-\varepsilon \leq 1^T y_i \leq \varepsilon \tag{2.66f}$$

where $\overline{h_i} = [h_{i1},\dots,h_{N_t}] \in \mathbb{R}^{N_t}$, and $\{\Gamma_y y \leq \beta + \Gamma_c C\}$ is a short notation for the $2N_t+2$ constraints $\{-C \leq y \leq C \ ; \ -\varepsilon \leq 1^T y \leq \varepsilon\}$. A classic method to transform the bilevel problem into a one-level problem is to use the Karush-Kuhn-Tucker (KKT) conditions [35].

$$\max_{C,\mu_i,y_i} \quad \lambda^T C \tag{2.67a}$$
$$\text{st} \quad -\overline{h_i}^T + \overline{\mu_i}^T \Gamma = 0 \tag{2.67b}$$
$$\Gamma y_i - \beta - \Gamma_c C \leq 0, \ \ \overline{\mu_i} \geq 0 \tag{2.67c}$$
$$\overline{\mu_i}(\Gamma y_i - \beta - \Gamma_c C) = 0 \tag{2.67d}$$
$$H_y y_i \leq b_y \tag{2.67e}$$
$$i \in \{1,\dots,N\}$$

Constraints (2.67b), (2.67c) and (2.67d) are the KKT conditions, which characterize the lower-level problem: respectively the stationarity condition, the feasibility conditions and the complementary slackness. Finally constraint (2.68f) ensures that the solution is feasible for the upper-level problem. This problem is not convex because of the complementary slackness condition (2.67d). A possible method to solve problem (2.67) is to introduce binary variables and transform the system into a Mixed Integer Linear Program (MILP):

$$\max_{C,\mu_i,y_i,z_i} \quad \lambda^T C \tag{2.68a}$$
$$\text{st} \quad -\overline{h_i}^T + \overline{\mu_i}^T \Gamma = 0 \tag{2.68b}$$
$$-L(1-z_i^k) \leq (\Gamma_y y_i - \beta - \Gamma_c C)_k \leq 0 \tag{2.68c}$$
$$0 \leq \overline{(\mu_i)}_k \leq L z_i^k \tag{2.68d}$$
$$z_i^k \in \{0,1\} \ \forall k \in \{1,\dots,2N_t+2\} \tag{2.68e}$$
$$H_y y_i \leq b_y \tag{2.68f}$$
$$i \in \{1,\dots,N\}$$

The appendix shows that the solution to the LP (2.65b) can take $2N_t+1$ different values $y_k^* = \Gamma_k c + \beta_k$, $k \in [1, 2N_t+1]$ where Γ_k, β_k (see Appendix B).

$$y^* = \Gamma c + \beta \text{ where}$$

$$\exists m \text{ st } \begin{cases} \gamma_{jj} = \text{sgn}(h_{ij} - h_{im}), \beta_j = 0 \text{ for } j \neq m, \\ \gamma_{mj} = -\text{sgn}(h_{ij} - h_{im}), \beta_m = \varepsilon \text{ for } j \neq m, \\ \gamma_{lk} = 0 \text{ otherwise} \end{cases} \tag{2.69a}$$

OR

$$\exists r \text{ st } \begin{cases} \gamma_{jj} = \text{sgn}(h_{ij} - h_{ir}), \beta_j = 0 \text{ for } j \neq r, \\ \gamma_{rj} = -\text{sgn}(h_{ij} - h_{ir}), \beta_r = -\varepsilon \text{ for } j \neq r, \\ \gamma_{lk} = 0 \text{ otherwise} \end{cases} \tag{2.69b}$$

OR

$$\gamma_{jj} = \text{sgn}(h_{ij}),\ \gamma_{lj} = 0,\ \beta_j = 0\ \forall i, j \text{ st } i \neq j \tag{2.69c}$$

We can derive simplified feasibility conditions for solutions (B.5). We define v_i^*, the maximum of LP (2.65b). If y_k^*, then v_i^* is higher than $\sum_j h_{ij} y_j^*$. This can be summarized as follows:

$$\text{(B.5a) is feasible} \quad \Leftrightarrow \begin{cases} \sum_{j=1}^{N_t} \text{sgn}(h_{im} - h_{ij}) c_j - c_m \leq -\varepsilon \\ \sum_{j=1}^{N_t} \text{sgn}(h_{im} - h_{ij}) c_j + c_m \geq -\varepsilon \end{cases} \Rightarrow v_i^* \geq \varepsilon h_{im} + \sum_{j=1}^{N_t} c_j |h_{im} - h_{ij}|$$

$$\text{(B.5b) is feasible} \quad \Leftrightarrow \begin{cases} \sum_{j=1}^{N_t} \text{sgn}(h_{ir} - h_{ij}) c_j - c_r \leq \varepsilon \\ \sum_{j=1}^{N_t} \text{sgn}(h_{ir} - h_{ij}) c_j + c_r \geq \varepsilon \end{cases} \Rightarrow v_i^* \geq -\varepsilon h_{ir} + \sum_{j=1}^{N_t} c_j |h_{ir} - h_{ij}|$$

$$\text{(B.5c) is feasible} \quad \Leftrightarrow \begin{cases} \sum_{j=1}^{N_t} \text{sgn}(h_{ij}) c_j \leq \varepsilon \\ \sum_{j=1}^{N_t} \text{sgn}(h_{ij}) c_j \geq -\varepsilon \end{cases} \Rightarrow v_i^* \geq \sum_{j=1}^{N_t} c_j |h_{ij}|$$

The above statements form a set of conditional constraints, which can be modeled by introducing integer variables [17]. δ is a small deviation and L is a large number.

$$\begin{cases} \sum_{j=1}^{N_t} \text{sgn}(h_{ij}) c_j \leq \varepsilon \\ \sum_{j=1}^{N_t} \text{sgn}(h_{ij}) c_j \geq -\varepsilon \end{cases} \Rightarrow v_i^* \geq \sum_{j=1}^{N_t} c_j |h_{ij}|$$

$$\Leftrightarrow \begin{cases} \sum_{j=1}^{N_t} \text{sgn}(h_{ij}) c_j \leq \varepsilon \\ \sum_{j=1}^{N_t} \text{sgn}(h_{ij}) c_j \geq -\varepsilon \end{cases} \text{false} \quad \text{OR} \quad v_i^* \geq \sum_{j=1}^{N_t} c_j |h_{ij}|$$

$$\Leftrightarrow \begin{cases} \sum_{j=1}^{N_t} \text{sgn}(h_{ij}) c_j > \varepsilon + \delta - Lx \\ \sum_{j=1}^{N_t} \text{sgn}(h_{ij}) c_j < -\varepsilon - \delta + Lz \\ v_i^* \geq \sum_{j=1}^{N_t} c_j |h_{ij}| - L(2 - (x+z)) \\ x, z \in \{0,1\};\ x + z \geq 1 \end{cases}$$

Finally, the problem can be written as a Mixed Integer Linear Program:

$$\max_{C,v^*,z,x} \quad \lambda^T C \tag{2.70a}$$

$$\text{st} \quad \forall i \in \{1,...,N_t\}, k \in \{1,...,2N_t+1\} \tag{2.70b}$$

$$\sum_{j=1}^{N_t} \overline{\alpha_{ij}^k} c_j > \overline{\theta_i^k} + \delta - L_i^k x_i^k \tag{2.70c}$$

$$\sum_{j=1}^{N_t} \underline{\alpha_{ij}^k} c_j < \underline{\theta_i^k} - \delta + L_i^k z_i^k \tag{2.70d}$$

$$v_i^* \geq v_i^k - L(2-(x_i^k+z_i^k)) \tag{2.70e}$$

$$x_i^k, z_i^k \in \{0,1\};\ x_i^k + z_i^k \geq 1 \tag{2.70f}$$

$$v_i^* \leq b_i \tag{2.70g}$$

2.7 Time series forecasting of the available capacity

With the PDE technique developed in this Chapter, the aggregator does not need to forecast travel behaviors for every car. Instead, we only needs to forecast the available capacity, i.e. the number of idle cars per time step. This is a unique characteristic, and strong advantage of this model as one driver's behavior is usually much harder to predict than one fleet's aggregate availability. In this section, we show how we can forecast fleet available capacity through time series.

Data is collected from more than 2000 non residential charging equipments in Northern California for the year of 2013 (see [61] for an extensive study of this dataset). For each charging session, we collect the start and end period, and each charging port reports the average consumed power every 15min. In this chapter, we are only interested in estimating the aggregate regulation signal that can be reached with idle cars. In our dataset, idle cars are the ones that are connected but already fully charged.

Figure (2.22) shows the number of idle cars for each 15-minute time step, for the year of 2013. Figure a) focuses on 5 weeks of the dataset and exposes a regular pattern of the time series. During weekdays, the number of idle PEVs seem to peak around 250 vehicles (in the late afternoon), and during weekends the number of idle PEVs stays pretty constant around 80 vehicles. Because of this very distinct profiles, we analyze and forecast separately the "weekday' time series and the "weekend" time series. In this chapter we focus on the "weekday' time series, which is represented in figure (2.22b). The number of PEVs in the system has increased along the year 2013, which results in a time series with increasing average and increasing variance. We preprocess the dataset with a log transformation in order to fit a standard seasonal ARIMA model.

Table 2.6 compares five models, and shows their AIC and BIC values. The model ARIMA $(1,0,1;1,1,0)$ has the lowest AIC and BIC values, and is therefore chosen. Figure 2.23 analyzes the residuals and 2.24 shows prediction results for this model.This analysis shows that the model is a good fit for the time series: Fig 2.23 shows that the standardized residuals distribution is normal.

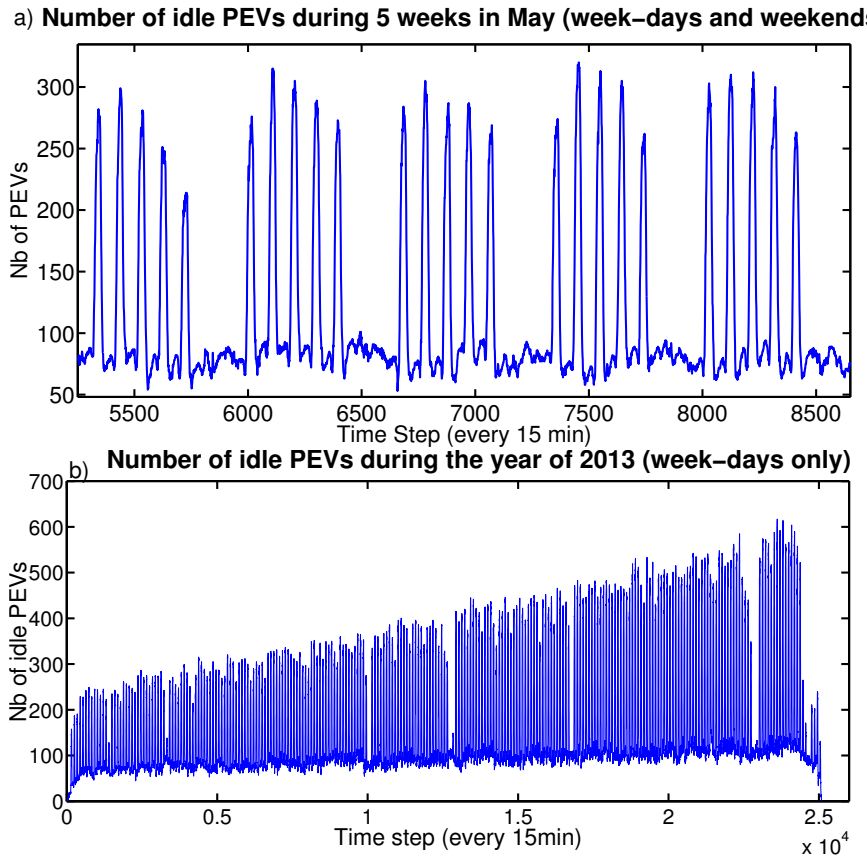

Figure 2.22: Number of idle cars for the year of 2013

Table 2.6: Fit from ARIMA models

Model	**AIC**	**AIC**
$ARIMA(1,1,0;1,1,0)$	-2.9131$\times 10^4$	-2.9096$\times 10^4$
$ARIMA(2,0,0;1,1,0)$	-2.9275$\times 10^4$	-2.9240$\times 10^4$
$ARIMA(1,0,1;1,1,0)$	-2.9297$\times 10^4$	-2.9255$\times 10^4$
$ARIMA(1,1,1;1,1,0)$	-2.9266$\times 10^4$	-2.9231$\times 10^4$
$ARIMA(2,0,1;1,1,0)$	-2.9138$\times 10^4$	-2.9096$\times 10^4$

Fig 2.24 illustrates the real time series, the ARIMA prediction with the 95% confidence interval, and shows that it can appropriately forecast five week-days in advance, which corresponds to one calendar week.

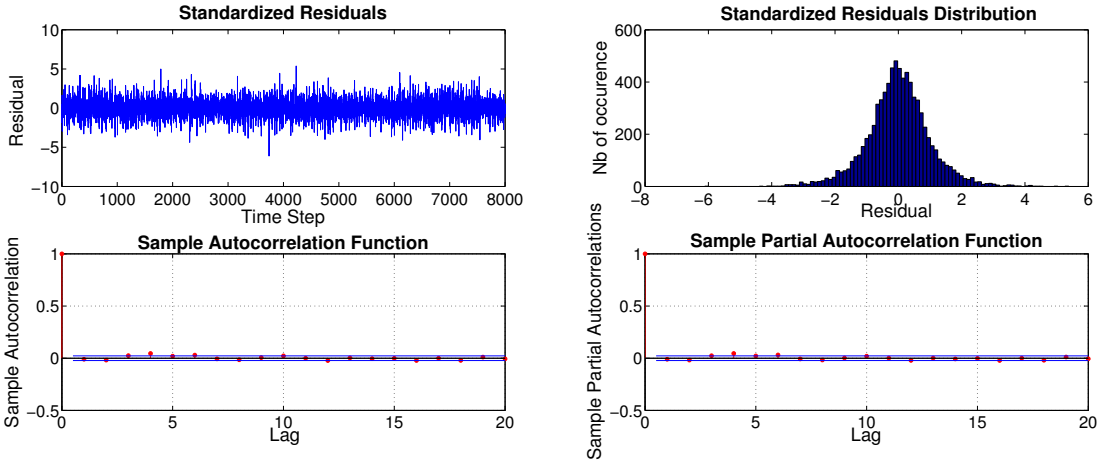

Figure 2.23: Analysis of residuals

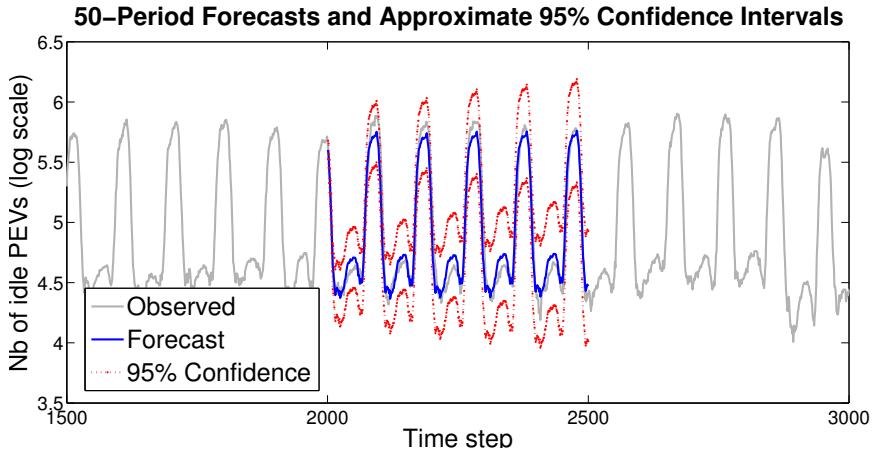

Figure 2.24: Forecasting result

Chapter 3

Dual Splitting Framework for Optimal Charging of Fleets of Electric Vehicles with Continuous Charging rates

3.1 EV charging with continuous charging rates

For the past five years, major efforts have been dedicated to develop the charging infrastructure in the US. This has resulted in an increasing number of charging stations, and more connected and smart equipment. In particular, with newer models of charging stations and their PEV battery communication protocols, it becomes possible to control power in a continuous charging setting. Instead of being controlled in an ON/OFF manner, charging stations can deliver power in a continuous range, between 0 and their maximum deliverable (i.e. limited by the station) or acceptable charging power (i.e. limited by the car).

Mathematically, this results in very different types of non-discrete problems. Prior work has studied this question, and the vast majority of proposed solutions are based on convex formulations of the PEV charging problem. This provides a wide variety of methods, which can be used to efficiently reach the optimal solution. This work can be classified into centralized or distributed protocols. Centralized algorithms [29], [119], [71] utilize a central infrastructure to communicate with each agent, collect information, and compute the optimal load profile of the fleet. The challenges for centralized methods are scalability, with respect to communication, computation and privacy.

In distributed optimization algorithms, each PEV solves a local problem and communicates information to its neighbors and/or a coordinator [106]. Previous work has studied various aspects of load shaping and PEV smart-charging, including filling the night valley of loads (valley filling) in [86, 47], more general driving behaviors in [127, 107], market bidding strategies and market uncertainty in [133, 52, 15] and grid constraints such as transformer overheating [115, 134] and local distribution grid constraints [26, 125, 84]. A wide range of distributed algorithms has been used including game theoretic approaches and Nash Equilibrium in [86], proximal methods in

[47], Alternating Direction Method of Multipliers (ADMM) in [127, 107], regret minimization in [**Ma2014Distributed**] and stochastic protocols in [48]. The aforementioned methods successfully address various aspects of PEV smart-charging but do not provide precise convergence analysis. In particular, finding the necessary number of iterations to reach a specific precision is crucial to assess implementation burdens for practitioners. In this chapter, we seek a tailored method for the distributed PEV smart charging problem, and derive computation requirements. We add to existing studies on optimal charging strategies for load shaping as follows:

- We derive a distributed dual-splitting optimization scheme that exploits the unique aggregate charging problem structure (i.e. a summed objective, strong convexity, and independent constraints). We additionally analyze convergence to yield explicit linear rate-of-convergence bounds, providing precise guidance on the relationship between iterations, error and algorithm parameters.
- We propose stochastic variations of the main dual-splitting algorithm. These variations provide communication and computation trade-offs, thus providing options for practitioners.

As a particular case study of interest we incorporate mobility and power system constraints to quantify demand response opportunities coming from PEVs to shape the California "Duck Curve".

3.2 Problem formulation

Table 3.1: Chapter 3 nomenclature

Symbol	Description
N	Number of PEVs
T_h	Time horizon
u_n^t	Charging rate of PEV n at time t
c_n^t	Discharging rate of PEV n at time t due to driving
x_n^t	State Of Charge (SOC) of PEV n at time t
D^t	Net Load at time t (consumption - renewable generation)
B_n	Battery capacity of PEV n
$\overline{P_n^t}$	Maximum charging power of PEV n at time t
$\underline{P_n^t}$	Minimum charging power of PEV n at time t

In this chapter, we use the notation in Table 3.1 and develop an optimization program for synthesizing PEV charging schedules. We use double brackets to denote a discrete set, e.g. $[[1,T_h]] = \{1,2,\cdots,T_h-1,T_h\}$ and we note the vector inner product: $\langle x,y\rangle = x^T y$, for $x,y \in R^n$. We use the vector notations: $u_n = (u_n^1,...,u_n^{T_h})$, $x_n = (x_n^1,...,x_n^{T_h})$, $c_n = (c_n^1,...,c_n^{T_h})$.

3.2.1 PEV Charging constraints

Let x_n^t denote the State of Charge (SOC) of vehicle n at time t, u_n^t denotes the charging rate when vehicle n is plugged-in, and c_n^t denotes the driving discharging rate when vehicle n is on road. The battery dynamics are described by a piecewise linear model, with a power conversion efficiency $\eta \leq 1$.

$$x_n^{t+1} = x_n^t + \frac{\eta^m u_n^t}{B_n}\Delta t - \frac{c_n^t}{\eta B_n}\Delta t. \tag{3.1}$$

$$m = \begin{cases} 1 & \text{if } u_n^t \geq 0, \\ -1 & \text{if } u_n^t < 0, \end{cases} \tag{3.2}$$

$$x_n^{min} \leq x_n^t \leq x_n^{max} \tag{3.3}$$

Equations (3.1), (3.2) and (3.3) define a constraint set, which is more binding as η increases, and attains the most binding case when $\eta = 1$ (in practice, $\eta = 1$ models a perfect battery efficiency). Therefore, satisfying the constraints associated with a perfect efficiency ensures that the constraints (3.1), (3.2) and (3.3) are true at every time step $t \in [\![1, T_h]\!]$, for any value of $\eta \leq 1$. For simplicity, and similarly to previous work ([55], [7], [57]), we will use $\eta = 1$ to determine the PEV energy constraints:

$$\frac{B_n}{\Delta t}(x_n^{min} - x_n^{init}) + \sum_{\tau=1}^{t} c_n^\tau \leq \sum_{\tau=1}^{t} u_n^\tau \leq \frac{B_n}{\Delta t}(x_n^{max} - x_n^{init}) + \sum_{\tau=1}^{t} c_n^\tau \tag{3.4}$$

$$\underline{P_n^t} \leq u_n^t \leq \overline{P_n^t}, \forall t \in [\![1, T_h]\!] \tag{3.5}$$

The variable u_n^t can be non zero if and only if PEV n is plugged-in at time t. We denote R_n as the indicator vector

$$R_n^t = \begin{cases} 1, \text{ if PEV } n \text{ is plugged in at time } t \\ 0, \text{ otherwise} \end{cases} \tag{3.6}$$

From this definition, we can derive the equality constraint:

$$(1 - R_n)^T u_n = 0 \tag{3.7}$$

3.2.2 Finite Time Horizon constraints

The above problem has a fixed time horizon T_h. In practice, the lack of a terminal constraint could deplete all the PEVs' energy at the end of the period T_h. For simplicity, we impose that every PEV reaches at least SOC x_n^{final} at the end of the period.

$$\sum_{\tau=1}^{T_h} u_n^\tau \geq \frac{B_n}{\Delta t}(x_n^{final} - x_n^{init}) + \sum_{\tau=1}^{T_h} c_n^\tau \tag{3.8}$$

This is a conservative constraint, which can be improved in future formulations of the problem.

3.2.3 Objective

We denote by D^t the aggregate uncontrollable electric loads combined with the uncontrollable renewable generation. Symbol D^t is the net load and does not include PEV loads [22].

We seek to minimize the variance of net load while preserving battery health. This is formulated by the following optimization program:

$$\min_{u} \sum_{t=1}^{T_h} (D^t + \sum_{n=1}^{N} u_n^t)^2 + \sigma \sum_{n=1}^{N} ||u_n||^2 \tag{3.9a}$$

$$\text{st } (1-R_n)^T u_n = 0 \quad \forall n \in [\![1,N]\!] \tag{3.9b}$$

$$\underline{P_n^t} \leq u_n^t \leq \overline{P_n^t} \qquad \forall n \in [\![1,N]\!], \forall t \in [\![1,T_h]\!] \tag{3.9c}$$

$$(3.4), (3.8) \qquad \forall n \in [\![1,N]\!], \forall t \in [\![1,T_h]\!] \tag{3.9d}$$

The first term $\sum_{t=1}^{T_h} (D^t + \sum_{n=1}^{N} u_n^t)^2$ accounts for the variance of the total load curve. The second term $\sigma \sum_{n=1}^{N} ||u_n||^2$ penalizes the distance from u_n to the zero vector. Therefore σ can be viewed as a battery degradation cost [91]. Battery degradation encompasses a variety of complex mechanisms, which partially depends on charging power magnitude among factors such as temperature, cell chemistry, manufacturing quality, etc. However, for simplicity, we will call this term "degradation cost" in the rest of the chapter.

The optimization program is a Quadratic Program (QP) with $T_h \times N$ linear equality constraints and $1 + 4T_h \times N$ linear inequality constraints. For context, consider the Zero Emission Vehicle (ZEV) Action Plan [20] to reach $N = 1.5$ million ZEVs in California by 2025. For $T_h = 24h$ and $\Delta t = 1h$, this yields a QP with $32M$ variables and $144M$ inequality constraints. Despite the structural simplicity of a QP, the shear problem size requires an untenable amount of memory, thus motivating parallelization methods.

3.3 Dual decomposition

In this section we develop a dual splitting method and provide a distributed protocol to solve problem (3.9). Dual splitting strategies are often used to parallelize large scale optimization problems and various methods have been applied to computer vision [18], machine learning [121] or signal processing [30]. Close to the setting under consideration here, the primal-dual approaches developed in [139, 25] deal with block constrained problems. In the following section, we leverage the particular structure of the PEV smart charging problem and develop a novel dual splitting strategy tailored to the average-based input in the objective and the independent constraints. We show that the resultant Gradient Ascent Method assumes updates from every PEV at each time step, and converges to the optimal solution with a linear rate. We later propose two variations based on the Incremental Stochastic Gradient Method (ISGM), which requires updates from only one agent at a time, but converges with a slower rate of convergence.

3.3.1 Dual splitting

In the remainder of this chapter, we will study the optimization program (3.9). Let Ω_n denote the feasible set of charging schedules for PEV n given by (3.9b), (3.9c), (3.9d). We define the consensus variable $z^t = D^t + \sum_{n=1}^{N} u_n^t$. Then (3.9) becomes:

$$\min_{u,z} \quad \sum_{t=1}^{T_h} (z^t)^2 + \sigma \sum_{n=1}^{N} ||u_n||^2 \tag{3.10a}$$

$$\text{st} \quad z^t = D^t + \sum_{n=1}^{N} u_n^t \tag{3.10b}$$

$$u_n \in \Omega_n \ \forall n. \tag{3.10c}$$

The above problem is a quadratic minimization problem with linear constraints, and therefore a convex program. We can dualize the equality constraint (3.10b) and form the Lagrangian with dual variable λ. Moreover, assume there exists a feasible point u in the convex set formed by constraints (3.10c) and (3.10b). Since (3.10b) is affine and always feasible, (3.10) is a convex program and admits a feasible point. Slater's condition holds (c.f. [19]) and the strong duality property gives the equivalent problem:

$$\begin{aligned} \max_{\lambda^t \in \Re} \min_{u,z} \quad & \sum_{t=1}^{T_h} (z^t)^2 + \sum_{t=1}^{T_h} \lambda^t (z^t - D^t - \sum_{n=1}^{N} u_n^t) + \sigma \sum_{n=1}^{N} ||u_n||^2 \\ \text{st} \quad & u_n \in \Omega_n \ \forall n. \end{aligned} \tag{3.11}$$

We first perform the minimization with respect to variable z;

$$\forall t \in [\![1, T_h]\!] \ z^{t*} = \text{argmin} \ [f_t(z^t) = {z^t}^2 + \lambda^t z^t]$$
$$z^{t*} = -\frac{\lambda^t}{2} \text{ and } f_t(z^{t*}) = -\frac{(\lambda^t)^2}{4}$$

Now, we define $\mu^t = -\lambda^t$ and plug the value of z^{t*} into (3.11). Then, the problem is equivalent to:

$$\max_{\mu \in \Re^{T_h}} \frac{-||\mu||^2}{4} + \mu^T D + \sum_{n=1}^{N} \begin{pmatrix} \min\limits_{u_n} & \mu^T u_n + \sigma ||u_n||^2 \\ \text{st} & u_n \in \Omega_n. \end{pmatrix} \tag{3.12}$$

Note that the contributions of u_n in the objective function (3.12) are decoupled along $n \in [\![1, N]\!]$. The N minimization subproblems are now independent from each other and can be solved in parallel. In the next sections we will study the Gradient Ascent Method and the Incremental Stochastic Gradient Method to solve this optimization program.

Algorithm 1 Gradient ascent

Initialization $\mu = \mu_0$; Choose $\alpha \geq 0$, $\beta \geq 0$
1) Find local optimal solution u_n^k
for n=1 **to** N **do**
Solve $u_n^k = \underset{u_n}{\operatorname{argmin}}\ {\mu^k}^T u_n + \sigma||u_n||^2$ st $u_n \in \Omega_n$.
end for
2) Update μ
Compute Gradient step $\mu^{k+1} = \mu^k + \frac{\alpha}{k^\beta}(-\frac{\mu^k}{2} + D + \sum u_n^k)$
if Stopping criteria not reached **then**
$k \leftarrow k+1$, Go to **1)**
end if

3.3.2 Gradient ascent method

Algorithm 1 gives the gradient ascent protocol to solve the optimization program with parameters $\alpha \geq 0$, $\beta \geq 0$, such that the gradient ascent step at iteration k is $\frac{\alpha}{k^\beta}$. In this section, we prove that Algorithm 1 converges to the optimal solution and we give complexity bounds. Let $g : \Re^{T_h} \to \Re$ denote the dual objective function:

$$g(\mu) = \frac{-||\mu||^2}{4} + \mu^T D + \sum_{n=1}^{N} \begin{array}{ll} \min\limits_{u_n} & \mu^T u_n + \sigma||u_n||^2 \\ \text{st} & u_n \in \Omega_n\ \forall n. \end{array}$$

Theorem 1 (Gradient Ascent with constant step-size)**.** *The dual problem in Eq (10) has a unique solution* μ^* *and the gradient ascent with step-size* $\alpha = \frac{2\sigma}{\sigma+N}$ *converges according to*

$$g(\mu^*) - g(\mu_k) \leq \big(\frac{N}{\sigma+N}\big)^k (g(\mu*) - g(\mu_0)) \tag{3.13}$$

Proof: We will prove Theorem 1 in two steps: (i) show strong concavity of g, then (ii) show that that function g admits Lipschitz gradients.

Step 1: The function $g : \Re^{T_h} \to \Re$ is strongly concave with constant $m = \frac{1}{2}$.

We refer to [19] for generic results about convex functions and for the detailed definition of the strong convexity constant m. Function g is a sum of a strongly concave quadratic function and N functions ψ_n defined by:

$$\psi_n(\mu) = \begin{array}{ll} \min\limits_{u_n} & \mu^T u_n + \sigma||u_n||^2 \\ \text{st} & u_n \in \Omega_n. \end{array}$$

The set Ω_n is a non-empty convex set. For each μ, $\psi_n(\mu)$ appears as a minimum of a strongly convex function over a convex set, thus it has a unique solution $u_n^*(\mu)$. Let $\tau \in [0,1]$, $\mu_1, \mu_2 \in \Re$.

$$\begin{aligned}
&\tau\psi_n(\mu_1) + (1-\tau)\psi_n(\mu_2) \\
&= \tau \min_{u_n \in \Omega_n} \mu_1^T u_n + \sigma||u_n||^2 + (1-\tau) \min_{u_n \in \Omega_n} \mu_2^T u_n + \sigma||u_n||^2 \\
&\leq \min_{u_n \in \Omega_n} \tau(\mu_1^T u_n + \sigma||u_n||^2) + (1-\tau)(\mu_2^T u_n + \sigma||u_n||^2) \\
&= \psi_n(\tau\mu_1 + (1-\tau)\mu_2)
\end{aligned} \tag{3.14}$$

Therefore, ψ_n is concave. Now, $g(\mu) = \frac{-||\mu||^2}{4} + \mu^T D + \sum_{n=1}^{N} \psi_n$. The quadratic part is strongly concave with constant $\frac{1}{2}$, therefore g is at least $\frac{1}{2}$ strongly concave.

Step 2: The function $g : \Re^{T_h} \to \Re$ has a Lipschitz continuous gradient with constant $L_g = \frac{1}{2}(1 + \frac{N}{\sigma})$. Since $\psi_n(\mu)$ admits a unique minimum and the function is linear in μ, ψ_n is differentiable and $\nabla\psi_n(\mu) = u_n^*(\mu)$ (see [14]). Using the characterization of minimum of convex functions with $u_n^{*1} = u_n^*(\mu_1)$ and $u_n^{*2} = u_n^*(\mu_2)$, we have:

$$\begin{aligned}
\langle \mu_1 + 2\sigma u_n^{*1}, u_n - u_n^{*1} \rangle \geq 0 \ \forall u_n \in \Omega_n \\
\langle \mu_2 + 2\sigma u_n^{*2}, u_n - u_n^{*2} \rangle \geq 0 \ \forall u_n \in \Omega_n
\end{aligned} \tag{3.15}$$

Applying these relations respectively to u_n^{*2} and u_n^{*1} we get:

$$\begin{aligned}
\langle \mu_1 + 2\sigma u_n^{*1}, u_n^{*2} - u_n^{*1} \rangle \geq 0 \\
\langle \mu_2 + 2\sigma u_n^{*2}, u_n^{*1} - u_n^{*2} \rangle \geq 0
\end{aligned} \tag{3.16}$$

Adding these lines, and using Cauchy Schwarz yields :

$$\begin{aligned}
\langle (\mu_1 - \mu_2) + 2\sigma(u_n^{*1} - u_n^{*2}), u_n^{*2} - u_n^{*1} \rangle \geq 0 \\
\langle (\mu_1 - \mu_2), u_n^{*1} - u_n^{*2} \rangle - 2\sigma||u_n^{*1} - u_n^{*2}||^2 \geq 0 \\
||\mu_1 - \mu_2||||u_n^{*2} - u_n^{*1}|| \geq 2\sigma||u_n^{*1} - u_n^{*2}||^2
\end{aligned} \tag{3.17}$$

We conclude that $||u_n^{*1} - u_n^{*2}|| \leq \frac{1}{2\sigma}||\mu_1 - \mu_2||$. Thus, with operations (3.15), (3.16) and (3.17) we can conclude:

$$||\nabla\psi_n(\mu_1) - \nabla\psi_n(\mu_2)|| \leq \frac{1}{2\sigma}||\mu_1 - \mu_2|| \ \ \forall n, \ \forall \mu_1, \ \forall \mu_2.$$

Coming back to the definition of function g, we obtain:

$$\begin{aligned}
\nabla g(\mu_1) - \nabla g(\mu_2) &= -\frac{\mu_1 - \mu_2}{2} + \sum_n (u_n^{*1} - u_n^{*2}) \\
||\nabla g(\mu_1) - \nabla g(\mu_2)|| &\leq \frac{\sigma + N}{2\sigma}||\mu_1 - \mu_2||
\end{aligned} \tag{3.18}$$

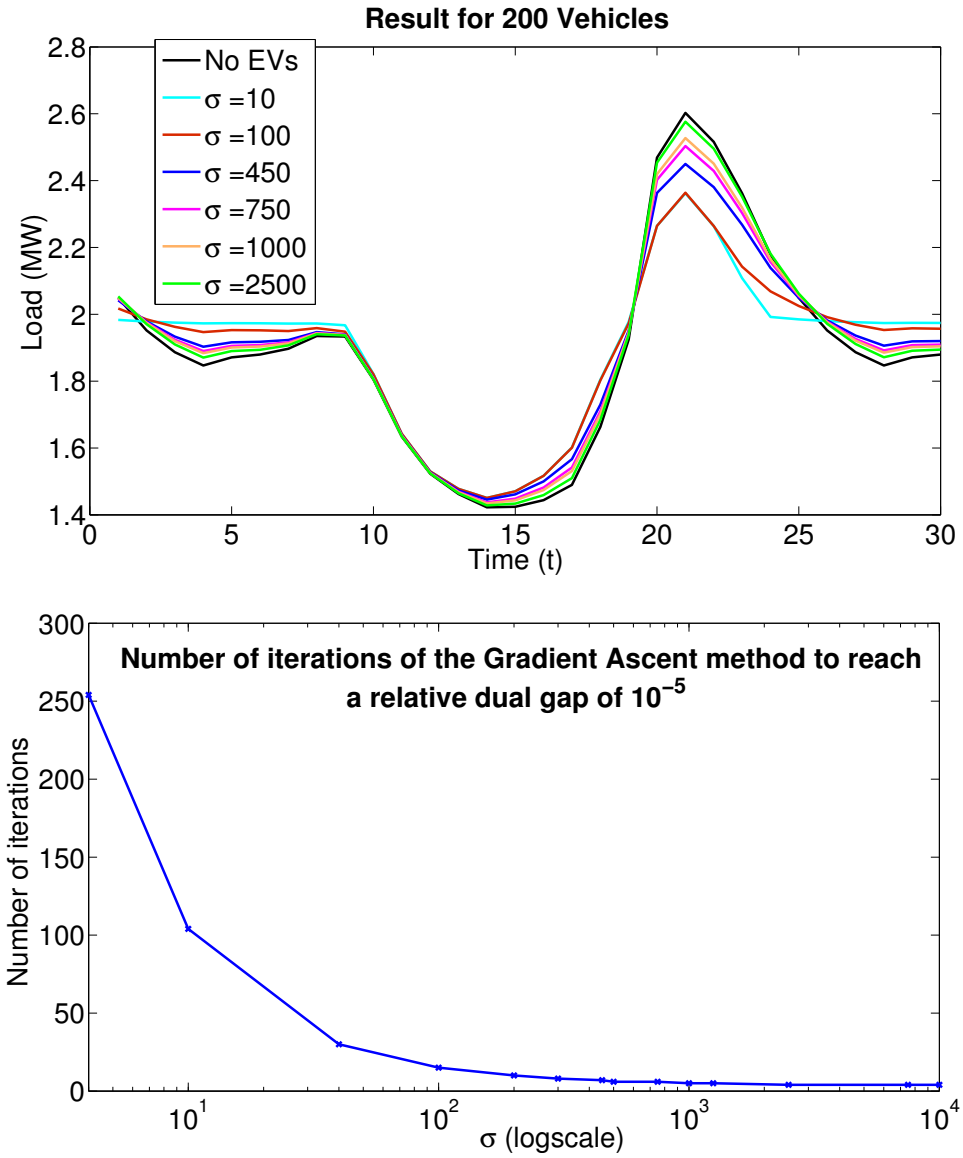

Figure 3.1: Impact of σ on convergence rate and results

Therefore, g has a Lipschitz continuous gradient with constant $L_g = \frac{\sigma+N}{2\sigma}$.
Now, from [19, Ch. 9, p. 466], the gradient ascent method with stepsize $\frac{1}{L_g}$ converges and gives

$$\begin{aligned} g(\mu^*) - g(\mu_k) &\leq \left(1 - \frac{m}{L_g}\right)^k (g(\mu*) - g(\mu_0)) \\ &\leq \left(\frac{N}{\sigma+N}\right)^k (g(\mu*) - g(\mu_0)) \end{aligned} \tag{3.19}$$

□

Remark 1. *Algorithm 1 with constant step-size converges to accuracy ε in $O\big((1+\frac{N}{\sigma})log(\frac{1}{\varepsilon})\big)$ iterations; the complexity is $O\big((N+\frac{N^2}{\sigma})log(\frac{1}{\varepsilon})\big)$. In other words, the convergence rate is linear with respect to parameter $\frac{\sigma}{N}$ and the complexity is quadratic with respect to N. Hence, it is important to tune the parameter $\frac{\sigma}{N}$ to accelerate the convergence. On the other hand, $\frac{\sigma}{N}$ measures how selfish the agents are: as $\frac{\sigma}{N}$ increases, the penalization for battery degradation increases and the result looses optimality in terms of variance minimization. Fig 3.1 illustrates this tradeoff for 200 agents. In each case $\mu_0 = D$ where D is the initial load curve. We stop the algorithm when we reach a relative duality gap of 10^{-5}. We note that for $\frac{\sigma}{N} \geq 1$, 10 iterations are enough to reach this precision.*

Remark 2. *The derived dual splitting algorithm and Theorem 1 apply for any feasible convex set of constraints Ω_n. Consequently, the algorithm can be adapted to similar problems where each agent has an independent set of convex constraints. This feature is useful for extensions that consider uncertainty via a robust convex set of constraints.*

3.3.3 Incremental Stochastic Gradient Method

Algorithm 2 Incremental Stochastic Gradient Method

Initialization $\mu = \mu_0$, Choose α, γ, $\beta \geq 0$
1) Find local optimal solution u_i^k
Select i at random in $[\![1,N]\!]$
Solve $u_i^k = \underset{u_i}{\operatorname{argmin}}\ \mu^{kT} u_i + \sigma||u_i||^2$ st $u_i \in \Omega_i$.
2) Update μ
Compute Gradient update step
$\mu^{k+1} = \mu^k + \frac{\alpha}{\gamma+k^\beta}(-\frac{\mu^k}{2N} + \frac{D}{N} + u_i^k)$
if Stopping criteria not reached **then**
$k \leftarrow k+1$, Go to **1)**
end if

This section develops a variation of the proposed dual-splitting optimization framework to solve (**??**), called the Incremental Stochastic Gradient Method (ISGM). The stochastic method is an iterative method, which uses unbiased estimates of gradients. This is similar to standard gradient methods in the sense that iterate directions are descent directions only in expectation. We keep the

same notations and remark that g can be expressed as:

$$g(\mu) = \frac{1}{N}\sum_{n=1}^{N} \frac{-||\mu||^2}{4} + \mu^T D + N \min_{u_n} \mu^T u_n + \sigma||u_n||^2 \quad \text{st } u_n \in \Omega_n.$$
$$= \frac{1}{N}\sum_{n=1}^{N} g_n(\mu) \tag{3.20}$$

The incremental gradient method is a version of Stochastic Gradient Method where we pick $i \in [\![1,N]\!]$ uniformly at random, and choose the iterate direction ∇g_i. Note μ^* is the optimum for g and μ_n^* is the optimum for g_n. Convergence of IGSM with constant and decreasing step-size are given by the following two theorems.

Theorem 2 (ISGM with constant step-size)**.** *ISGM with constant step-size* $\alpha \in [0, \frac{1}{(1+N/\sigma)^2}]$ *reaches the ball* $B(\mu^*, r)$ *with precision* ε *where* $r = \frac{1}{1+2\alpha L_g^2}\frac{2\alpha}{N}L_g^3 \sum_{i=1}^{N} ||\mu_i^* - \mu^*||^2$ *in* $\frac{1}{\alpha(1-2\alpha L_g^2)}\ln(\frac{||\mu_0-\mu^*||}{\varepsilon})$ *iterations.*

Theorem 3 (ISGM with decreasing step-size)**.** *ISGM with decreasing step-size* $\alpha_k = \frac{1}{(1+N/\sigma)^2+k}$ *converges to the optimal solution* μ^* *and*

$$\mathbb{E}(g(\mu^*) - g(\mu_k)) \leq \frac{1}{N}\sum_{i=1}^{N} ||\mu_i^* - \mu^*||^2 \frac{1}{(1+N/\sigma)^2+k} \tag{3.21}$$

Proof of Theorems: We prove Theorem 2 and 3 by showing that we can find L and B such that $\mathbb{E}\big(||\nabla g(\mu)||^2\big) \leq L^2||\mu - \mu^*||^2 + B^2$.

Step 1: The function $g_n : \mathfrak{R}^{T_h} \to \mathfrak{R}$ has a Lipschitz continuous gradient with constant $L_n = L_g = \frac{1}{2}(1+\frac{N}{\sigma})$. This is shown by following the same procedure as Step 2 of Theorem 1 proof.

Step 2: Show $\mathbb{E}\big(||\nabla g_i(\mu)||^2\big) \leq 2L_g^2||\mu - \mu^*||^2 + B^2$ with $L_g = \frac{1}{2}(1+\frac{N}{\sigma})$ and $B^2 = \frac{1}{2N}(1+\frac{N}{\sigma})^2 \sum_{i=1}^{N} ||\mu_i^* - \mu^*||^2$. Using the Cauchy Schwarz inequality and the Lipschitz condition, we obtain:

$$\begin{aligned}
\mathbb{E}\big(||\nabla g_i(\mu)||^2\big) &\leq \mathbb{E}\big(L_i^2||\mu - \mu_i^*||^2\big) \\
&\leq \mathbb{E}\big(2L_i^2||\mu - \mu^*||^2 + 2L_i^2||\mu_i^* - \mu^*||^2\big) \\
&= \frac{2}{N}\sum_{i=1}^{N} L_g^2||\mu - \mu^*||^2 + \frac{2}{N}\sum_{i=1}^{N} L_g^2||\mu_i^* - \mu^*||^2 \\
&= 2L_g^2||\mu - \mu^*||^2 + B^2
\end{aligned} \tag{3.22}$$

This is the condition $\mathbb{E}\big(||\nabla g(\mu)||^2\big) \leq L^2||\mu - \mu^*||^2 + B^2$. With these particular values of L and B, results in [93] can be used to establish the step-sizes and convergence rates of Theorem 2 and 3. □

Remark 3. *Similarly to Remark 1, Theorem 2 and Theorem 3 show that the computation time depends only on the parameter $\frac{\sigma}{N}$. Parameter $\frac{\sigma}{N}$ measures the tradeoff between the regularity of the objective function (convergence speed) and the optimality of the solution (load shaping performance). In particular, when $\frac{\sigma}{N}$ increases, the number of necessary iterations decreases but the optimal solution becomes less optimal in terms of load shaping.*

3.3.4 Comparison of algorithms

This sections shows computation and communication tradeoffs between the algorithms.

3.3.4.1 Convergence speed

Theorem 2 states that the convergence rate of Algorithm 2 with constant step size is linear, similar to Algorithm 1. Theorem 3 states that the convergence rate of Algorithm 2 with decreasing step size is $\frac{1}{k}$, which is much slower than Algorithm 1. Note that an Incremental Method iteration is N times faster than a Gradient Ascent iteration. Thus, the convergence speed of Algorithm 2 with constant step-size is usually faster, but converges only to a certain precision r. Algorithm 2 should be used when the aggregator needs a fast convergence and is satisfied with an approximate solution.

3.3.4.2 Privacy

In the stochastic configuration, only one random PEV needs to communicate with the aggregator at each time step. This significantly reduces the required communication between each PEV and the aggregator, thus increasing resistance to hacking attacks and improving cyber-security [118]. Consequently, Algorithm 2 with decreasing step-size should be used when the aggregator is concerned about privacy.

Figure 3.2 and 3.3 show the values of the primal and dual objectives for each of the three methods. We stop Algorithm 1 and 2 when the number of iteration exceeds 2×10^5, or the relative duality gap reaches 10^{-3}; N_{it} denotes the number of necessary iterations to converge to the desired precision $\varepsilon = 10^{-3}$. For each case, we choose the starting point $\mu_0 = D$ where D is the load curve ("Duck Curve"). This shows that all the algorithms converge faster as the parameter $\frac{\sigma}{N}$ increases. For $\sigma = 200$, Algorithm 1 and Algorithm 2 with constant step-size converge to the required precision:

- Algorithm 1 needs 5 full-gradient iterations.
- Algorithm 2 needs 6193 stochastic iterations, which corresponds to $\frac{6193}{200} \simeq 31$ full-gradient iterations.

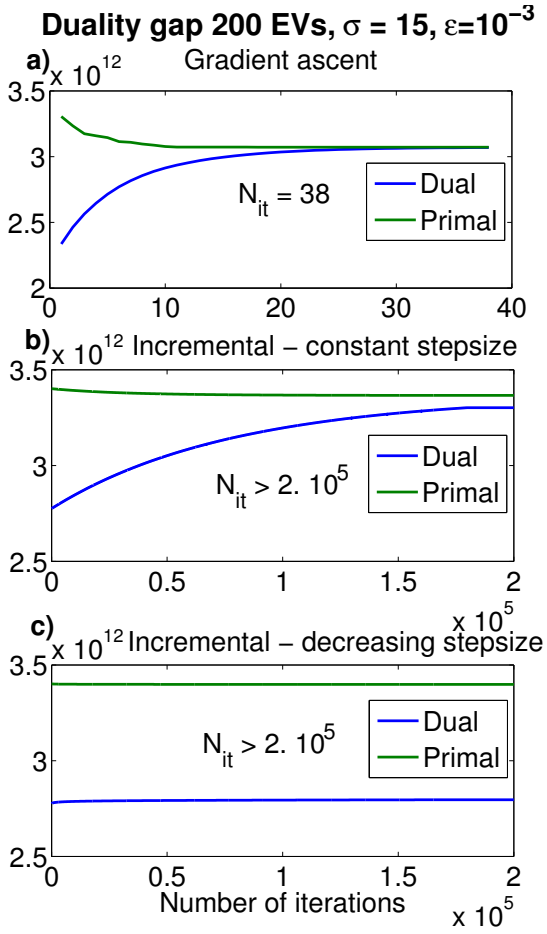

Figure 3.2: Duality gap $\sigma = 15$

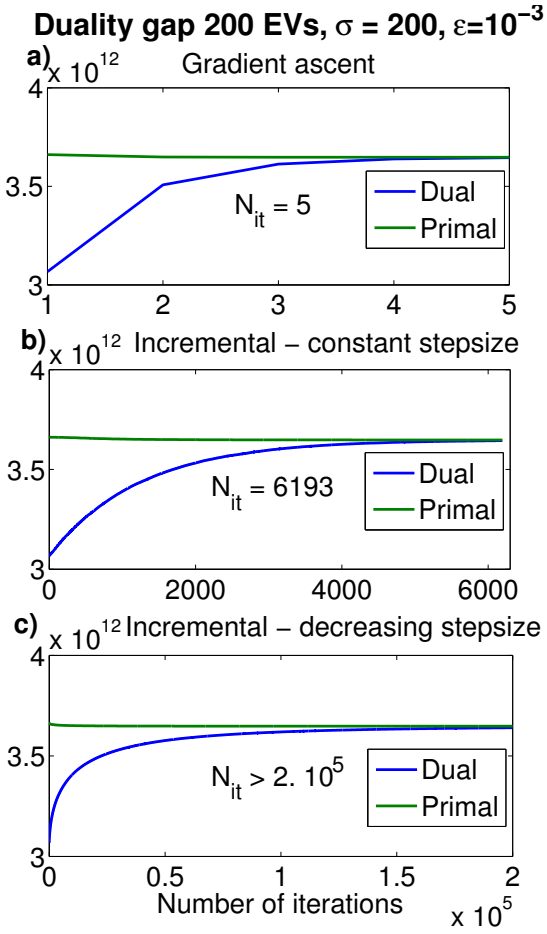

Figure 3.3: Duality gap $\sigma = 200$

3.4 Power network capacity constraints

In this section we adapt the above methodology to include grid capacity constraints, as studied in [115, 134].

3.4.1 Integration of congestion constraints

The algorithms from Section 3.3 are likely to create scenarios where most vehicles charge during low net-load hours, and discharge during high net-load hours. This coordination pattern may provoke power congestion and reverse power flows on distribution lines. In particular, distribution system substations may become overloaded and induce equipment failure and large power outages [128, 65]. We consider preventing these dangerous side effects by setting active power capacity constraints for each feeder.

We consider a network with S feeders and denote by $\mathbb{S}_d$ the set of agents that are connected to the feeder d. The aggregator constrains the aggregated PEV power as follows:

$$L_d^t \leq \sum_{j \in \mathbb{S}_d} u_j^t \leq M_d^t \; \forall d \in [\![1,S]\!], t \in [\![1,T_h]\!]. \tag{3.23}$$

where M_d^t and L_d^t denote the remaining capacity of $\mathbb{S}_d$ at time t and can be determined by forecasting the net load connected to $\mathbb{S}_d$ at time t (without PEVs). In this chapter we do not model the impact of PEVs at the distribution network bus level, instead we assume an independent system operator or utility provides constraints for the aggregated PEV power at the feeder level and ensures grid reliability. The optimization problem with congestion constraints is:

$$\min_u \sum_{t=1}^{T_h} (D^t + \sum_{n=1}^{N} u_n^t)^2 + \sigma \sum_{n=1}^{N} ||u_n||^2 \tag{3.24a}$$

$$\text{st } \forall n \in [\![1,N]\!], u_n \in \Omega_n \tag{3.24b}$$

$$\forall d \in [\![1,S]\!], L_d \leq \sum_{j \in \mathbb{S}_d} u_j \leq M_d \tag{3.24c}$$

We define the same consensus variable $z^t = D^t + \sum_{n=1}^{N} u_n^t$, and the conclusions from equation (3.11) still hold. Then, the distributed problem becomes:

$$\begin{aligned} \max_{\mu \in \Re^{T_h}} \frac{-||\mu||^2}{4} + \mu^T D \quad + \quad & \sum_{d=1}^{S} \sum_{n \in S_d} \min_{u_n} \mu^T u_n + \sigma ||u_n||^2 \\ \text{st} \quad & \forall n \in [\![1,N]\!], u_n \in \Omega_n \\ & \forall d \in [\![1,S]\!], L_d \leq \sum_{j \in S_d} u_j \leq M_d \end{aligned} \tag{3.25}$$

We can further dualize the congestion constraints with dual variables λ_d, γ_d to obtain:

$$\max_{\substack{\mu \in \Re^{T_h} \\ \lambda_d, \gamma_d \in \Re^{+T_h}}} \frac{-||\mu||^2}{4} + \mu^T D + \sum_{d=1}^{S} \sum_{n \in S_d} \min_{u_n} \mu^T u_n + \sigma ||u_n||^2 + \lambda_d^T (u_n - M_d) + \gamma_d^T (L_d - u_n) \tag{3.26}$$

$$\text{st } \forall n \in [\![1,N]\!], u_n \in \Omega_n$$

Equations (3.25) and (3.26) show two ways to solve the optimization program with congestion:

- In (3.25), the problem is semi-distributed (see fig 3.4). Each subsystem S_d is associated with a Quadratic Program of size $T_h \times N_d$ where N_d is the number of vehicles in S_d. Thus, the complexity of each Quadratic Program scales as $O(T_h^3 \times N_d^3)$. All the results from Section 3.3 still hold, where N agents are replaced by S subsystems. This formulation is not scalable, but may be computationally tractable if the size of each subsystem is small.

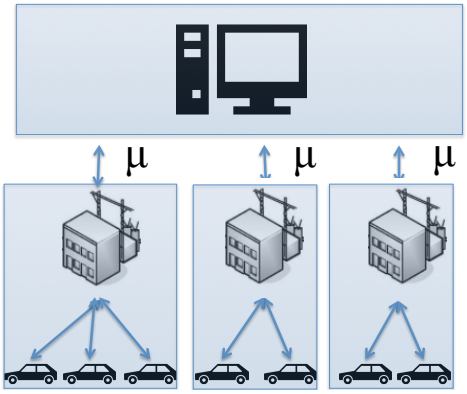

Figure 3.4: Semi distributed

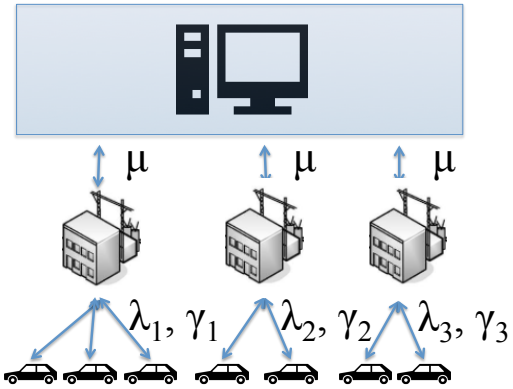

Figure 3.5: Fully distributed

- In (3.26), the introduction of dual variables λ_d and γ_d enables a fully distributed system (see fig 3.5). The triplet of dual variables (μ, λ, γ) is comprised of the global price μ and the congestion prices (λ_d, γ_d).

3.4.2 Distributed optimization under congestion constraints

In this subsection we study formulation (3.26) in more detail. Algorithm 3 proposes an accelerated projected gradient ascent to solve (3.26). Let y denote the full dual variable $[\mu, \lambda, \gamma]$, the dual objective $f : (\mathbf{R} \times \mathbf{R}^+ \times \mathbf{R}^+) \to \mathbf{R}$ is:

$$f(y) = \frac{-||\mu||^2}{4} + \mu^T D + \sum_{d=1}^{S} N_d(\gamma_d^T L_d - \lambda_d^T M_d) \sum_{d=1}^{S} \sum_{n \in S_d} \min_{u_n} (\mu^T + \lambda_d^T - \gamma_d^T) u_n + \sigma ||u_n||^2$$
$$\text{st } \forall n \in [\![1, N]\!], u_n \in \Omega_n$$

Let Pr denote the projection on the set $(\mathbf{R} \times \mathbf{R}^+ \times \mathbf{R}^+)$. We can find the optimal solution of (3.26) with a projected gradient ascent. Algorithm 3 presents an accelerated projected gradient ascent using Nesterov iterations [95].

Theorem 4 (Accelerated Projected Gradient Method)**.** *The accelerated projected gradient ascent in Algorithm 3 with step-size $\alpha = \frac{2\sigma}{\sigma+N}$ converges to an optimal solution y^* with*

$$f(y^*) - f(y_k) \leq \frac{2(\sigma + N)}{\sigma(k+2)^2} ||y^* - y_0||$$

Proof: Note that f is weakly concave and has Lipschitz continuous gradients with constant $L_g = \frac{\sigma+N}{2\sigma}$ (see proof of Theorem 1 for details). Reference [95] gives the corresponding convergence rate for the accelerated Nesterov method.

Algorithm 3 Accelerated Projected Gradient Method

Initialization y_0, y_1, $\theta_0 = 1$, Choose α
1) Find local optimal solution u_n^k
for d=1 **to** S **do**
  for n=1 **to** N_d **do**
    Solve Local Quadratic Program $QP_n(\mu^k, \lambda^k, \gamma^k)$
    $u_n^k = \underset{u_n}{\text{argmin}} \ (\mu^k + \lambda_d^k - \gamma_d^k)^T u_n + \sigma||u_n||^2$ st $u_n \in \Omega_n$
  end for
end for
2) Compute β_k
$\theta_k = \frac{1}{2}(-\theta_{k-1}^2 + \sqrt{\theta_{k-1}^4 + 4\theta_{k-1}^2})$
$\beta_k = \theta_k(\frac{1}{\theta_{k-1}} - 1)$
3) Nesterov Gradient update step $y = (\mu, \lambda, \gamma)$
$z_k = y_k + \beta_k(y_k - y_{k-1})$
$y_{k+1} = y_k + \alpha \ \Pr(\Delta f(z_k))$
if Stopping criteria not reached **then**
  $k \leftarrow k+1$, Go to **1)**
end if

Figure 3.6 shows the result for 500 EVs and 5 distribution subsystems with and without congestion constraints. For the 5 subsystems we simulate congestion constraints, which are proportional to the number of PEVs and charger power rate, such that all PEVs cannot be charging or discharging at the same time.Figure 3.6 shows that the congestion constraints limit the charging and discharging flexibility of the aggregator, especially during the peaks of underconsumption (2pm) and overconsumption (9pm).

Remark 4. *A simple projected gradient ascent could be performed to find the optimal solution of problem (3.26). However, Theorem 4 states that the number of iterations to reach precision ε scales as $\frac{1}{\sqrt{\varepsilon}}$ for the accelerated method, as compared to $\frac{1}{\varepsilon}$ for a simple projected gradient ascent. Figure 3.6 b) and 3.6 c) show the distance from the feasible set after 200 iterations for both the accelerated and standard projection methods. In these two plots the feasible set is the half plan of positive Remaining Capacity values. This shows that 200 iterations are sufficient to approach feasibility with the accelerated method but not with the standard method.*

3.5 Results, application to the Duck Curve

In this section we apply the proposed dual splitting algorithm to flatten the California "Duck Curve" via managed PEV charging. In this section, we do not consider capacity constraints. The Vehicle-to-Grid Simulator (V2G-Sim), developed at Lawrence Berkeley National Labora-

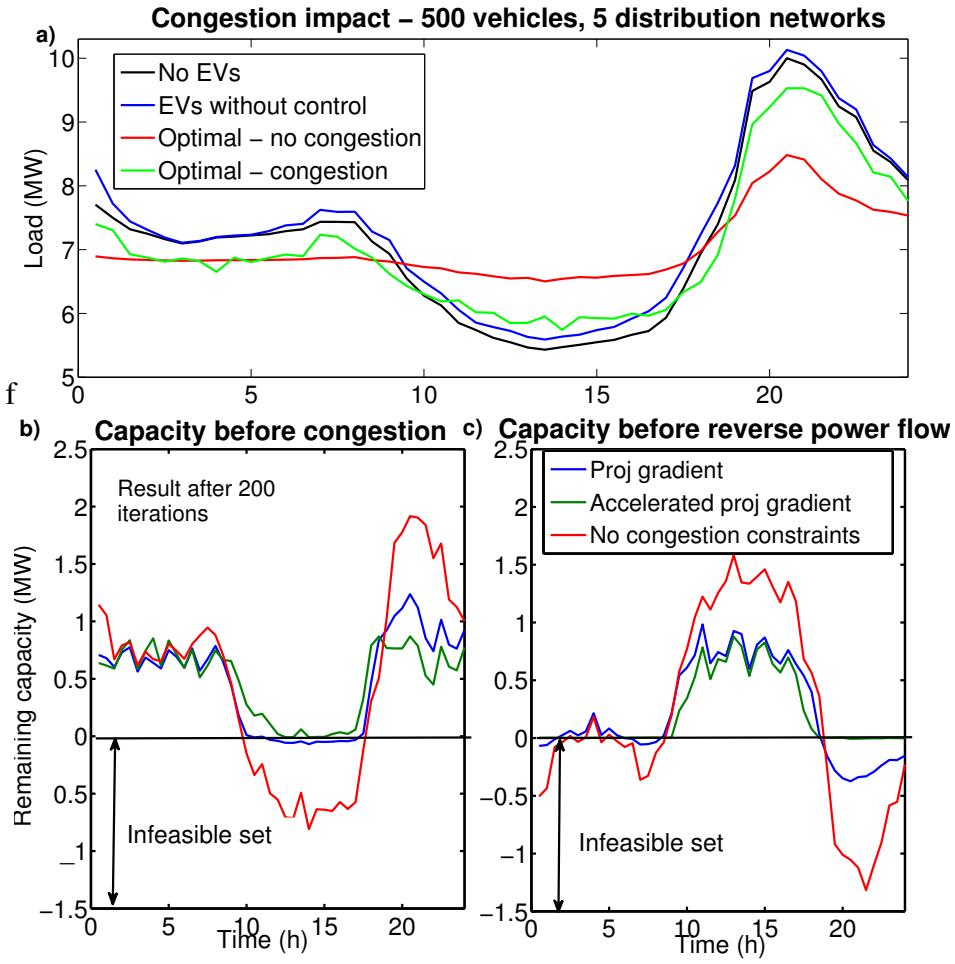

Figure 3.6: Impact of congestion constraints

tory [132], is used to model the driving and charging behavior of individual PEVs. V2G-Sim is an agent-based simulator that incorporates mobility data from the 2009 National Household Travel Survey (NHTS) [131]. Reference [113] provides more details about the V2G-Sim modeling methodology.

3.5.1 Impact of PEV penetration on Demand Response

In this section, we fix the scale $\frac{\text{Number of cars}}{\text{Maximum Peak Load}}$. We assume that the total peak load in California is 26000 MW and the total number of cars in California is 13.3×10^6. This ratio is kept constant to simulate areas of different size and study the impact of PEV penetration in California. Figure 3.7 shows the impact of PEV penetration on a 3MW peak area, which approximately corresponds to 1600 cars. We consider the only available charging infrastructure is Level 1 chargers at home.

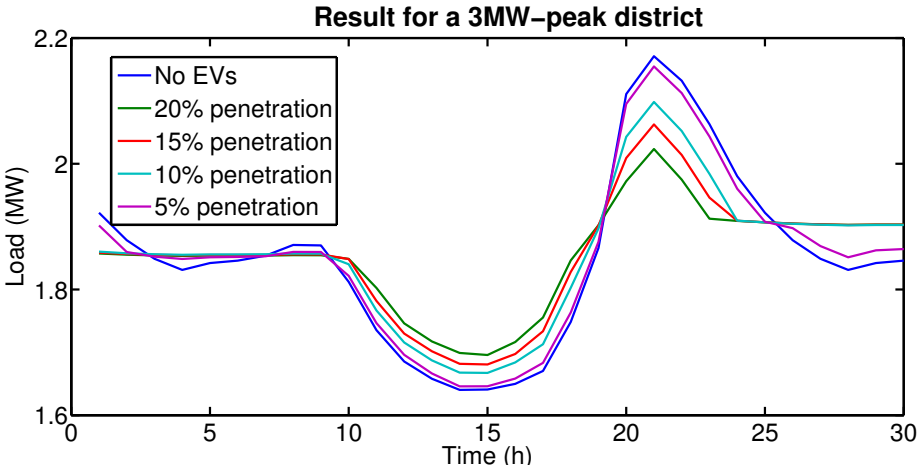

Figure 3.7: Impact of PEV penetration on Demand Response

It is interesting to see that 20% penetration (315 PEVs) suffices to reduce the evening ramp by a factor of 2.

3.5.2 Comparison with other algorithms

In this section, we compare the load shaping performance of the proposed distributed algorithm against decentralized strategies, such as exogeneous marginal pricing and Time Of Use (TOU) pricing ([86, 37]). We seek to assess the performance with respect to the demand response impact. As such, other distributed methods are not considered, since they would yield the same load shaping result, although may require different numbers of iteration.

- *Exogenous Marginal Price*: In this scenario, we consider a fixed pricing signal $\mu^t = \frac{\sigma 10^4}{Cap} D^t$, where Cap is the maximum Load capacity from loads and PEVs, and D is the Net Load without PEVs. This price signal is synthesized by multiplying the net load signal D by scaling factor $\frac{\sigma 10^4}{Cap}$. Thus, this method naturally assigns high prices to peak consumption times, and low prices when total net load is low. This concept is explored in [86] for example.

- *TOU Price*: This pricing method is based on off-peak, partial peak and peak periods. It has been used by several utilities to regulate the demand (see *PG&E* for example [37]). In this scenario we divide the 24h period into 3 groups and assign the corresponding *PG&E* rates for off-peak, partial-peak, and peak periods.

Figure 3.8 shows the effect of the 3 price signals in two different penetration scenarios. In general, the three methods tend to flatten the net load curve, however TOU and Exogenous prices are suboptimal. Figure 3.8 b) shows that TOU pricing yields non-flat load for a large penetration of PEVs. Because we assume that all the agents are price takers, the transitions between partial-peak and off-peak periods (9am and 6pm) create large undesirable ramping. That is, all the PEVs start charging at 9am and stop at 6pm.

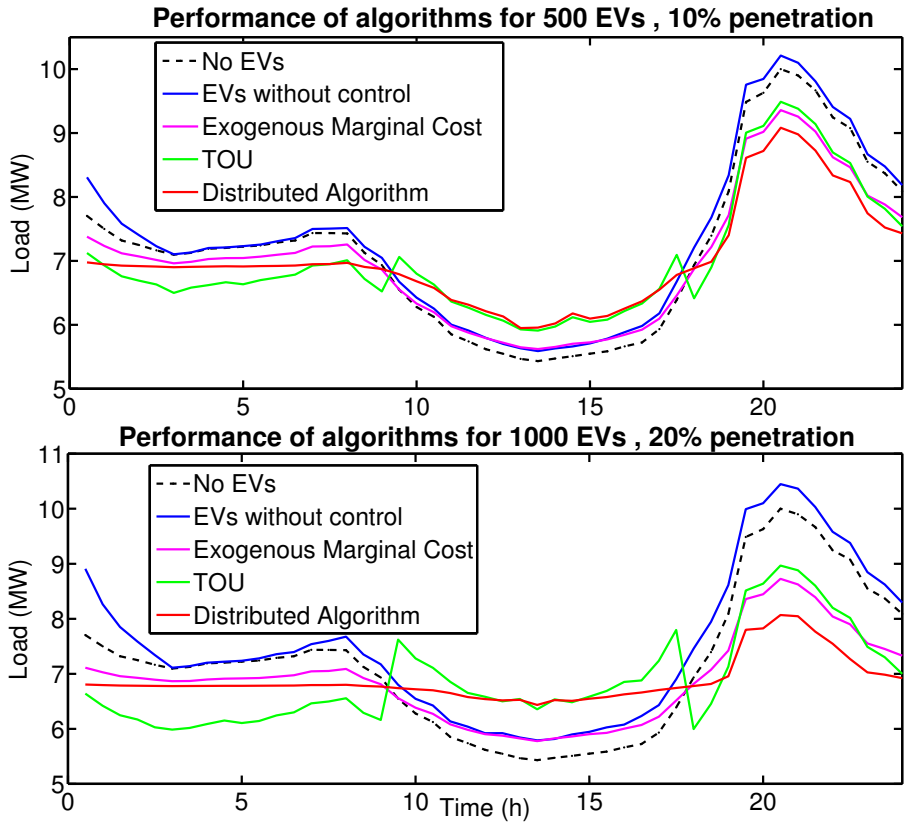

Figure 3.8: Comparison of various pricing methods

This example shows that exogenous methods can be counterproductive in certain scenarios. It is preferable to have a systematic, model-based method to determine price signals.

3.5.3 Load continuity and real implementation

Equation 3.9 is a finite time horizon optimization program. In practice, this method could create discontinuities (ramping) between two separate time periods. This is critical in the context of load shaping since we aim to flatten a continuous energy curve. This point can be handled with rolling horizon techniques. Let T_r define the Rolling Horizon and T_e the execution horizon, we augment the objective function (3.9a) with additional costs due to time steps $t \in [\![T_e, T_r]\!]$ but implement the given solution only for time steps in $[\![1, T_e]\!]$:

$$\min_u \sum_{t=1}^{T_e} (D^t + \sum_{n=1}^{N} u_n^t)^2 + \sum_{t=T_e+1}^{T_r} (D^t + \sum_{n=1}^{N} u_n^t)^2 + \sigma \sum_{n=1}^{N} ||u_n||^2 \tag{3.27}$$

Figure 3.9 shows a four day implementation. Figure 3.9 a) shows the case where $T_e = T_r = 24$h and Figure 3.9 b) shows the case where $T_e = 24$h and $T_r = 48$h. In Figure 3.9 b) there are no

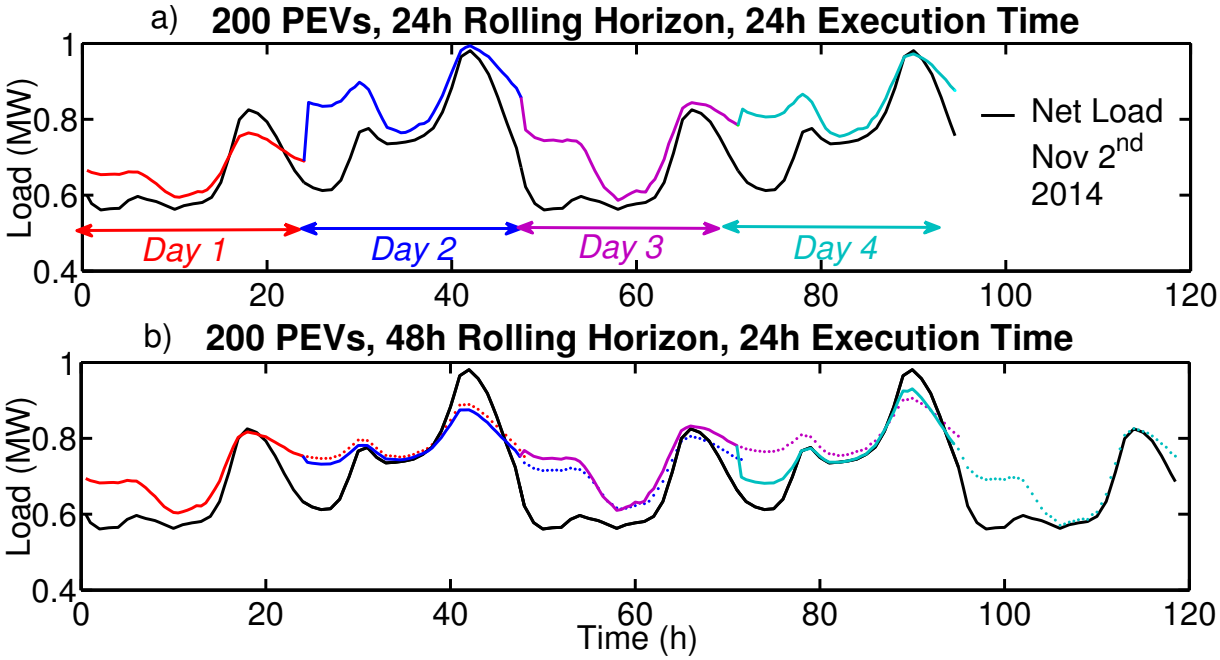

Figure 3.9: Rolling horizon implementation: the colored lines represent the load shape after PEV smart charging, full lines are real implementation and dashed lines planned implementation

discontinuities between two distinct execution periods (full lines), whereas figure a) shows some high power ramping between two different days (particularly between Day 1 and Day 2). The plot illustrates that this implementation method ensures load continuity between different execution periods.

3.6 Summary

In this chapter, we have proposed a method to solve the opetimal PEV scheduling problem with power network congestion constraints. However, power congestion is not the only risk associated wit PEV aggregation, and voltage deviation is also a major threat. To prove complete safety of PEV aggregation, it is necessary to consider a complete model of the power network, and incorporate detailed power and voltage constraints at every node of the grid. Next chapter studies this extended problem, and proposes Plug & Play Model Predictive Control for real time implementation in a computationally efficient manner.

Chapter 4

Electric Vehicle Charging in the Smart Grid: Plug-and-Play Model Predictive Control techniques

4.1 Controlling PEV charging in the broader context of smart grids

The development of smart meters has led to the modernization of distribution networks by enabling real-time bidirectional communication [135]. In this context of smart grids, demand side management allows system operators to control the energy consumption at the household level, offering new opportunities to improve the reliability, efficiency and sustainability of the grid [97, 50]. In particular, automated load shifting is expected to play a key role in stabilizing the grid in the case of high penetration of plug-in Electric vehicles (PEVs) and uncontrollable renewable sources, such as photovoltaic solar energy [72, 82]. Many efficient distributed algorithms have been proposed to address the load scheduling problem, but neglecting distribution grid constraints [73, 47, 87]. In Chapter 2, no grid constraints is considered, and in Chapter 3 only potential line congestion is considered. As a result, these approaches may result in infeasible solutions for the distribution grid [85]. In particular, with the growing penetration of renewable and distributed resources, the risk of voltage instability and reverse power flow increases, and it becomes essential to coordinate loads by considering the extensive set of distribution grid constraints. In this Chapter, we develop a control scheme that integrates flexible loads in the existing distribution network, provides local and aggregated grid services and satisfies users' requirements, as well as grid constraints.

There are two key challenges in designing such a controller. First, it should be able to handle variations in the number of connected loads, i.e. plugging in and out operations. In a real scenario, a user can request to connect or disconnect any load at any desired time and bus. Modeling all the possible requests results in a very large scale and uncertain system, which has been studied through model predictive control (MPC) [34], maximum sensitivity selection [33], and solved by using parallel computing methods [117]. These solutions with fixed-order models (centralized

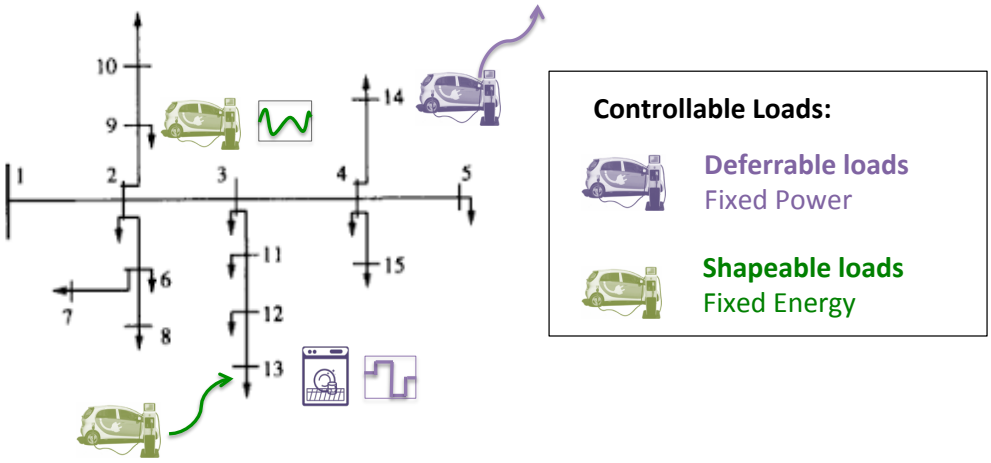

Figure 4.1: Schematic representation of the protocol: loads plugging in and out of the distribution network.

or distributed) do not account for changes in state dimension when PEVs plug-in and plug-out. In contrast, the proposed framework models only the static state of the network and deals with plug-in requests when new loads require supply. Contrary to most available results, the proposed controller is not based on flexible load forecasting, but is redesigned each time a new load is connected. Second, the controller should consider two different objectives and time scales: local voltage regulation and aggregate load shaping. Previous work has proposed multilevel and multi-horizon approaches [34, 114, 81] and decentralized protocols [90] but does not consider the available distribution grid control devices. In opposition, this method does not only include the state of the network, but also the control of battery banks and capacitors, which are jointly optimized with the load profiles.

The proposed solution is based on a two-stage plug-and-play model predictive controller. While the main focus of MPC so far has been on the control of networks with constant topology, the concept of plug and play (P&P) MPC [109, 138, 123] considers network changes by subsystems that want to join or leave the network, while ensuring feasibility and stability of the global system. By providing an automatic redesign of the control laws in response to changing network conditions, P&P MPC is an attractive scheme for modern control systems of increasing complexity. We provide a P&P framework to deal with the connection and disconnection of loads from the grid, which requires an online feasibility handling as introduced in [7]. Compared to previous work in [7], which considers voltage control in a distribution grid, we propose a methodology to control loads with fixed charging deadlines, and achieve both load shaping and voltage control. A procedure for updating the controller together with a transition scheme is proposed, which prepares the system for the requested modifications, and we provide a new proof of recursive feasibility, i.e. satisfaction of network constraints and user deadlines. A schematic representation of the protocol is given in Fig. 4.1.

4.2 Preliminaries

This section introduces the different elements of the network, including deferrable and shapeable loads, battery banks and capacitors. The overall system is modeled as a constrained dynamic system with linear dynamics and energy constraints.

4.2.1 Load modeling

Let consider a load with proposed energy profile $e(k)$ and power profile $c(k)$, where k is the discrete time step. The role of the scheduling operator is to generate another energy profile $\widetilde{e} = \tau(e)$. Three types of loads with different maps τ are distinguished (see Fig. 4.1):

- *Fixed loads* do not participate in demand response and cannot be controlled : $\widetilde{e}^f(k) = e^f(k)$.
- *Deferrable loads* can be delayed but have a fixed load profile. In this case $\widetilde{e}^{def}(k) = e^{def}(k-d)$ with d bounded by a constraint on the maximum allowable delay. This includes PEVs with constant charging rate.
- *Shapeable loads* have a flexible profile but need a fixed amount of energy in a fixed time period T: $\sum_{k=0}^{T} \widetilde{e}^{shp}(k) = \sum_{k=0}^{T} e^{shp}(k)$. It includes PEVs with continuous charging rate.

In the following sections, we model the load dynamics.

4.2.1.1 Deferrable loads

Consider a deferrable load with a proposed power profile $c_0^{def}(k) > 0$ (see Ref [36, 66] for typical profile examples). As soon as the deferrable load plugs in, its power profile c^{def} becomes deterministic:

$$\begin{aligned} e^{def}(k+1) &= e^{def}(k) + \eta^{def} \Delta T c^{def}(k) && \text{(4.1a)} \\ c^{def}(k) &= c_0^{def}(k) && \text{(4.1b)} \end{aligned}$$

In Eq (4.1a), ΔT and $\eta^{def} \leq 1$ are parameters corresponding respectively to the duration of time intervals and the efficiency coefficient, which accounts for energy conversion losses.

Remark 5. *The only control on deferrable loads comes from P&P operations, which determines when to plug-in the load. After it is connected, the load is deterministic and can be considered as a fixed load.*

4.2.1.2 Shapeable loads

Power at shapeable loads c^{shp} can take values in a continuous range $[0, c_{max}^{shp}]$. We define e_{low}^{shp}, e_{max}^{shp}

Table 4.1: Nomenclature - Load dynamics

Symbol	Description
Variables	
$e^{def}(k)$	Deferrable load energy level at time k (kWh)
$c^{def}(k)$	Deferrable load power at time k (kW)
$e^{shp}(k)$	Shapeable load energy level at time k (kWh)
$e^{shp}_{min}(k)$	Minimum shapeable load energy at time k (kWh)
$c^{shp}(k)$	Shapeable load power at time k (kW)
$e^{bat}(k)$	Battery energy level at time k (kWh)
$p^{bat}(k)$	Battery power at time k (kW)
Parameters	
ΔT	Duration of time step (h)
η^{def}	Deferrable load efficiency coefficient (1)
c^{def}_0	Deferrable load fixed power profile (kW)
η	Shapeable load efficiency coefficient (1)
e^{shp}_{low}	Shapeable load energy physical lower limit (kWh)
e^{shp}_{max}	Shapeable load energy physical maximum limit (kWh)
e^{shp}_{des}	Shapeable load desired energy level (kWh)
c^{shp}_{max}	Shapeable load maximum power (kW)
k^{out}	Charging deadline (h)
p^{bat}_{max}	Battery maximum power (kW)
p^{bat}_{min}	Battery minimum power (kW)

and e^{shp}_{des} as the physical lower limit, physical upper limit and desired energy level of the load, respectively. The dynamics of shapeable loads are given by:

$$e^{shp}(k+1) = e^{shp}(k) + \eta \Delta T c^{shp}(k) \tag{4.2a}$$
$$e^{shp}_{min}(k) \leq e^{shp}(k) \leq e^{shp}_{max} \tag{4.2b}$$
$$0 \leq c^{shp}(k) \leq c^{shp}_{max} \tag{4.2c}$$

where $\eta < 1$ is an efficiency parameter. The user's constraint implies that the load is fully charged by time k^{out}, where k^{out} is a parameter communicated to the controller when the load requests supply: $e^{shp}(k^{out}) \geq e^{shp}_{des}$. As a result, the lower bound constraint $e^{shp}_{min}(k)$ is due to two independent factors: (i) the user's constraint in Eq (4.3), and (ii) the physical energy lower limit in Eq (4.4):

$$e^{shp}_{min}(k) \geq e^{shp}_{des} - (k^{out} - k) c^{shp}_{max} \Delta T \eta \qquad \forall k \leq k^{out} \tag{4.3}$$
$$e^{shp}_{min}(k) \geq e^{shp}_{low} \quad \forall k \tag{4.4}$$

Equations (4.3) and (4.4) can be combined as follows:

$$e^{shp}_{min}(k) = \max[e^{shp}_{des} - \max(0,(k^{out}-k)c^{shp}_{max}\eta\Delta T), e^{shp}_{low}]. \tag{4.5}$$

We use the notation:

$$1_{k<k^{out}} = \begin{cases} 1 & \text{if } k < k^{out} \\ 0 & \text{otherwise} \end{cases}$$

4.2.2 Battery banks

On-site batteries are modeled with a linear state space model:

$$e^{bat}(k+1) = e^{bat}(k) + \Delta T\, p^{bat} \tag{4.6a}$$
$$e^{bat}_{low} \leq e^{bat}(k) \leq e^{bat}_{max} \tag{4.6b}$$
$$p^{bat}_{min} \leq p^{bat}(k) \leq p^{bat}_{max} \tag{4.6c}$$

where e^{bat}_{low}, e^{bat}_{max} are the fixed physical lower and upper limits of the battery's energy level and p^{bat}_{min}, p^{bat}_{max} are the minimum and maximum power. This model assumes perfect battery efficiency, which is a simplified approximation of the battery dynamics. The introduction of an efficiency factor $\eta < 1$ would result in a non-convex program as shown in [77, 70]. As a result, the perfect efficiency assumption in (Eq 4.6) is frequently used in the power system literature to formulate the overall system as a linear dynamical system, and to simplify the resulting control scheme ([55, 7, 57]).

4.2.3 Network Model

We consider a radial distribution network, which is a structure commonly used in the power systems literature. To characterize the power flow in this network we adopt the DistFlow equations first introduced in [9] and the notation introduced in [40], restated here for completeness.

The power flow equations for a radial distribution network can be written as the following DistFlow equations [8]:

$$P_{ij} = p^l_j + p^{bat}_j + p^{def}_j + p^{shp}_j + r_{ij}L_{ij} + \sum_{k:(j,k)\in\mathscr{L}} P_{jk} \tag{4.7a}$$

$$Q_{ij} = q^l_j - q^g_j + x_{ij}L_{ij} + \sum_{k:(j,k)\in\mathscr{L}} Q_{jk} \tag{4.7b}$$

$$v^2_j = v^2_i + (r^2_{ij} + x^2_{ij})L_{ij} - 2(r_{ij}P_{ij} + x_{ij}Q_{ij}) \tag{4.7c}$$

$$L_{ij}v^2_i = P^2_{ij} + Q^2_{ij} \tag{4.7d}$$

$$\forall j \in \mathscr{N}\backslash\{1\}, \text{ and } (i,j) \in \mathscr{L}$$

Table 4.2: Nomenclature - Radial distribution network

Symbol	Description
Sets	
$\mathscr{N}$	Set of buses, $\mathscr{N} := \{1,\dots,n\}$
$\mathscr{L}$	Set of lines between the buses in $\mathscr{N}$
$\mathscr{L}_i$	Set of lines connecting bus 0 to bus i
Parameters	
M_i	Number of shapeable loads connected at bus i
Variables	
p_i^l	Real power consumption by fixed loads at bus i (kW)
p_i^{bat}	Real power consumption by battery banks at bus i (kW)
p_i^{shp}	Real power consumption by shapeable loads at bus i (kW)
p_i^{def}	Real power deferrable loads at bus i (kW)
q_i^l, q_i^g	Reactive power consumption and generation at bus i (Var)
r_{ij}, x_{ij}	Resistance and reactance of line $(i,j) \in \mathscr{L}\Omega$
P_{ij}, Q_{ij}	Real and reactive power flows from bus i to j (kW, Var)
v_i	Voltage magnitude at bus i (V)
L_{ij}	Squared magnitude of complex current from bus i to j (A^2)

where P_{ij}, Q_{ij}, v_j and L_{ij} are defined in Table 4.2. Because the above formulation is non-convex, the Second Order Cone relaxation (SOCP) defined in [41] is used, and equation (4.7d) is relaxed as follows:

$$L_{ij} \geq \frac{P_{ij}^2 + Q_{ij}^2}{v_i^2}. \tag{4.8}$$

The variables are the reactive power generation input (column) vector $q^g := (q_1^g,\dots,q_n^g) \in \mathbb{R}^n$, the battery input vector $p^{bat} := (p_1^{bat},\dots,p_n^{bat}) \in \mathbb{R}^n$ and the shapeable, deferrable and fixed loads: p^{shp}, p^{def}, $p^l \in \mathbb{R}^n$, where $p_i^{shp} \in \mathbb{R}^+$ and $p_i^{def} \in \mathbb{R}^+$ denote the net shapeable loads and net deferrable loads charging at bus i, respectively. Symbols M_i^{shp} and M_i^{def} denote the number of shapeable and deferrable loads connected at bus i, respectively. These values can vary over time due to plugging and unplugging operations. This relates with the notation in Section 4.2.1 as follows:

$$p_i^{shp} = \sum_{j=1}^{M_i^{shp}} c_j^{shp}, \quad p_i^{def} = \sum_{j=1}^{M_i^{def}} c_j^{def} \tag{4.9}$$

The substation voltage v_0 is assumed to be given and constant. Furthermore, load profiles p^l and q^l are time-varying but their 24-hour forecast is assumed to be given.

4.2.4 Network Constraints

Depending on the load, bus voltages can fluctuate significantly. For reliable operation of the distribution network, it is required to maintain the bus voltages v within a tight range around the nominal value v_{nom} at all times (generally 5% deviation): $v_{nom} - \Delta v_{max} \leq v \leq v_{nom} + \Delta v_{max}$. We define the variable $V_i = v_i^2$ and write this condition as:

$$V_{min} \leq V_i \leq V_{max}. \tag{4.10}$$

Moreover, storage devices can supply energy at the nodes of the network when $P_{bat} < 0$, which may introduce reverse power flow in the lines [10] and create operational issues in traditional power networks [79]. This issue is avoided by imposing the following constraint:

$$P_{ij} \geq 0 \;\; \forall (i,j) \in \mathscr{L} \tag{4.11}$$

In addition, there are inherent physical limitations on the capacitor control input, which is limited to:

$$q_{min} \leq q^g \leq q_{max}. \tag{4.12}$$

4.2.5 Dynamic System

In this section, the overall system is represented as a constrained dynamic system with energy levels as states. Recalling that $p_i^{shp} = \sum_{j=1}^{M_i^{shp}} c_j^{shp}$, we can write $p^{shp} = K^{shp} u^{shp}$ where $u^{shp} := (c_1^{shp}, \ldots, c_{M^{shp}}^{shp})^T \in \mathbb{R}^{M^{shp}}$, and M^{shp} is the total number of shapeable loads connected to the grid, i.e. $M^{shp} = \sum_{j=1}^{n} M_j^{shp}$. Matrix $K^{shp} \in \mathbb{R}^{n \times M^{shp}}$ is defined such that:

$$K_{ij}^{shp} = \begin{cases} 1 & \text{if shapeable load j is connected to bus i} \\ 0 & \text{otherwise} \end{cases}$$

The overall system model is described as follows:

$$x(k+1) = Ax(k) + Bu(k) \tag{4.13a}$$
$$(x(k), u(k)) \in \mathscr{Z}_k \tag{4.13b}$$

$$x = \begin{bmatrix} x_1, x_2 \end{bmatrix}^T = \left[(e_1^{shp}, \ldots, e_{M^{shp}}^{shp}), (e_1^{bat} \ldots, e_n^{bat}) \right]^T, \qquad u = \begin{bmatrix} q^g \; u^{shp} \; p^{bat} \end{bmatrix}^T$$

$$A = I, \quad B = \begin{bmatrix} 0 & \eta \Delta T & 0 \\ 0 & 0 & \Delta T \end{bmatrix}$$

$$\mathscr{Z}_k = \{\,(x(k),u(k),P_{ij}(k),Q_{ij}(k),V_i(k),L_{ij}(k)) : \tag{4.14}$$
$$(4.7a),(4.7b),(4.7c),(4.8),(4.11), \tag{4.15}$$
$$V_{min} \le V_i(k) \le V_{max},\ \ e_{min}(k) \le x(k) \le e_{max}, \tag{4.16}$$
$$p^{bat}_{min} \le p^{bat} \le p^{bat}_{max},\ \ q_{min} \le q^g(k) \le q_{max}, \tag{4.17}$$
$$0 \le u^{shp}(k) \le c^{shp}_{max}\}. \tag{4.18}$$

4.3 Controller Design

The controller is designed with three control objectives:

- *Peak reduction*: Smooth the aggregated power profile.
- *User satisfaction*: Provide the desired energy to shapeable and deferrable loads.
- *Voltage control*: Ensure that voltage deviation from nominal voltage remains within bounds.

For the purpose of this section, the number of loads connected to the grid is assumed constant. Plug and play connections are introduced in Section 4.4.

4.3.1 Stage 1: Feasible reference

In the remainder of this Chapter, Eq. (4.13) with $p^{def} = 0$, $u^{shp} = 0$ refers to the dynamics with no deferrable and no shapeable loads. We assume that the system has a feasible trajectory and has the following periodic property, with period N_r:

Assumption 2. *There exists an initial value $\hat{x}_0$ and a sequence of control inputs $\hat{u}(k)$, such that the corresponding sequence of states $\hat{x}(k)$ according to dynamics (4.13a) with $p^{def} = 0$, $u^{shp} = 0$ satisfies the constraints in (4.13b), i.e. $(\hat{x}(k),\hat{u}(k)) \in \mathscr{Z}_k$ for all $k \in \{0,...,N_r-1\}$.*

Assumption 3. *If problem (4.13) with $p^{def} = 0$, $u^{shp} = 0$, $x(k) = x_0$ is feasible at time k, then problem (4.13) with $p^{def} = 0$, $u^{shp} = 0$, $x(k+N_r) = x_0$ is feasible at time $k+N_r$.*

In practice, Assumption 2 means that the traditional control devices (battery banks and capacitors) are selected according to the traditional fixed loads p^l. When new loads, such as PEVs, are not plugged-in, traditional control devices have enough flexibility to regulate voltage. Assumption 3 means that if the problem is feasible at time k, then the problem with same initial state is feasible at time $k+N_r$, where the period N_r is typically a day. Deferrable and shapeable loads increase power demand and voltage drop, which requires extra control capacity. In this case, the problem with extra loads may not be feasible, requiring to solve the problem in a hierarchical way. First an optimal solution is computed for the system without extra loads, second this reference signal

is used to formulate a model predictive controller. The optimization problem for computing the solution with only fixed loads $(\hat{x}(k);\hat{u}(k))$ is referred to as *stage-1*:

$$
\begin{aligned}
(\hat{x}(k),\hat{u}(k)) := \underset{\tilde{x},\tilde{u}}{\operatorname{argmin}} \sum_{i=0}^{N_r-1} ||\tilde{u}(i)||_{T_1}^2 + ||V(i)-V_{nom}||_{T_2}^2 \\
\text{s.t. } \tilde{x}(i+1) = A\tilde{x}(i) + B\tilde{u}(i) && (4.19a)\\
\tilde{x}(0) = A\tilde{x}(N_r-1) + B\tilde{u}(N_r-1) && (4.19b)\\
(\tilde{x}(i),\tilde{u}(i)) \in \mathscr{Z}_i;\ \ i=0,\ldots,N_r-1 && (4.19c)\\
M^{def} = M^{shp} = 0
\end{aligned}
$$

where T_1 and T_2 are respectively positive definite and positive semi-definite weight matrices of appropriate dimensions (see [129, Chapter 1] for details about weighted norms). The terminal constraint (4.19b) ensures that batteries recover their initial energy level at the end of the control horizon.

Remark 6. *At* stage-1*, a cost function is chosen that penalizes the generation control input and the deviation of voltage from its nominal value. The matrix T_2 is defined positive semi-definite since tracking the nominal voltage improves the power quality for loads, but the constraint (4.19c) is enough to ensure that voltage remains between operational bounds at every time step $i \in \{0,\ldots,N_r-1\}$.*

4.3.2 Stage 2: Model Predictive Controller

In the second stage, a predictive controller is designed to minimize the overall cost of the system for time steps in $\{0,..,N-1\}$, with $N < N_r$. Problem *stage-1* is computed once, at the begining of the horizon, and the corresponding solution is used to ensure that the *stage-2* problem remains recursively feasible under a receding horizon strategy. Let $\lambda(t)$ denote the price of electricity at time t. The price $\lambda(t)$ is given as an input to the MPC and reflects demand peaks and congestion in the grid. This price can change at every time step, and reflect dynamic price markets. We propose the following MPC problem (referred to as *stage-2*):

$$
\begin{aligned}
\min_{x,u} \quad & \sum_{i=0}^{N-1} \lambda(i+k)\Big(\sum_{j=1}^{M^{shp}} u_j^{shp}(i+k)\Big) + ||V-V_{nom}||_{T_3}^2 && (4.20a)\\
\text{s.t} \quad & x(i+1+k) = Ax(i+k) + Bu(i+k) && (4.20b)\\
& x(k) = x_k && (4.20c)\\
& (x(i+k),u(i+k)) \in \mathscr{Z}_{i+k};\ \ i=0,\ldots,N-1 && (4.20d)\\
& x(N+k) \in \mathbb{X}_{N+k} && (4.20e)
\end{aligned}
$$

In the MPC problem (4.20), the first term achieves peak reduction through the time-varying price λ, while the second term penalizes voltage deviation. In the first term, the contribution from

fixed loads p^l, and deferrable loads p^{def} is uncontrollable, therefore load shaping can only be achieved by controlling u^{shp}. The loads directly respond to the price, and we refer to [72, 70] for methods to set this price. In the second term, the weight matrix T_3 is positive semi-definite and can be used to penalize large voltage deviations from v_{nom}.

Remark 7. *The solution from* stage-1 *is used to define the terminal set $\mathbb{X}_{N+k}$ in the next Section. Thus, the horizon time N is chosen such that $N < N_r$.*

4.3.3 Terminal Set

In this section, we detail the terminal set (4.20e). This constraint ensures that the system has enough flexibility to charge shapeable and deferrable loads before their plug-out time k^{out}, and keep voltage between the regular bounds after the control horizon N. The terminal set is defined such that the battery banks have enough energy to meet the real power demand of additional (shapeable and deferrable) loads at the end of horizon. Moreover, the capacitors supply the reactive power to satisfy the network constraints under base load. Feasibility of the *stage-1* problem thus ensures that all network constraints are satisfied even with the additional loads.

The terminal constraint for the shapeable loads' energy $x_1 = (e_1^{shp}, \ldots, e_{M^{shp}}^{shp})^T$ should guarantee that each load can be fully charged before their plug-out time. This is given by Eq. (4.5), which ensures the recursive feasibility of the constraint $e_{min}(k) \leq x(k) \leq e_{max}$, where $e_{min}(k^{out}) = e_{des}^{shp}$.

The terminal constraint for the battery banks' energy $x_2 = (e_1^{bat} \ldots, e_n^{bat})^T$ guarantees that batteries have enough capacity at time N to track the reference signal from *stage-1* and supply the additional deferrable and shapeable loads. We denote $(\hat{q}_i,\ \hat{e}_i^{bat})$ the optimal solution to the *stage-1* problem in (4.19), and k_{max}^{out} the maximum plug-out time of all the deferrable and shapeable loads that are currently connected to the grid.

Definition 1. *The terminal set $\mathbb{X}_{N+k}$ at time $N+k$ is defined as follows:*

$$\mathbb{X}_{N+k} := \begin{cases} \left[x_1(N+k), x_2(N+k)\right]^T = \left[e^{shp}(N+k), e^{bat}(N+k)\right]^T \\ \quad \textit{such that } \ \forall i \in \{1,...,n\} \ \ \forall j \in \{1,...,M^{shp}\} \\ \\ e_j^{shp}(N+k) \geq e_{des,j}^{shp} \text{ - } max(0, (k_j^{out} \text{ - } (N+k))\eta \Delta T c_{max,j}^{shp}) \\ e_j^{shp}(N+k) \geq e_{low,j}^{shp} \\ \\ e_j^{shp}(N+k) \leq e_{des,j}^{shp} \\ e_j^{bat}(N+k) = \hat{e}_i^{bat}(N+k) + \sum_{l=N+k}^{k_{max}^{out}} \Delta T p_i^{def}(l) + \tilde{p}_i^{shp}(l) \end{cases}$$

$$\tilde{p}^{shp}(l) = K^{shp} \tilde{c}^{shp}(l) \tag{4.21}$$

$$\tilde{c}_j^{shp}(l) = \frac{e_{des,j}^{shp} - e_j^{shp}(N+k)}{(k_j^{out} - (N+k))\eta \Delta T} 1_{l<k_j^{out}} \tag{4.22}$$

Lemma 1. *If the following conditions hold:* $\forall l \in [N+k, k_{max}^{out}]$, $\forall i \in 1,...,n$:

$$\hat{p}_i^{bat}(l) - p_i^{def}(l) - \tilde{p}_i^{shp}(l) \geq p_{imin}^{bat} \tag{4.23}$$

$$\hat{e}_i^{bat}(l) + \sum_{m=l}^{k_{max}^{out}} \Delta T\, p_i^{def}(m) + (e_{des,i}^{shp} - e_i^{shp}(N+k)) \frac{(k_i^{out} - l)}{\eta(k_i^{out} - (N+k))} \leq e_{max,i}^{bat} \tag{4.24}$$

then problem (4.20) with terminal set $\mathbb{X}_{N+k}$ *as defined in Definition 1, is recursively feasible, i.e. if the MPC optimization problem is feasible for* $x(k)$*, then it is also feasible for* $x(k+1)$ *defined in Eq. (4.13).*

Proof. We provide an outline of the proof, which can be found in the Appendix C. A feasible control sequence for *stage-2* at time $k+N$, $(p^{shp}(k+N), p^{bat}(k+N), q(k+N))$ is defined based on the solution of *stage-1* at time $k+N$, $(\hat{p}^{shp}(k+N), \hat{p}^{bat}k+(N), \hat{q}(k+N))$:

$$c_j^{shp}(N+k) = \frac{e_{des,j}^{shp} - e_j^{shp}(N+k)}{(k_j^{out} - (N+k))\eta\Delta T} 1_{N+k<k_j^{out}} \tag{4.25}$$

$$q_i(N+k) = \hat{q}_i(N+k) \tag{4.26}$$

$$p_i^{bat}(N+k) = [\hat{p}_i^{bat} - p_i^{def} - p_i^{shp}](N+k) \tag{4.27}$$

In practice, Eq (4.21) and (4.22) define a feasible control sequence after time $k+N$ where the shapeable power $\tilde{c}_j^{shp}$ at load j is constant until the plug-out time k_j^{out}. Then, Problem (4.20) is recursively feasible assuming that Equations (4.23), (4.24) are true. □

Remark 8. *Lemma 1 shows that under conditions (4.23), (4.24) the MPC problem is feasible at all times, if it is feasible for an initial state* x_0*. The next section shows that the P&P operation ensures that conditions (4.23), (4.24) are always satisfied, proving constraint satisfaction at all times.*

4.4 Plug-And-Play PEV Charging

In real distribution systems, users can connect or disconnect their appliances randomly. This changes the overall load on the system and can affect bus voltages significantly. This section extends the MPC scheme to the case where the system dynamics in (4.13) change due to loads joining or leaving the network by employing the concept of P&P MPC in [138]. The introduction of P&P capabilities poses two key challenges ([138], [108]): (i) P&P operations may produce infeasible operating conditions; (ii) the control law has to be redesigned for the modified dynamics. In the considered case, the problem is reduced to the first issue since the controller is computed centrally by the *stage-2* MPC (Section 4.3). In this section, the first challenge is addressed by means of a preparation phase ensuring recursive feasibility and stability during P&P operation. We first address the case of shapeable, then deferrable loads.

4.4.1 Shapeable loads

As shown in Eq. (4.2c), shapeable loads can be plugged-in without drawing energy from the grid: $0 \leq c^{shp} \leq c^{shp}_{max}$. Therefore it is always optimal for a shapeable load to plug-in as soon as it requests it: it can plug-in with $c^{shp} = 0$ and wait for the system to allow strictly positive values $c^{shp} > 0$. Thus, the output of the P&P stage is to accept shapeable requests immediately. Additionally, we assume that it is feasible to meet the user's requirements, i.e. fully charge the load before the maximum required time k^{out}, and satisfy equations (4.23), (4.24). In practice, if a user makes an infeasible request, he would be asked to lower his/her requirements by allowing a later k^{out} or a lower desired energy e^{shp}_{des}.

4.4.2 Deferrable loads

The goal of the P&P operation is to find a time to safely connect deferrable loads, and modify the response of shapeable loads and control devices to allow this connection as soon as possible. In this section, a Mixed Integer Program (MIP) is defined to find the minimum time to safely plug-in a deferrable load. After finding this time, the list of connected deferrable loads is updated, and *stage-2* is executed with the new system.

Deferrable loads do not impact the dynamics of the system, and only change the feasible set. An additional deferrable load at node j modifies the set $\mathscr{Z}_k$ via the equality:

$$P_{ij} = p^l_j + p^{bat}_j + p^{def}_j + p^{shp}_j + r_{ij}L_{ij} + \sum_{k:(j,k)\in\mathscr{L}} P_{jk}$$

Moreover, it modifies the terminal set $\mathbb{X}_{N+k}$. In the following, $\overline{\mathscr{Z}}_k$ (respectively $\overline{\mathbb{X}}_{N+k}$) denote the feasible set (respectively terminal set) constraints that remain unchanged when a deferrable load plugs in. Let's consider a P&P request from a deferrable load at time k. The request can be postponed by $d_{max} < N$ maximum time steps. This creates d_{max} possible load shapes. For each possible time-delay $0 \leq d \leq d_{max}$ we note $p^{new,d}_j$ the corresponding shifted vector:

$$p^{new,d}_j = [\underbrace{0,...,0}_{\text{size d}}, p^{new,0}_j] \tag{4.28}$$

Thus the following constraints are defined when a deferrable load requests to plug-in at node j and is delayed by d time steps:

$$P_{ij}(l) = [p^l_j + p^{bat}_j + p^{def}_j + p^{shp}_j](l) + r_{ij}L_{ij}(l) + \sum_{m:(j,m)\in\mathscr{L}} P_{jm}(l) + \sum_{d=0}^{d_{max}} z_d p^{new,d}_j(l) \tag{4.29}$$

$$e^{bat}(N+k) = \hat{e}^{bat}(N+k) + \frac{1}{\eta}K^{shp}\left(e^{shp}_{des} - e^{shp}(N+k)\right) + \sum_{r=N+k}^{k^{out}_{max}} \Delta T[p^{def} + \sum_{m=0}^{d_{max}} z_m p^{new,m}](r) \tag{4.30}$$

The solution (x^*, u^*, z^*) of the Mixed Integer Program (MIP) (4.31) gives the optimal transition time $d^* = \sum_{m=0}^{d_{max}} m z_m^*$.

$$\min_{x,u,z} \quad V_3(u,z) = \sum_{m=0}^{d_{max}} m z_m \tag{4.31a}$$

s.t *System Dynamics:*

$$x(l+1) = Ax(l) + Bu(l), \quad x_0 = x(0) \tag{4.31b}$$

$$(x(l), u(l), P_{ij}(l), Q_{ij}(l), V_i(l), L_{ij}(l)) \in \overline{\mathscr{Z}_l}$$

$$x(N+k) \in \overline{\mathbb{X}}_{N+k} \tag{4.31c}$$

Connection:

$$z_m \in \{0,1\}\ \forall m \in \{0,1,...,d_{max}\}, \quad \sum_{m=0}^{d_{max}} z_m = 1 \tag{4.31d}$$

$$(4.29), (4.30) \tag{4.31e}$$

Power flow: (4.29) (4.31f)

Battery banks: (4.30) (4.31g)

$$p_{j_{min}}^{bat} \leq \hat{p}_j^{bat}(s) - [p_j^{def} + \sum_{m=0}^{d_{max}} z_m p_j^{new,m}](s) \frac{e_{des,j}^{shp} - e_j^{shp}(N+k)}{(k_j^{out} - (N+k))\eta} \tag{4.31h}$$

$$e_{max,j}^{bat} \geq \sum_{r=s}^{k_{max}^{out}} \Delta T [p_j{}^{def} + \sum_{m=0}^{d_{max}} z_m p_j^{new,m}](r) + \frac{(e_{des,j}^{shp} - e_j^{shp}(N+k))(k_j^{out} - s)}{\eta(k_j^{out} - (N+k))} + \hat{e}_j^{bat}(s) \tag{4.31i}$$

$$s \in [N+k, k_j^{out}], \quad l = k, \ldots, k+N-1$$

Objective (4.31a) minimizes the transition delay and ensures that the problem remains feasible when the load plugs in.

Remark 9. *Constraints (4.31h), (4.31i) correspond to the conditions in Lemma 1 Eq. (4.23), (4.24) respectively.*

We execute the request by (i) updating the system with the new load that plugs in at time d^*, and (ii) going back to *stage-2*. If $d^* > 0$, then the control devices and shapeable loads update their signal during the transition phase $[N+k, N+k+d^*]$. The full controller is shown in Fig. 5.1.

Theorem 5. *The model predictive controller (4.20) with network reconfigurations and transition times given by the MIP (4.31) is recursively feasible. For all initially feasible state x_0 and for all optimal sequences of control inputs, the MPC problem (4.20) with P&P network modifications (Fig. 5.1) remains feasible for all time.*

Proof. Assume the problem is feasible at time k and a request occurs at time k. The P&P MIP (4.31) ensures that all constraints are satisfied during the transition time and that the conditions in

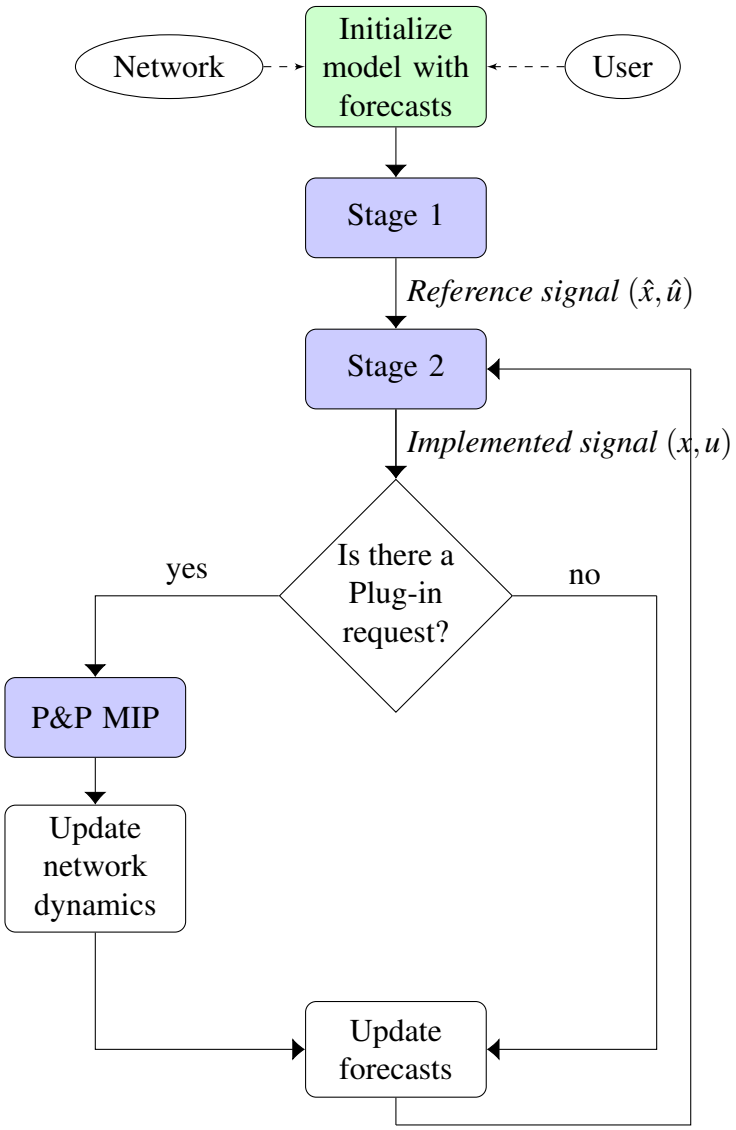

Figure 4.2: Full controller flow: the solution at *stage-1* is used to define the terminal set at *stage-2*. When a new deferrable load requests to plug-in, the MIP determines the optimal plug-in time, the system is updated with the new load and the controller executes *stage-2* on the new system.

Lemma 1 are satisfied for the modified network. Hence the overall procedure maintains feasibility during transition, and recursive feasibility is ensured after the modification. □

4.5 Numerical results

This section shows simulation results on a 55 bus Southern California Edison distribution network (see Fig. 4.3). This network was previously studied in [42]. Seven additional storage devices are modeled at nodes 2, 8, 10, 14, 21, 30, 41. We assume that the price of electricity is given and reflects the requirements of the system operator. In this case study, we choose the time step $\Delta t = 0.5$h, the *stage-2* MPC time horizon $\frac{N}{\Delta T}$ =5h and the *stage-1* time horizon $\frac{N_r}{\Delta T}$ =48h. The controller response is illustrated for a period of 30h in order to show daytime and night-time load schedules. These parameters are chosen for illustration purposes, and may be set differently to meet practical grid requirements. It is important to note that the choice of ΔT contains a tradeoff between reactivity and planning horizon. In particular, the controller response may be up to 30 minutes (ΔT) later than the request time of a load, and in practice, aggregators may require a smaller interval ΔT to reduce the response time and satisfy grid and users' requirements, however generally at the cost of not being able to plan optimally over a long time period of a day or more.

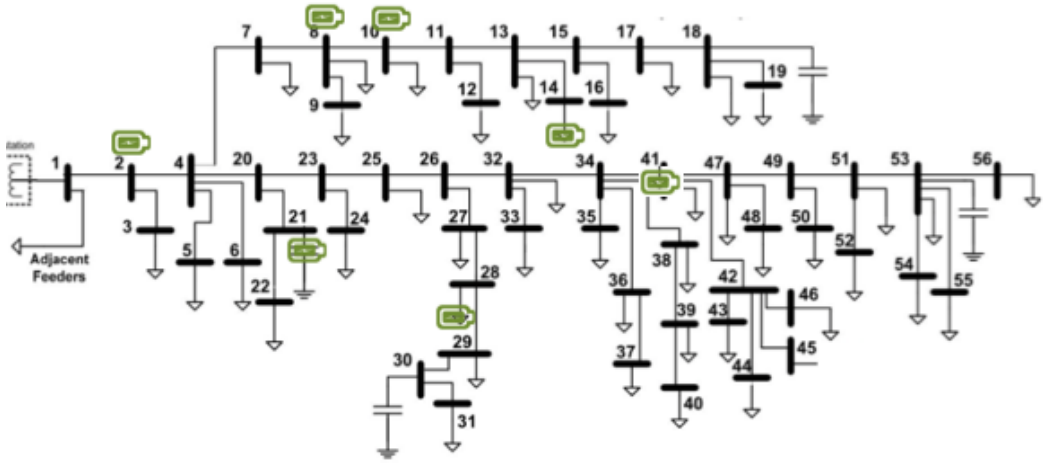

Figure 4.3: 55 bus feeder. Additional battery banks are indicated in green (capacitors are not represented here).

4.5.1 Load scheduling

As mentioned in Section 4.4.1, shapeable loads plug-in as soon as they requests it, can be zero-power during a certain time and fully charge before their desired plug-out time k^{out}. Figure 4.4 shows the power and SOC at three shapeable loads. The vertical green lines show the connected period: the first green line is the request time, the second green line is k^{out}. Figure 4.4a shows that loads draw power only when they are plugged-in and Fig. 4.4b shows that they reach their desired SOC before k^{out}. In these three examples, the loads tend to charge when the price of electricity is cheaper. In particular, the load at bus 4 avoids the evening peak time (5pm to 9pm), and charges

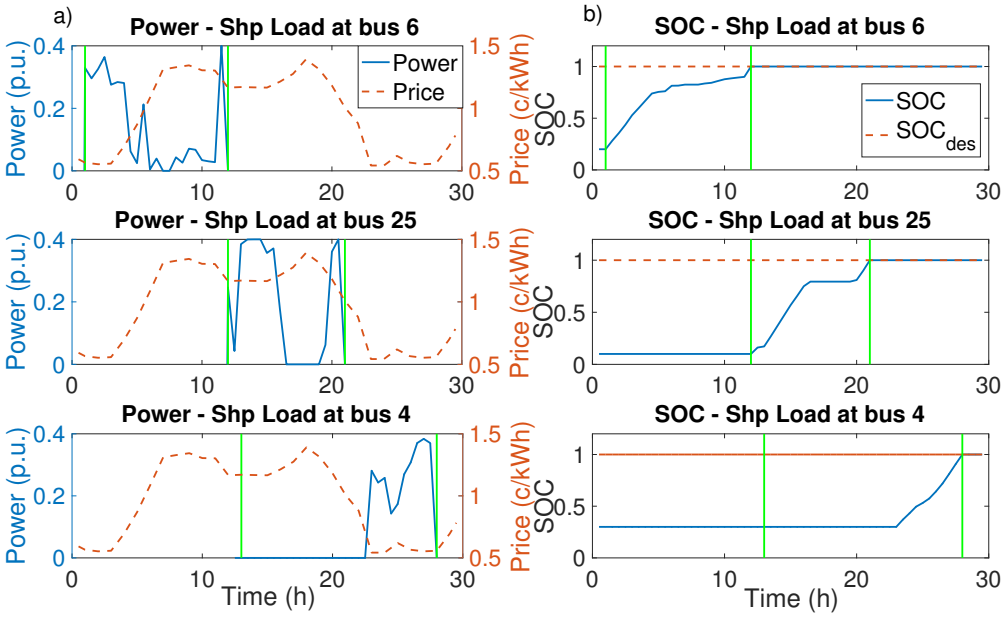

Figure 4.4: Power and SOC of three different Shapeable Loads in the network. Green vertical lines show when the load requests to plug in and plug out.

Table 4.3: Description of Defferable Loads in the System

Request Time (h)	Requests	Bus number	Plug-in Time
4	1	8	4
6	1	33	6
10	5	4, 5, 5, 16, 17	10, 10, 10, 10, 10
11	1	28	11.5
12	2	19, 38	14.5, 12
17	3	8, 20, 22	17, 17, 17
18	1	12	18
18.5	2	5, 22	18.5, 18.5
19.5	1	12	19.5

during the night time (10pm to 6am). Shapeable loads have the flexibility to adapt their power signal to the conditions and constraints of the network. In particular, they can adapt their response when a deferrable load requests to plug-in, allowing the new load to connect without violating the network constraints. Table 4.3 details all the plug-in requests and shows that only two deferrable loads need to be deferred in this case: one load at time 11h and bus 28 and one load at time 12h and bus 19. Figure 4.5 shows the overall state of the system when the deferrable load is delayed at 11h. It shows the total implemented and planned loads (shapeable in the top plot and deferrable

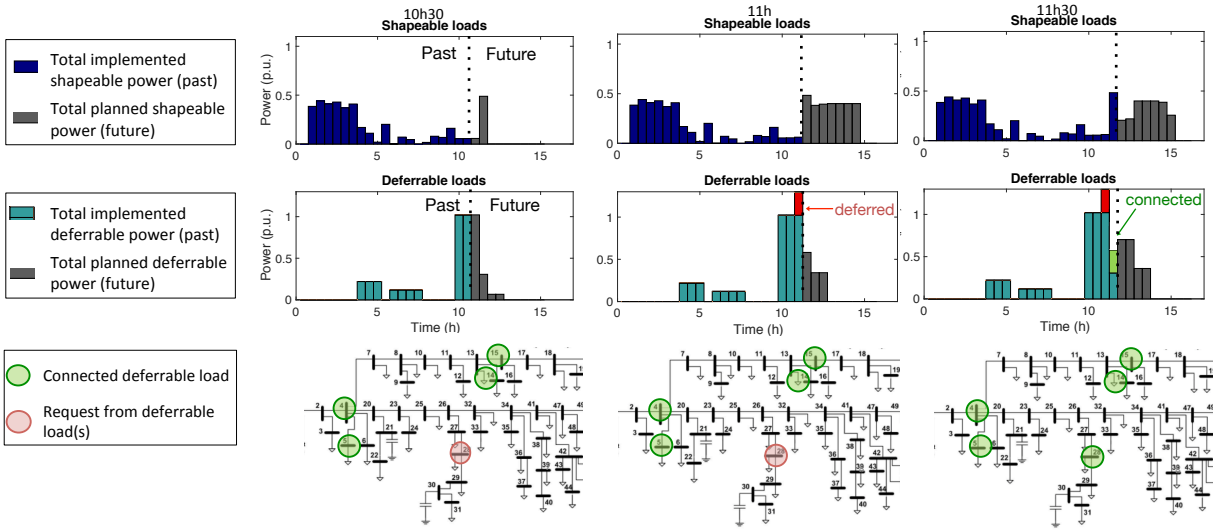

Figure 4.5: Evolution of loads: one deferrable load requests to plug-in at 11h and is delayed to connect at 11h30. During the transition phase (11h-11h30), shapeable loads adapt their signal to enable safe connection of the deferrable load.

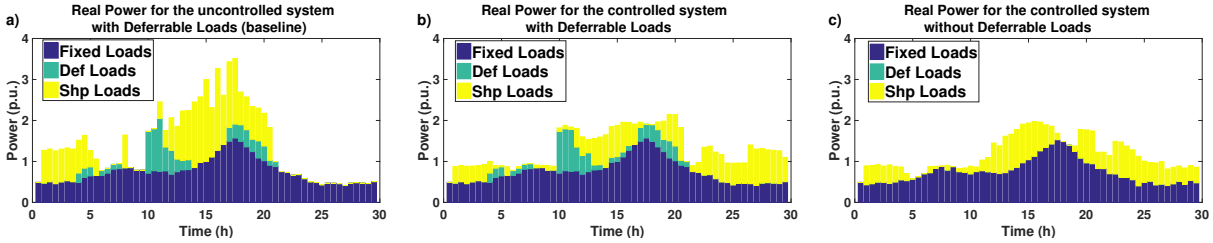

Figure 4.6: Cumulative real power in the network for a) the uncontrolled system with deferrable loads, b) the controlled system with deferrable loads, c) the controlled system without deferrable loads

in the middle plot) before and after the delayed request. During the transition phase (11h-11h30), shapeable loads adapt their signal, i.e. reduce their demand, to enable safe connection of the deferrable load at 11h30.

4.5.2 Peak reduction impact

In this section the peak reduction impact of the controller is illustrated. Figure 4.6 shows the aggregate load in the network in three cases: a) in the uncontrolled case, b) when the controller is applied to the network with deferrable and shapeable loads and c) when the controller is applied to the network without deferrable loads. In the uncontrolled case, every load plugs in as soon as it requests it. The total peak in the uncontrolled case (Fig. 4.6a) is 3.5 p.u. whereas it is 2 p.u in the controlled case (Fig 4.6b), providing 40% reduction. In the uncontrolled case, a lot of additional

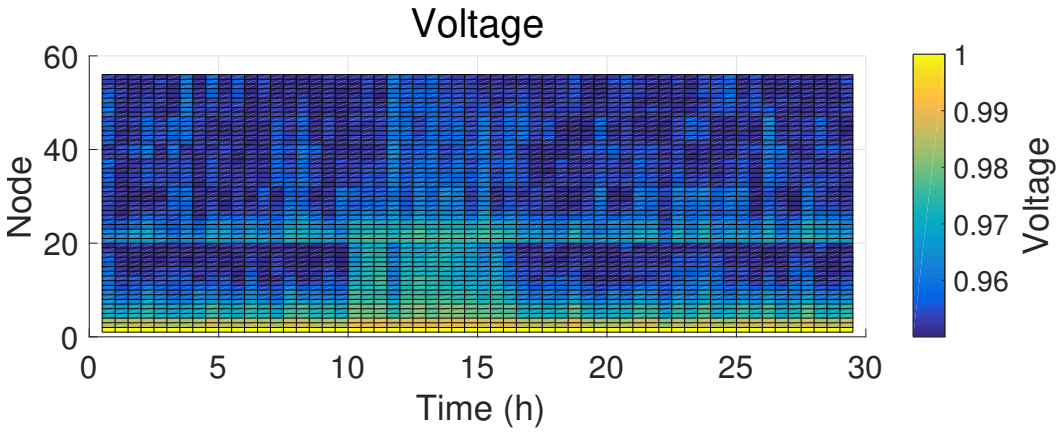

Figure 4.7: Voltage at each mode of the network

loads plug-in during the peak time (3pm to 9pm) and immediately charge. On the contrary, in the controlled case, shapeable loads are delayed to the night time, which results in a smoother load curve. The difference between Fig. 4.6b and Fig. 4.6c illustrates how shapeable loads' schedules change when deferrable loads are connected to the network. Fig 4.6b shows that shapeable loads adapt their load profile to enable connection of deferrable loads: in Fig 4.6b shapeable power tends to be delayed to the night time, in order to allow connection of deferrable loads in the evening (6pm to 9pm).

4.5.3 Network constraints

Network constraints include voltage and battery banks constraints. Figure 4.7 illustrate the voltage at each bus and time step and shows that voltage remains between the bounds 0.95 and 1. Figure 4.8 shows the power and SOC at the seven battery banks and Fig. 4.9 shows the aggregated real power over time. Figure 4.8a shows that batteries tend to highly discharge, i.e. have high negative power, around 10h, 15h and 20h. Figure 4.9 shows that these are times when the network is highly loaded, i.e. a lot of shapeable loads and deferrable loads are connected and fixed loads are high. Storage devices are used to supply additional power in case of load peaks. Note that we impose the minimum SOC, $e^{bat}_{low} = 0.12$ however the SOC never goes below 0.3. This limit is due to the terminal constraints (4.19b): the initial SOC has to be recoverable at the final time $N_h = 48h$. Fig 4.10 and Fig 4.11 show the output of *stage-1*, for capacitors and batteries respectively. We use a different color scale to highlight that the variation is very different from the *stage-2* response. Indeed, the objective in *stage-1* penalizes large control inputs whereas the objective in *stage-2* penalizes large peak consumptions, as a result the input in *stage-1* is lower than in *stage-2*. Fig 4.11 a) and b) show that the SOC at battery banks remains between 0.42 and 0.57. Batteries supply energy around 15h (peak consumption) and consume energy during the night to be able to recover the initial SOC. This *stage-1* response is used as a reference signal in *stage-2*.

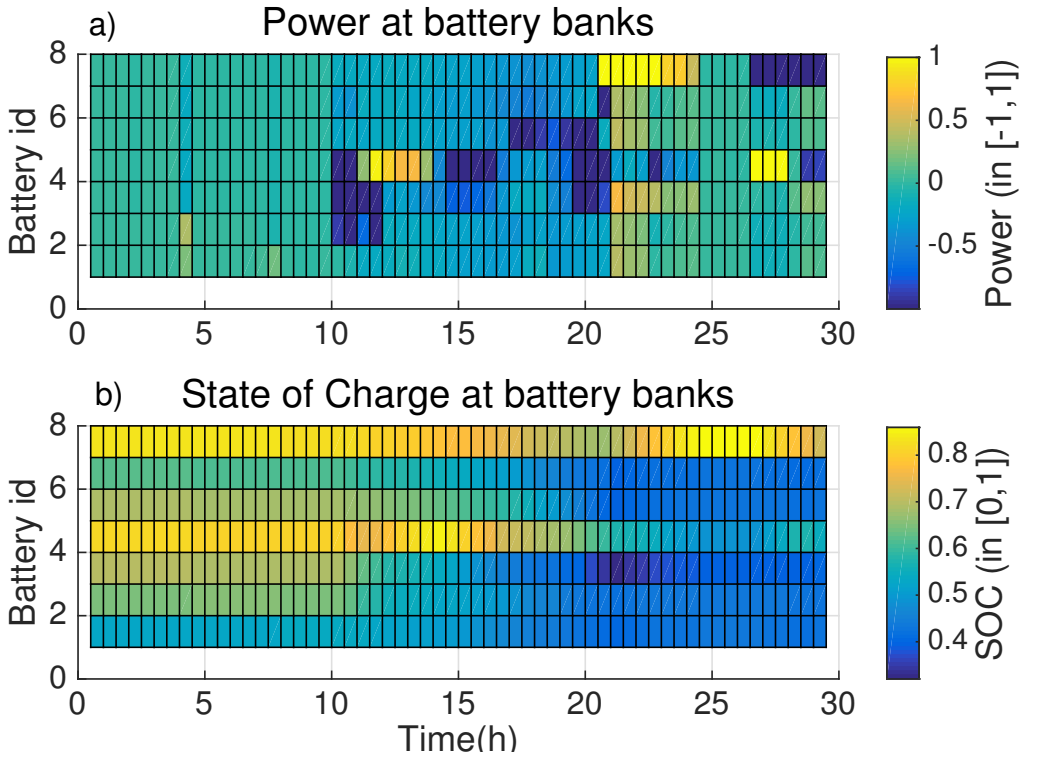

Figure 4.8: a) Real power and b) SOC at battery banks. Values are normalized

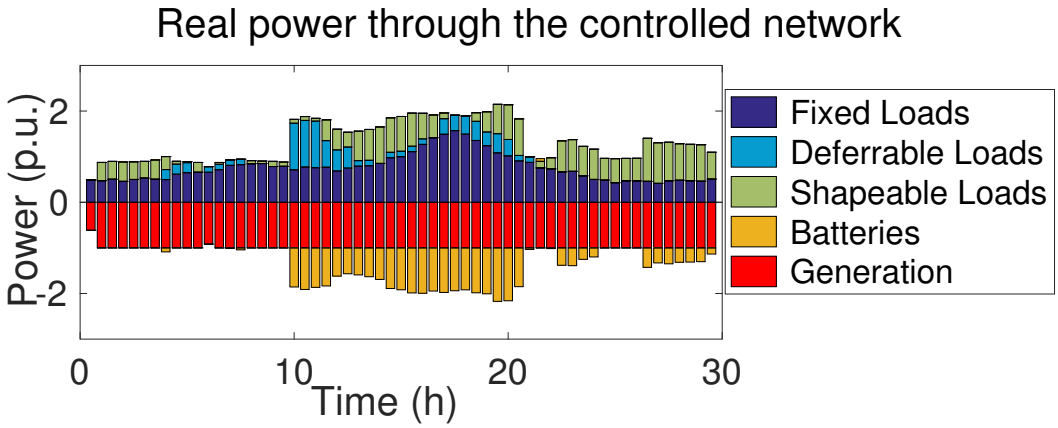

Figure 4.9: Real power across the different devices of the networks

4.6 Summary

In this Chapter, a predictive controller capable of handling P&P requests of flexible and deferrable loads, is proposed. First, an MPC approach for minimizing the global cost of the system is used to aggregate flexible loads and provide load shaping objectives under distribution grid constraints.

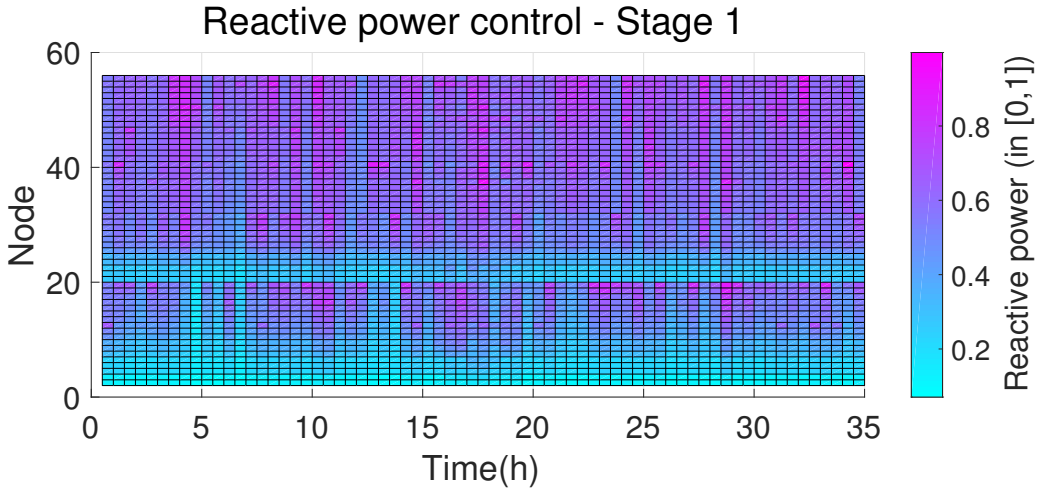

Figure 4.10: Capacitor reactive power computed at Stage 1

Second, a MIP is defined to safely connect loads and minimize waiting times. The article proved that the algorithm achieves recursive feasibility, by appropriately defining the connection conditions and the terminal constraint set. The performance of the proposed method was demonstrated for the control of a radial distribution system with 55 buses.

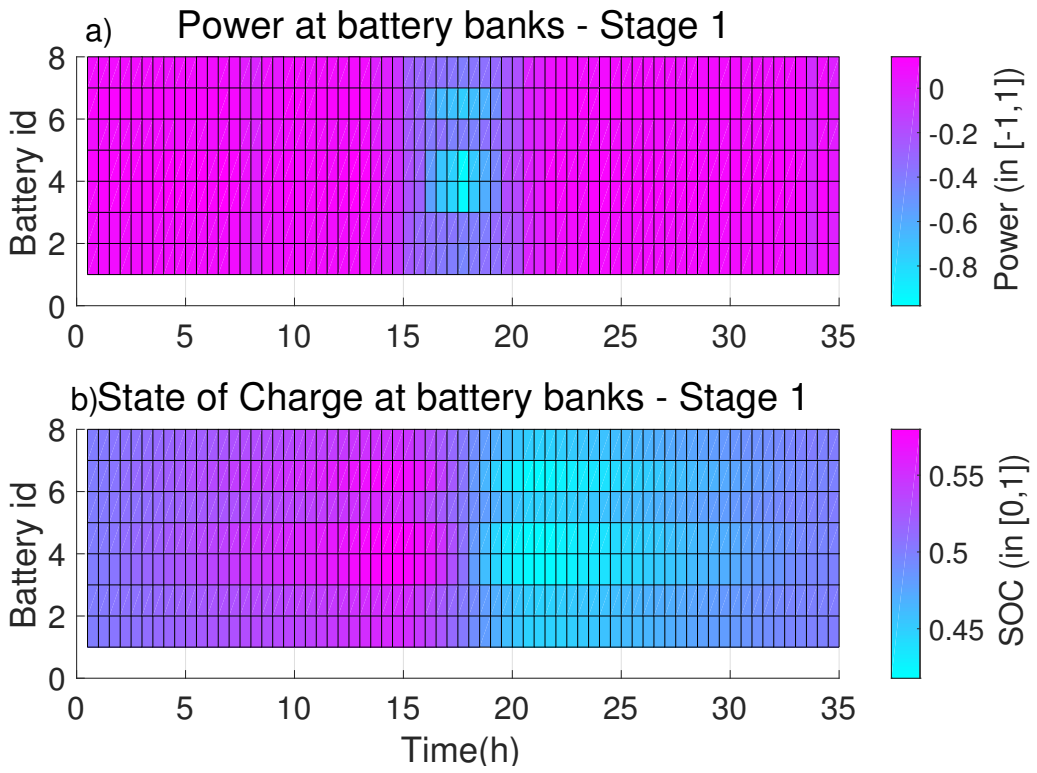

Figure 4.11: a) Real power and b) SOC at battery banks computed at Stage 1 (values are normalized)

Chapter 5

Behavioral study of Demand response Programs

5.1 Motivation: the irrational driver

Previous chapters have proposed optimization methods to solve the PEV optimal charging problem in various scenarios. If the three proposed methods highly vary with their use case and mathematical techniques, they share one common aspect: driver behaviors are assumed "perfect". The common underlying assumption is that drivers minimize their charging costs and require enough battery capacity to meet their mobility constraints at all time. However, current PEV charging behaviors tend to go against this assumption, as many PEV drivers decide to charge as soon as they plug-in, without seeking to minimize their cost. In particular, the choice of when to charge seems to be driven by two important factors: cost and range anxiety. Smart-charging implies that drivers choose to give up their charging flexibility in exchange of lower charging costs, but this is not unanimous. For example, risk averse drivers choose to maximize battery SOC at all time and charge as soon as they plug-in, in order to ensure enough capacity in case of unexpected trips. On the other hand, cost-sensitive drivers choose to charge when the price is lower, with the risk of lacking battery capacity if they need to take an unexpected trip.

With the observation that charging behaviors vary across drivers, it becomes fundamental to understand and characterize how people choose their PEV charging schedule. In particular, what is the tradeoff between range anxiety and charging costs? In this chapter, we seek to provide answers to this question by studying price sensitivity in the context of energy consumption. Understanding electricity price sensitivity will help practitioners design effective PEV charging programs that incentivize drivers to minimize their costs and benefit the electricity grid. A small number of PEV smart charging programs currently exist, and very little data is available today. As a result, we study electricity price sensitivity in the broader context of Demand Response (DR). We analyze the Smart Grid Smart City Trial data in Australia, which proposes more than four electricity tariffs and measures how households respond to price through smart meter readings.

5.2 Data analytics for Demand Response programs

The development of smart meters has led to the modernization of distribution networks by enabling real-time bidirectional communication between utilities and households [135]. In this context of smart grids, demand side management allows system operators to shape the energy consumption at the household level, offering new opportunities to improve the reliability, efficiency and sustainability of the grid [97, 50]. Demand response programs are designed to change energy consumption behavior with two objectives: (i) reduce energy consumption and (ii) shift peak consumption from peak times to off-peak times. In that regard, it is essential to understand how to effectively incentivize households in to modify energy habits.

Over the past 20 years, more than twenty Demand Response (DR) trials have been conducted worldwide. These trials have looked at two main types of programs to institute energy behavior change: (i) information and feedback technologies like In Home Displays (IHD) or mobile applications [45, 116], and (ii) economics incentives through time-of-use tariffs and dynamic pricing [3, 44, 60, 59]. Although it is widely accepted that information and feedback technologies result in energy-saving outcomes [45], the effectiveness of price-based demand response programs is still under debate, and past trials have resulted in mixed conclusions [96]. Faruqui et al review 15 price-based experiments and find that time-of-use rates induce a drop in peak demand that ranges between 3 to 6 percent whereas critical-peak pricing tariffs induce a drop in peak demand that ranges between 13 to 20 percent [44]. Similarly, Alberini et al [3] finds beneficial impacts in price-based demand response, and shows that price elasticity of electricity demand ranges between -0.860 and -0.667 over the ten-year period 1997-2007 in the United States. Conversely, Jessoe et al [60] study a time-of-use experiment through a regression discontinuity framework, and shows that the impact is opposite from what was expected: households tend to reduce energy consumption when the price goes down.

These mixed findings make it difficult to draft recommendations for designing a successful and effective demand response program, and have created confusion amongst policymakers, utilities, and system operators. In this chapter we seek to improve the understanding of demand response behavior by segmenting households based on their energy consumption profile. In particular, previous work has showed that households have very diverse reactions to demand response, and this high diversity results in few actionable insights for policymakers and utilities. We intend to define 'Demand Response Profiles' that group households which have similar reactions to Demand Response events. Based on these profiles, a successful demand response program would be composed of a portfolio of offers that target different behaviors. For example, price sensitive households should be offered time-of-use and peak pricing tariffs, whereas environment-conscious households may better respond to information and feedback.

A growing body of literature addresses the question of customer profiles in the context of electricity consumption. Specifically, with the transition towards Advanced Metering Infrastructure (AMI, also called 'smart meters'), utilities now measure household electricity consumption at the hour or 15-minute interval. This creates very rich datasets that bring new opportunities to study and understand energy consumption patterns. As a result, past research has proposed different methods for analyzing smart meter data, including Kmeans clustering [46, 68, 67, 104], follow-

the-leader algorithms and self-organizing maps [27], Hidden Markov Models [5] and Hierarchical clustering and Ward's method [53]. More recently, several articles have focused on combining smart meter data with external data sources to understand more general behavior patterns. For example, Gouveia and Seixas [53] perform a door-to-door survey, and study the correlation between demographics and energy clusters. Similarly, Kwac et al in [68] seek to determine lifestyle patterns based on smart meter and demographics data, but do not associate lifestyle patterns with DR program effectiveness. Albert and Maasoumey [4] address DR program effectiveness by defining predictive customer segments that share similar demographics attributes, and have a higher probability of enrolling into DR programs than the population as a whole. However, the latter article does not study how these customer segments respond to DR programs after their enrollment decision.

Previous work has considered energy segmentation for DR enrollment, but to the best of our knowledge, prior literature does not propose methods to predict both likelihood of a consumer enrolling in a DR program, and the resulting response to DR events. We add to previous literature by studying more comprehensive DR patterns that describe how households behave when presented with DR opportunities. For the first time, we study DR customer segments based on both enrollment choices and energy consumption, i.e. energy saving and peak shifting behaviors (see Fig 5.1). We use smart meter data to identify seven representative energy profiles, and combine these energy consumption characteristics with survey-based attributes such as income, climate and dwelling type. We add to the literature by showing how these household characteristics influence both enrollment and energy consumption during DR events, providing complete DR pattern specifications. We develop new discrete choice models that show how household attributes influence DR choices, and regression models that show how household attributes influence response to DR events. The chart in Fig 5.1 depicts the proposed method.

The chapter is organized as follows: Section 5.3 presents the Australia Smart-Grid Smart-City (SGSC) trial data, while Section 5.4 introduces the method to cluster households into energy use profiles based on smart meter data. Section 5.5 shows a logit binary regression model that takes into account energy profile, demographics and DR program attributes to predict DR enrollment choices. Section 5.6 measures the impact of Dynamic Peak Pricing (DPP) events and hourly electricity prices on energy consumption, and shows how it differs with household profiles. Section 5.7 concludes and summarizes our findings.

5.3 Background on the Smart Grid Smart City trial

The Smart Grid Smart City (SGSC) program was initiated in 2010 by the Australian government to explore the economic benefits of smart grid technologies. The SGSC trial dataset contains demographic information and smart meter data for more than 10,000 households over a 2-year period in 2012-2014. Several DR programs were offered to participants, including Dynamic Peak Pricing (DPP), Seasonal Time Of Use (STOU) and Dynamic Price Rebate (DPR). The complete SGSC trial program and resulting dataset is described in [89], and summarized by the Venn diagram in Fig 5.2. Figure 5.2 shows the number of households in the three main tables, namely the demo-

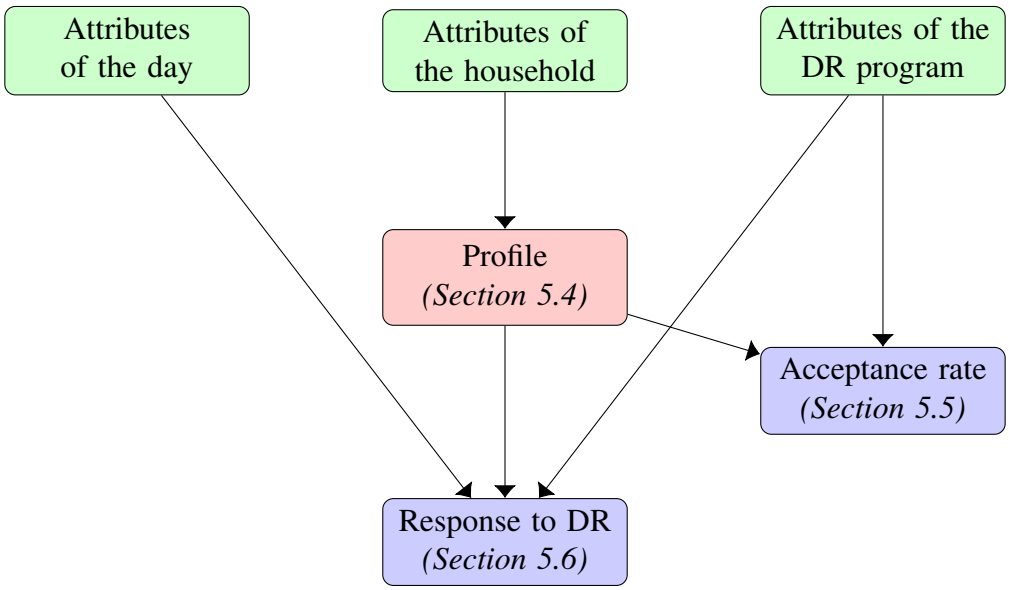

Figure 5.1: Depiction of model structure: green blocks shows the original data features, the red color shows the electricity consumption profiles obtained after clustering smart meter data, and the blue color shows the model outputs.

graphics statistics data in green, smart meter readings in red and DR offering data in blue. For the treatment group, the set of customers with complete information is described by demographics, smart meter and DR offering data, and composed of 5,110 households. For the control group, most participants are not offered any DR choices, and the set of customers with complete information is described by demographics and smart meter data, and composed of 3,292 households. In the remainder of this chapter, we jointly analyze these three tables to provide a comprehensive analysis of DR behaviors. In Section 5.4, we analyze meter data to define energy consumption profiles. In Section 5.5, we analyze demographics, meter and DR offering data to understand why customers decide to accept or decline a DR product. In Section 5.6, we analyze meter data for the treatment group and the control group, and evaluate the impact of DR programs on energy consumption.

5.4 Smart meter data clustering

The smart meter table records household energy consumption every 30 minutes. In order to evaluate the impact of energy consumption on DR acceptance and DR energy response, we need to transform this large and unstructured dataset into meaningul information. As a result, in this section we seek to define a discrete number of energy consumption patterns, that will be further used to segment bouseholds and better characterize DR behaviors.

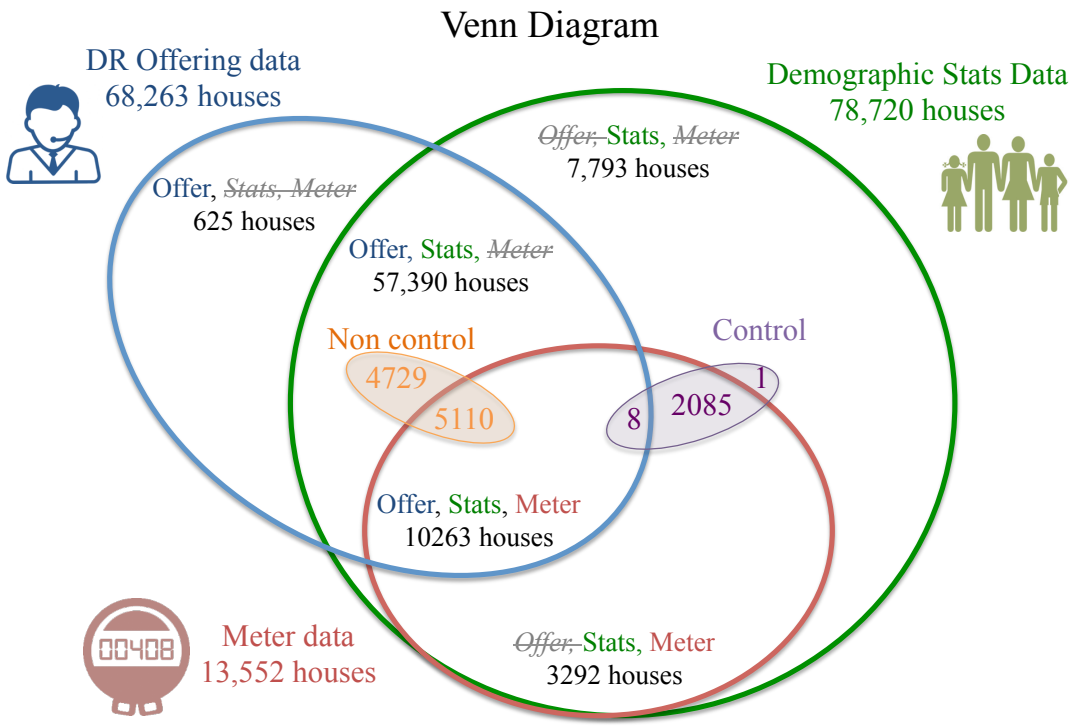

Figure 5.2: Venn diagram of the Smart grid Smart City trial dataset. The dataset contains three types of data: DR offering data, demographics data and meter data.

Table 5.1: Nomenclature - Clustering method

Symbol	Description
K	Total number of clusters
p	Data point: daily consumption curve as a 48-element consumption vector
C_i	Cluster i: set all of points p assigned to cluster i - $\{p$ s.t. $p \in C_i\}$
m_i	Center of cluster i
$P_n(C_i)$	Probability that household n has a daily energy consumption $p \in C_i$
S_n	Entropy of household n
T_n	Highest cluster frequency of household n

5.4.1 Clustering Method

The energy profiles should represent both the shape and the magnitude of the consumption. The shape gives information about how the consumer distributes his/her energy during the day (e.g. morning peak, evening peak) whereas the magnitude gives information about how much total energy the household consumes during the day. We use the notations described in Table 5.1 and measure the performance of the clustering result with 4 metrics:

- **Inertia**, or within-cluster sum of squares, is the sum of the Euclidean distances between each pattern and its cluster center. The K-means algorithm aims at minimizing this metric:

$$\sum_{i=1}^{K} \sum_{p \in C_i} ||p - m_i||^2 \tag{5.1}$$

- **Average Silhouette Index** measures the separation of clusters between each others (see [111] for complete definition). It ranges between -1 and 1, where the best value is 1 and the worst value is -1. Values near 0 indicate overlapping clusters. Negative values generally indicate that a sample has been assigned to the wrong cluster, as a different cluster is more similar.

- **Entropy** as defined by Kwac in [67]. The entropy of household n is calculated as:

$$S_n = -\sum_{i=1}^{K} \mathrm{P}_n(C_i) \log(\mathrm{P}_n(C_i)) \tag{5.2}$$

  The entropy is highest if all the clusters are equally likely (i.e. $\mathrm{P}_n(C_i) = \frac{1}{K}$ and $S_n = \log(K)$) and lowest if household always use the same cluster (i.e. $S_n = 0$).

- **The highest cluster frequency**, which represents how well the household is defined by its most likely cluster.

$$T_n = max(\mathrm{P}_n(C_i)) \in [\frac{1}{K}, 1] \tag{5.3}$$

  In practice, we will use the center of the most probable cluster as an approximation of the household's consumption shape. As a result, this should be a good proxy of the actual energy consumption, and we will favor higher values of T_n.

5.4.2 Clustering Results

In general, energy consumption is strongly dependent on season (i.e. summer vs winter) and the day of the week (i.e. week-day vs weekend). In this work, we research consumption patterns that are caused by household characteristics. To mitigate the effect of seasonal and weekday/weekend confounding variables, we choose to study only summer week-days. This subset is of greatest interest to utilities when considering programs to manage peak demand.

The selected dataset is composed of two years of summer weekdays in Australia, with 11,057 households and 1,110,076 datapoints in total. We use the K-means clustering method as implemented in the Scikit-learn package in Python [99]. The four metrics are shown in figure 5.3 for the total number of clusters $K \in [2, 21]$. The objective of the standard K-means algorithm is to minimize inertia, for a given number of clusters. Consequently, it is logical that inertia decreases monotonically with number of clusters, which is illustrated by the green line in figure 5.3. The black line shows the silhouette, which decreases monotonically between 2 and 6 clusters, and increases between 6 and 7 clusters. The blue line shows the entropy, which increases with the number

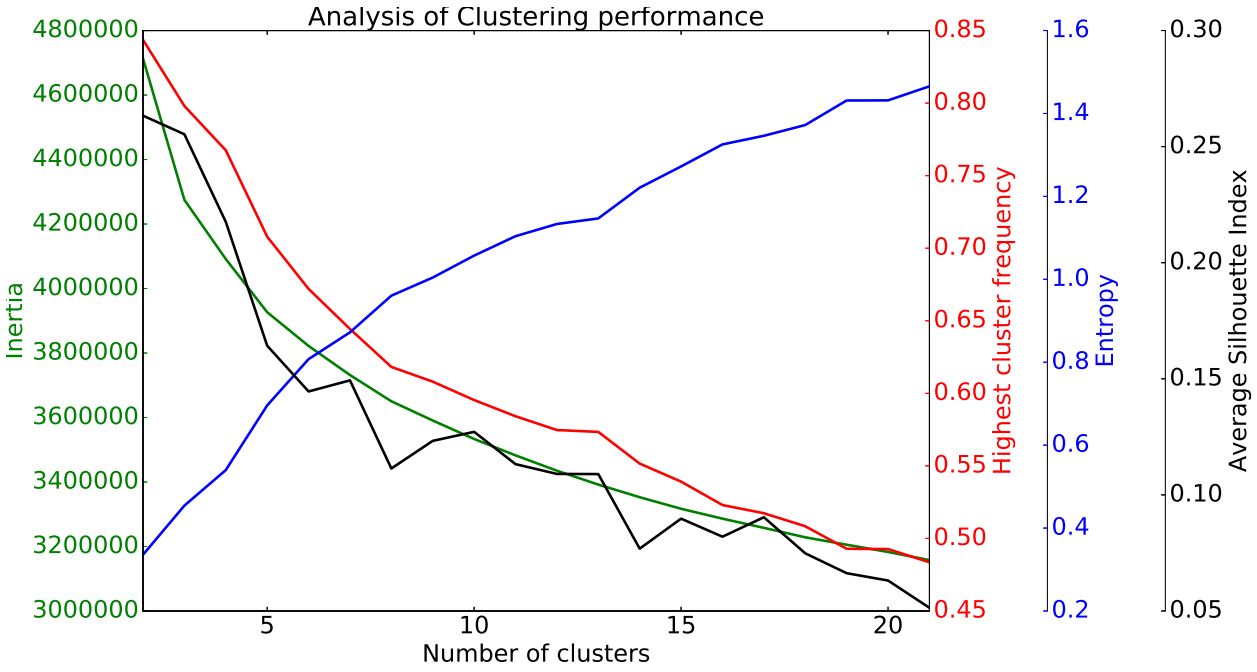

Figure 5.3: Analysis of K-means performance for the number of clusters ranging between 2 and 21

of clusters. The entropy is a measure of chaos, and quantifies energy consumption heterogeneity. Conversely, the red line shows the average proportion of time that household's most probable shape is the best cluster. This metric decreases with the number of clusters, but always remains higher than 0.5. Note that no single metric is uniformly best for selecting the appropriate number of clusters. These four metrics, however, provide different views on clustering performance. Consequently, analyzing all four metrics together provide a comprehensive decision support tool for selecting the appropriate number of clusters.

After considering the metrics shown in Figure 5.3, we choose to keep seven clusters. The clustering results with seven clusters gives a particularly good silhouette index, with the highest cluster frequency exceeding 60%. The resulting clusters are visualized in Fig 5.4. This shows consumption in kWh of the 7 typical energy consumption at each hour of the day. Figure 5.5 represents the number of points falling in each cluster, and shows that clusters C1 and C3 are particularly frequent. In comparison with other clusters, C1 seems to be a low-consumption profile and C3 a medium consumption profile. Figure 5.6 shows the normalized shapes of these two profiles, which is defined as the consumption divided by the total daily consumption, i.e. the area under the curve. As a result, Fig 5.6 shows how households distribute their energy consumption during the day, and shows that both profiles correspond to double peak consumption: the first peak at morning around 6am and a second peak during the evening (4pm- 9pm). By combining Fig 5.5 and Fig 5.6 we find that the most probable energy profiles are low double peak consumption and medium double peak consumption.

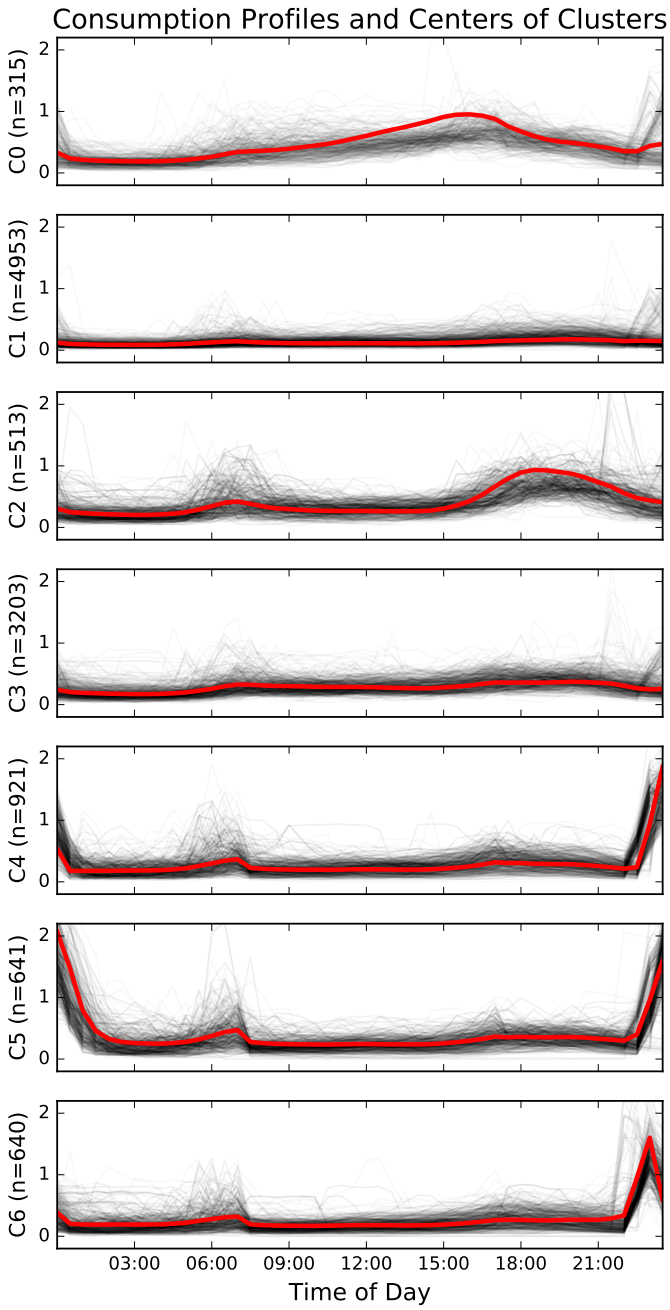

Figure 5.4: Seven energy clusters, showing both cluster centroids (red) and individual households' consumption as thin traces. The y axis shows the cluster identification number, and n denotes the number of data points belonging to that cluster.

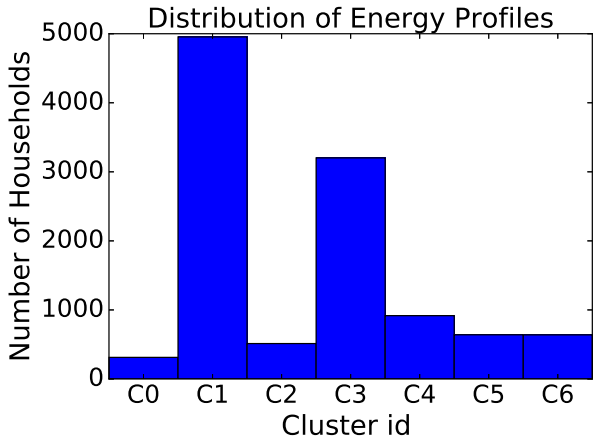

Figure 5.5: Number of households assigned to each cluster

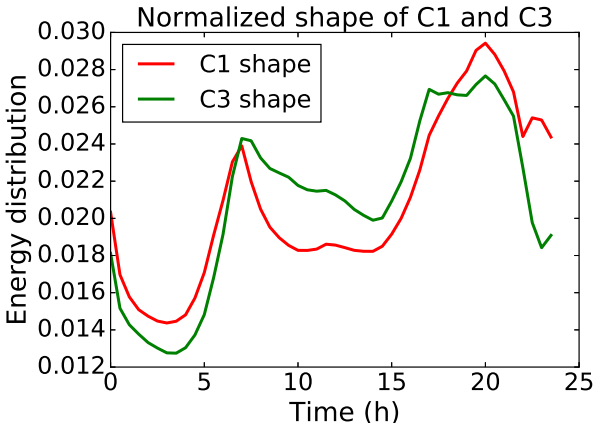

Figure 5.6: Normalized shape of the two most probable clusters (Cluster C1 and C3)

In the rest of this chapter, we will describe energy consumption profiles by using the clustering results in this Section, and defining key energy characteristics:

- *Cluster*: number between 0 and 6 describing the most probable cluster for each household. The distribution is shown in Fig 5.5.
- *Entropy*: measure of energy consumption heterogeneity as defined in Section 5.4.1. The distribution is shown in Fig 5.7.
- *Average daily consumption*: the distribution is shown in Fig 5.7.
- *The standard deviation of daily consumption*

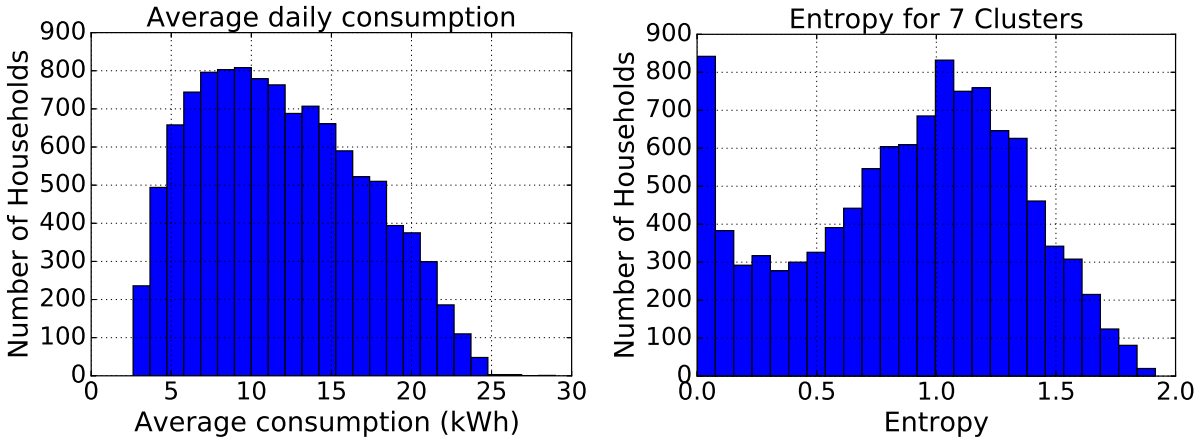

Figure 5.7: Average daily consumption and entropy distribution across the population

The clustering process has segmented daily load profiles into seven representative loads, and transformed large unstructured smart meter data into four simple and meaningful energy metrics. Next sections will show that these metrics characterize households' energy consumption, and impact how households choose and respond to DR programs.

5.5 Demand Response program enrollment

In this section, we seek to understand what attributes have an impact on DR enrollment, and use the the results of Section 5.4 to define energy profile attributes. As shown in Fig 5.1 we consider both household attributes (e.g.: demographics, energy profile...) and product attributes (e.g. dynamic pricing, time-of-use, feedback technology...). In particular, for utilities and energy providers it is important to understand which customers should be targeted with each product in order to improve marketing efficiency and reduce customer acquisition costs.

5.5.1 Data

Tables 5.2, 5.3 and 5.4 show the available variables for estimating DR choice models. Table 5.2 shows the list of initial categorical variables, with the possible values and frequency of each value. Table 5.3 shows the continuous variables defined from the clustering results in Section 5.4, i.e. average daily consumption, standard deviation of daily consumption, and entropy. We further define categorical variables for average consumption and entropy by defining three group levels: the lower third is defined as 'Low', the second third is defined as 'Medium' and the highest third is defined as 'High'. Table 5.4 shows these categorical variables which are derived from the clustering results in Section 5.4.

5.5.2 Model

In this work, we use the binary logit regression model, and refer to [13, 78] for a detailed exposition of this model and its properties. Binary choice models are a specific case of discrete choice models, which are generally defined by four elements:

- *Decision makers*: in our case decision makers are households who receive at least one DR offer. Decision makers can receive more than one offer, and therefore, make more than one choice. Decision makers are described by characteristics, which can influence their choice (see Table 5.5).
- *Alternatives*: the options available to the decision maker. In our case, decision makers have only two options - accept or refuse the DR offer. Therefore, this is a case of binary choices.
- *Attributes*: alternatives are described by a set of attributes (see Table 5.5). Decision makers make choices based on these attributes and their own characteristics.

Table 5.2: Categorical variables from initial dataset

Variable	**Value**	**Frequency**
Income	High	3201
	Med	4320
	Low	4263
Climate	Mild temperate	990
	Warm temperate	19794
Dwelling	Single-family	9999
	Multi-Unit	1785
Electricity usage	High	1586
	Med	4127
	Low	6071
Has Children	No	7886
	Yes	3898
Has Generation	No	11503
	Yes	281
Has solar	No	11549
	Yes	235
Has Poolpump	No	10429
	Yes	1355
Has HVAC	No	3467
	Yes	8317
Product	EA-DPP	2740
	EA-ILAC	392
	EA-STOU	1835
	EA-TOPUP	2793
	NetAir	11
	NetDPRPPE	962
	None	2951
Feedback	No	4671
	Yes	7113
Feedback 2	No	686
	Yes	11098

Table 5.3: Continuous variables, obtained after clustering results

	Average daily consumption	**Standard Deviation of daily consumption**	**Entropy**
Mean	13.02	3.80	0.929
Std	5.06	1.74	0.44
Min	2.67	0.20	0
Max	28.99	10.99	1.88

Table 5.4: Categorical variables obtained after clustering results

Variable	Value	Frequency
Measured Entropy	Low	2723
	Med	6195
	High	2866
Average daily consumption	Low	4750
	Med	5926
	High	1108
Energy Profile	0	471
	1	4018
	2	620
	3	3760
	4	1239
	5	768
	6	908

- *Decision rule*: the process used by decision makers to choose their preferred alternative. The decision maker's preference is described by the utility function U, and the logit distribution is applied to measure the probability of choosing an alternative with utility U.

We define the utility function of decision maker n for alternative i as follows:

$$U_{i,n} = \beta^T X_{i,n} + \varepsilon_{i,n} \tag{5.4}$$

where $X_{i,n}$ is a vector of attributes for alternative i and characteristics for decision maker n, β is the vector of model parameters, and $\varepsilon_{i,n}$ is the random component. The logit model is particularly well suited for discrete choices, as it offers a closed form for the choice probability. In this case, $\varepsilon_{i,n}$ is logistically distributed and the probability of choosing alternative i versus alternative j, with utility functions described in Eq 5.4 can be written:

$$P_n(i) = P(U_{i,n} \geq U_{j,n}) \tag{5.5}$$

$$= \frac{1}{1+e^{-\beta(X_{i,n}-X_{j,n})}} \tag{5.6}$$

5.5.3 Results

Decision makers are faced with two alternatives: accepting or rejecting the Demand Response offer, denoted by:

$$y_n = \begin{cases} 1 \text{ if household } n \text{ accepts the DR offer} \\ 0 \text{ otherwise.} \end{cases} \tag{5.7}$$

In a utility-maximizing model, only the difference in utilities matters. As a result, U_n measures the utility of accepting relative to not accepting:

$$U_n = \beta X_n + \varepsilon_n \tag{5.8}$$

$$y_n = \begin{cases} 1 & \text{if } U_n > 0 \\ 0 & \text{if } U_n \leq 0 \end{cases} \tag{5.9}$$

The proposed model includes all regressors described in Tables 5.2, 5.3, 5.4, except the discrete energy profiles, as we find that these are highly correlated with other energy characteristics and do not improve the discrete choice model. We use the discrete choice regression software Biogeme [16] to estimate parameter values β. Two optimization algorithms are used to estimate parameters using the global maximum of the likelihood function, and both converge to the solution in Table 5.5. The first algorithm is a trust region algorithm explained in [16, 32], and the second algorithm is a sequential equality constrained quadratic programming method, developed by Spellucci [120].

The result from the Logit regression model is shown in Table 5.5, where all regressors are normalized to take value on $[0,1]$. It is remarkable to see that all coefficients are significant at the 95% level, except *poolpump ownership*. The Alternative Specific Constant (ASC) value is negative (-0.993), which means that people generally prefer refusing the offer rather than accepting it.

5.5.3.1 Energy product attributes

The proposed product has a large impact on the decision making, as the difference in parameter values of DPP (Dynamic peak Pricing), STOU (Seasonal Time of Use) and DPR (Dynamic Price Rebate) shows. The DPP and DPR products share many similarities, namely customers are notified one day in advance of an energy reduction event, although the incentive differs. In the case of DPP, households pay higher prices during peak times, whereas in the case of DPR, households receive rebates if they lower their energy consumption during peak times. The rebate incentive is more than four times more popular than the pricing incentive and five times more popular than time-of-use tariff. It is also interesting to notice that offering a feedback system increases the probability of accepting the offer.

$$U_{feedback} = ASC + \beta_{Feedback} = -0.993 + 1.98 = 0.987 > 0 \tag{5.10}$$

Equation (5.10) shows that, while accepting the offer is generally less favored than refusing the offer, this is reversed as soon as the household is offered a feedback system along with the energy product.

5.5.3.2 Household characteristics

Table 5.5 shows eight household characteristics that are statistically significant in DR enrollment choices. Households who live in single family homes, who are equipped with solar panels, and who have higher income are more likely to accept a DR product. Conversely, households with children, with HVAC systems, and who live in warmer areas are less likely to accept DR programs. In this

dataset, all sample households are in Australia, where a large portion of electricity consumption is due to cooling systems. Our model confirms that customers in warm areas and equipped with cooling systems are less likely to commit to energy reduction programs.

5.5.3.3 Electricity consumption behaviors

The last two parameters measure the impact of electricity consumption habits on DR enrollment. Our model shows that customers with higher average consumption and higher entropy are more reluctant to accept DR offers. Entropy is a measure of heterogeneity in energy consumption, and previous work has assumed that higher entropy would result in less interest in demand response [68, 67]. This model verifies and quantifies this assumption: being in the highest entropy group tends to increase refusal rates by 13%. For the first time, this model confirms that higher entropy customers are more reluctant to commit to DR programs, and utilities should target households with more consistent energy habits. On the other side, although customers with higher energy consumption on average have more flexibility to reduce and shift their usage, Table 5.5 shows that they are less likely to enroll in DR programs.

5.5.3.4 Summary

This section has characterized DR program acceptance choices, while the next sections will analyze responses to DR events for households who enroll in one of the offered programs. From the above analysis, we conclude that rebate-based DR programs are preferred, and that feedback systems are very efficient at incentivizing households to accept DR programs, probably because they bring more transparency to DR. The analysis of demographic characteristics shows that Australian utilities should target customers with low entropy, who live in colder areas, and who live in single-family housing. Some characteristics like owning a solar panel anecdotally tend to be a sign of environment-awareness, which is a good target profile for DR programs. In the next section, we deepen our analysis of DR programs, by evaluating the response to DR events and electricity prices for customers who enrolled in DR.

5.6 Demand Response Impact and Price of flexibility

5.6.1 Difference-in-difference Analysis of Dynamic Peak Pricing

As shown in Section 5.3, DPP is the most common product accepted in the SGSC trial. More generally, DPP has become an attractive solution for utilities, as it is easy to implement and can be dynamically set to regulate the grid during peak-consumption days. As a result, we study this specific tariff and seek to measure the response to DPP events. Our objective is to estimate the quantity of load reduction as a response to a DPP event signal,and investigate if load shape clusters (as defined in Section 5.4) can improve these estimates. In this section, we use the difference-in-difference method [6] method, as has been used in prior literature to measure the impact of

Table 5.5: Logit regression for DR enrollment choice

Parameter	**Value of β**	**Std**	**t-test**	**p-value**
ASC (constant)	-0.993	0.116	-8.56	0.00
Attributes				
DPP	0.668	0.0553	12.54	0.00
STOU	-0.596	0.069	-8.63	0.00
DPR	4.40	0.165	26.64	0.00
Feedback	1.98	0.0561	35.26	0.00
Decision maker's characteristics				
Single family home	0.204	0.0710	2.87	0.00
Has Children	-0.127	0.0495	-2.56	0.01
High income	0.157	0.0515	3.04	0.00
Has poolpump	-0.102	0.0749	-1.35	0.18*
Has Solar	1.50	0.186	8.05	0.00
Has HVAC	-0.474	0.0533	-8.90	0.00
Warm climate	-0.624	0.0831	-7.51	0.00
Avg daily consumption	-2.297	0.144	-2.07	0.00
High entropy	-0.139	0.0621	-2.25	0.02

DPP treatments on energy consumption [44, 43]. We build on this approach, and show that the clustering results presented in Section 5.4 can improve the predictability of load reduction..

Table 5.6: Variables for DPP impact assessment

Symbol	**Description**
Variables	
$W_{i,t} \in \mathbb{R}^+$	Hourly consumption of household i during peak hours on day t
$G_i \in \{0,1\}$	Binary variable for household i being in the DPP group
$P_{i,t} \in \{0,1\}$	Binary variable for household i experiencing a peak event during day t
$C_i^k \in \{0,1\}$	Binary variable for household i being part of cluster k
Parameters	
u_t	Day level effects
b_{peak}	Impact of the DPP event on the DPP group
$b_{peak,Ck}$	Impact of the DPP event on the Cluster k DPP group
b_{dpp}	DPP group fixed effect
b_{Ck}	Cluster k group fixed effect

Three regression models are tested, with the notations presented in Table 5.6. The dependant variable $W_{i,t}$ is the average hourly consumption during peak hours on day t for customer i. More precisely, for each day with a dynamic peak event, utilities set a period of 2 to 10 hours during

which the price of electricity is elevated. For each peak-event day, we average the hourly consumption of customer i in the predetermined peak period, and note this value $W_{i,t}$. We compare three regression models that include day-level effects, treatment effects, and use the information obtained from the clustering analysis in Section 5.4:

(M1) Difference in differences:

$$W_{i,t} = b_0 + u_t + b_{dpp}\mathrm{G}_i + b_{peak}\mathrm{P}_{i,t} + \varepsilon_{i,t} \tag{5.11}$$

(M2) Difference in differences with cluster level fixed effects:

$$W_{i,t} = b_0 + u_t + b_{dpp}\mathrm{G}_i + b_{peak}\mathrm{P}_{i,t} + \sum_{k=0}^{6} b_{Ck}\mathrm{C}_i^k + \varepsilon_{i,t} \tag{5.12}$$

(M3) Difference in differences with treatment parameters depending on cluster:

$$W_{i,t} = b_0 + u_t + b_{dpp}\mathrm{G}_i + \sum_{k=0}^{6} [b_{Ck} + b_{peak,Ck}\mathrm{P}_{i,t}]\mathrm{C}_i^k + \varepsilon_{i,t} \tag{5.13}$$

5.6.1.1 Model (M1)

Model (M1) presented in Eq (5.11) is a difference-in-differences model with day-level fixed effects. Parameter u_t is the day-level effect, which accounts for all specific aspects of day t (e.g: weather, holiday, etc). Parameter b_{dpp} measures the overall difference between the DPP group and the control group, irrespective of peak events. Parameter b_{peak} is the main parameter of interest, as it measures the impact of the peak event. The value and statistics of (M1) parameters are shown in Table 5.7, where the green color means that DPP treatments have a beneficial impact on electricity consumption, i.e. result in lower energy consumption during peak times. From this measure, we can conclude with more than 95% confidence that the DPP program results in lower energy consumption during peak times. More precisely, Fig (5.8) shows the estimated impact of each DPP event, as the estimated percentage of electricity reduction r_j for peak event index j:

$$r_j = \frac{b_{peak}}{b_0 + b_{dpp} + u_{peak_j}} \tag{5.14}$$

In Eq (5.14), u_{peak_j} denotes the day-level effect for the day corresponding to peak event index j. Figure (5.8) shows that the (M1) estimated impact is between 15% and 20% energy reduction per peak event. This is in accordance with previous DPP experiments [44], which found an impact of between 13% and 20%.

5.6.1.2 Model (M2) and (M3)

We seek to improve our understanding of DPP impact by using the concept of energy clusters as defined in Part 5.4. Model (M2) in Eq. (5.12) assumes that clusters have different baseline

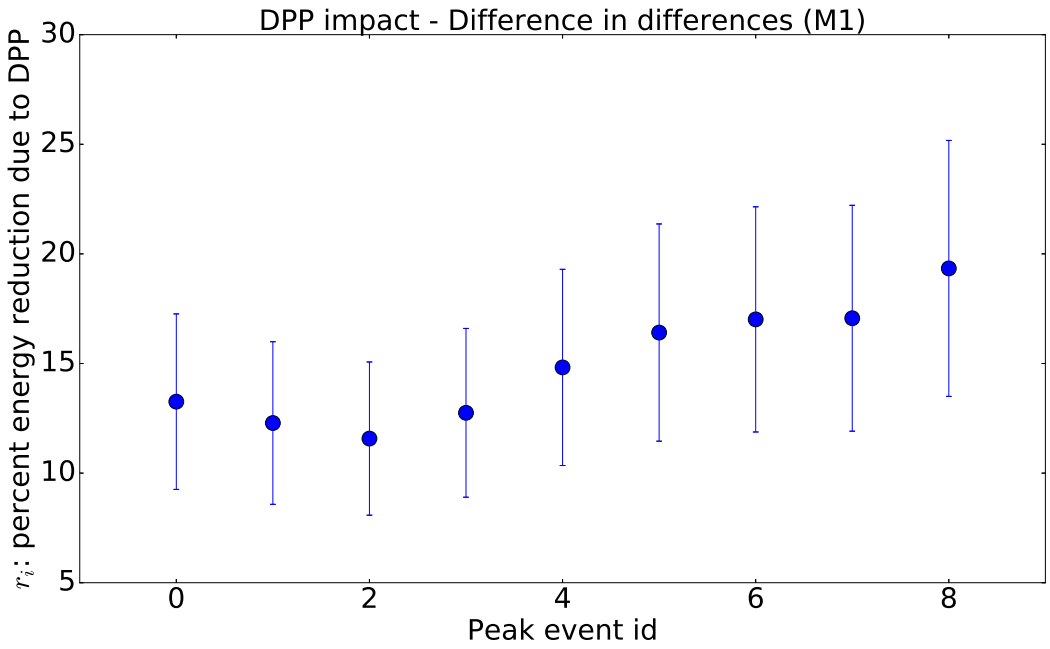

Figure 5.8: Estimated electricity reduction due to peak events, as defined in Eq 5.14 - model (M1). Blue lines show 95% confidence intervals.

Table 5.7: (M1) model parameters

	(M1) Difference in differences			
	Coef	Pvalue	95 conf interval	
b_0	0.1989	0.000	0.193	0.205
b_{dpp}	0.0755	0.000	0.073	0.078
b_{peak}	-0.0488	0.000	-0.064	-0.034

consumption, and include a cluster-level fixed effect b_{C_k} for each cluster C_k. Model (M3) in Eq. (5.13) assumes that clusters have different reactions to peak events, and include a cluster-level treatment parameter b_{peak,C_k} for each cluster C_k. Table 5.8 shows the regression results, where the green color means that DPP has a beneficial impact on energy consumption, red means that it has a negative impact and blue means that it is not statistically significant. Table 5.9 shows comparison metrics for the three models, and shows that clustering information tends to improve the model. Indeed, model (M3) has the largest adjusted R-squared value, and the lowest Bayesian Information Criterion (BIC) and Aikaike Information Criterion (AIC). Moreover, Table 5.8 shows that all the cluster-specific parameters are significant, except $b_{peak,C4}$. Fig 5.9 shows the percentage of energy reduction during peak times, per peak event. Each line corresponds to a different cluster, and shows clear heterogeneity in the energy reduction as a function of cluster index. This obser-

Table 5.8: (M2) and (M3) model parameters

	(M2) Cluster level fixed effects				**(M3) Cluster level dpp coefficient**			
	Coef	Pvalue	95 conf interval		Coef	Pvalue	95 conf interval	
b_0	0.2369	0.000	0.231	0.243	0.02054	0.000	0.199	0.212
b_{dpp}	0.0290	0.000	0.027	0.031	0.0764	0.000	0.074	0.079
b_{peak}	-0.0486	0.000	-0.063	-0.035	NA	NA	NA	NA
b_{C0}	0.0259	0.000	0.254	0.264	0.2531	0.000	0.248	0.258
b_{C1}	-0.0839	0.000	-0.087	-0.081	-0.0837	0.000	-0.087	-0.080
b_{C2}	0.1337	0.000	0.129	0.138	0.1343	0.000	0.130	0.139
b_{C3}	0.0619	0.000	0.059	0.065	0.0614	0.000	0.058	0.065
b_{C4}	-0.0114	0.000	-0.016	-0.007	-0.0133	0.000	-0.018	-0.009
b_{C5}	0.0129	0.000	0.009	0.017	0.0128	0.000	-0.008	0.017
$b_{peak,C0}$	NA	NA	NA	NA	0.1292	0.000	0.101	0.157
$b_{peak,C1}$	NA	NA	NA	NA	-0.0700	0.000	-0.085	-0.055
$b_{peak,C2}$	NA	NA	NA	NA	-0.0836	0.000	-0.107	-0.060
$b_{peak,C3}$	NA	NA	NA	NA	-0.0473	0.000	-0.062	-0.032
$b_{peak,C4}$	NA	NA	NA	NA	0.0035	0.739*	-0.024	0.017
$b_{peak,C5}$	NA	NA	NA	NA	-0.0624	0.000	-0.085	-0.040
$b_{peak,C6}$	NA	NA	NA	NA	-0.0628	0.000	-0.084	-0.041

Table 5.9: Model comparison - cluster information in (M2) and (M3) tends to improve model performance

	(M1)	(M2)	(M3)
Adj R^2	0.063	0.162	0.163
BIC	3.07 10^4	-4237	-4444
AIC	3.62 10^4	-7776	-8058

vation is true for models (M2) and (M3), and suggests that clustering is a useful tool for targeting customers with high DR potential. In particular, customers belonging to Cluster 1 have the most beneficial response to peak events, reducing their consumption between 15% and 60% during peak periods. In contrary, customers in Cluster 0 have the worst response to DPP, as Model (M3) finds that DPP is counter-effective and customers tend to increase consumption during peak times. For electrical utilities using conventional customer segmentation, Cluster 0 might seem to be a good target for DPP programs, as Fig 5.4 shows that customers in Cluster 0 have a late afternoon peak consumption. However, this study shows that the DPP program fails to induce energy reduction within this part of the population. In contrary, utilities should target customers in Clusters 1, 2, 3 or 5, who tend to reduce energy consumption during peak events.

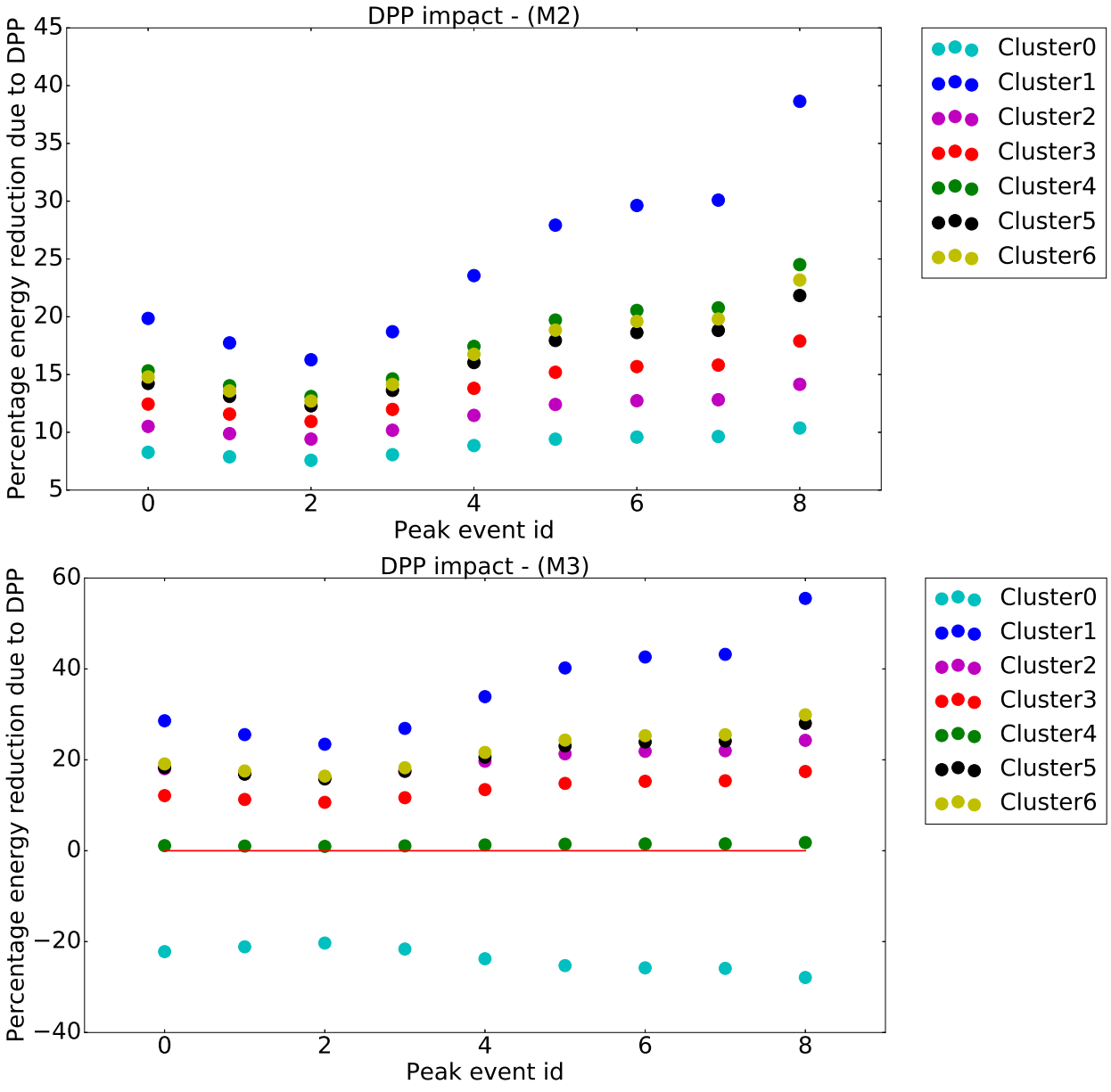

Figure 5.9: Percentage energy reduction due to DPP events, per cluster

5.6.2 Customer-Level DPP assessment

While we have demonstrated a significant opportunity for improving predictions of demand response by clustering households, electric utilities would like to be able to further target programs at the household level. This section shows how we analyze the response of individual households, by matching each households in the DPP program to a similar household in the control group, and performing a difference-in-differences analysis. We then compare the results with the profile-cluster approach above.

To perform this matching, we scale each household's consumption to $[0,1]$ and remove the average consumption in each hour. This creates a vector of each household's consumption relative to the average baseline. From this vector, which includes all hours in the study period, we extract the data for the peak consumption hours of the day, i.e. 13:00-18:30.

We then matched each household in the DPP experimental group with the n nearest neighbors in the control group, excluding days when DPP calls were made. In this model, we use mean Euclidean distance between the vectors described above, as a metric of fit quality. A number of different specifications were considered, and we found that $n = 9$ neighbors from the control group produced the highest-quality fit (lowest RMSE averaged across all households participating in the DPP).

This matching allows us to estimate baseline consumption of each household, in order to calculate the effect of the DPP treatment. Using the non-DPP hours to inform our matching, we then compute the difference in consumption between the experimental household and the baseline household during the DPP call hours. The average response of each household, as a portion of its peak consumption, is shown in Figure 5.10.

We find significant variance in results that is hidden in the profile-level analysis, although the average response of 17% reduction in consumption during DPP periods is consistent with the results found above.

The set of households in each profile group were analyzed, but a strong correlation between profile groups and fit quality or variance was not found.

Attempting to improve model fit by including the household attributes from Table 5.2 2 did not produce a significant improvement in fit quality, and instead led to over-fitting and a loss in statistical power.

These results show that predicting energy reduction for individual households during DPP hours is extremely difficult due to variations in appliance use and consumer behavior. By showing the relative weakness of household-level approaches, this section gives strength to the profile-cluster approach advanced in this chapter. While still able to differentiate between the response patterns of different consumption profiles, using clusters allows for improved prediction quality thanks to the law of large numbers.

5.6.3 Price sensitivity

The goal of this section is to understand the impact of price on energy consumption, instead of considering a binary indicator for peak event occurrence only. The DPP study above shows how

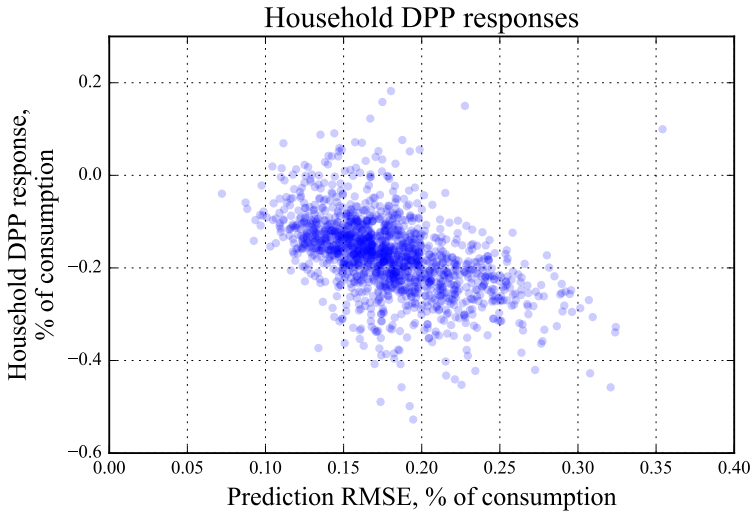

Figure 5.10: Response of each household to dynamic peak pricing events, along with the fit quality for each household's prediction. The response is computed as the difference between the DPP household's power consumption and the mean power consumption of the 9 households in the control group with the most similar power consumption patterns. The quality of the fit between the DPP household and the baseline reference is shown on the x-axis.

people react to DPP events, but cannot capture if this is due to the psychological impact of the event, or if this is due to price. In other words, if the DPP peak event was half the price or twice as expensive, would that change how people behave? For each day and each hour of the day, we report the hourly price of electricity, i.e. the price will be very high during DPP events. We include all the studied utility rates, and seek to understand how people respond to price. We find that price sensitivity highly depends on time of the day and cluster, and we find two clusters with good price sensitivity.

In the studied experiment, most energy products are price-based incentives: the electricity price is higher during peak times, when utilities seek to lower the energy demand. Because this dataset includes more than four different pricing products, the price of electricity takes between 2 and 5 different values at each hour of the day, across the customer database. This a unique characteristics of the SGSC dataset, when most past trials have studied one unique DR program and cannot cover a range of energy prices. As a result, we can use this dataset to capture price sensitivity (kWh/$) and inversely define a 'price of flexibility', which measures the monetary value of 1 kWh energy flexibility, from the customer perspective. We augment the dataset with temperature data, in order to account for the impact of weather on energy consumption. Table 5.10 shows the notations used in this section. Similarly to Section 5.6.1, we run three regression models, which include different price dependence and cluster dependence. For each hour, we run the

Table 5.10: Variables for Price impact assessment

Symbol	Description
Variables	
$W_{i,t} \in \mathbb{R}^+$	Hourly consumption of household i during hour t
$T_{i,t} \in \mathbb{R}$	Ambient temperature for household i at time t
$R_{i,t} \in \mathbb{R}^+$	Electricity rate for household i at time t
$C_i^k \in \{0,1\}$	Binary variable for household i being part of cluster k
Parameters	
u_t	Day level effects
b_{temp}	Impact of temperature on energy consumption
$b_{temp,Ck}$	Impact of temperature on energy consumption for Cluster k
b_{price}	Impact of electricity rate on energy consumption
$b_{price,Ck}$	Impact of electricity rate on energy consumption for Cluster k

three following models:

(Mp1) General regression:

$$W_{i,t} = u_t + b_{temp}T_{i,t} + b_{price}R_{i,t} + \varepsilon_{i,t} \tag{5.15}$$

(Mp2) Regression with cluster level fixed effects:

$$W_{i,t} = u_t + \sum_{k=1}^{C} b_{Ck}C_i^k + b_{temp}T_{i,t} + b_{price}R_{i,t} + \varepsilon_{i,t} \tag{5.16}$$

(Mp3) General regression with treatment parameters depending on cluster:

$$W_{i,t} = \sum_{k=1}^{C} [u_{t,C_k} + b_{Ck} + b_{temp,C_k}T_{i,t} + b_{price,C_k}R_{i,t} + \varepsilon_{i,t}]C_i^k \tag{5.17}$$

Model (Mp1) includes day-level fixed effects, temperature and price, without cluster information. Model (Mp2) includes cluster-level fixed effects and Model (Mp3) includes cluster-level parameters for each parameter. Fig 5.11 represents energy consumption data as a function of temperature, and confirms the relevance of the linear regression approach. Fig 5.12 shows the price coefficient, temperature coefficient and adjusted R-squared of models (Mp1) and (Mp2). Price coefficients and temperature coefficients are plotted with the 95% confidence interval. For most hours of the day, the temperature coefficient is strictly positive with more than 95% confidence, which confirms that households consume more energy when the temperature is higher, probably by increasing the usage of HVAC systems. On the other hand, the impact of price highly varies during the day. Model (MP1) and (Mp2) find that the price parameter is strictly negative with statistical significance, at 6am and from 9pm to 12am. During these times, customers reduce their energy consumption when the price is higher. The Adjusted R-squared of (Mp2) is higher than

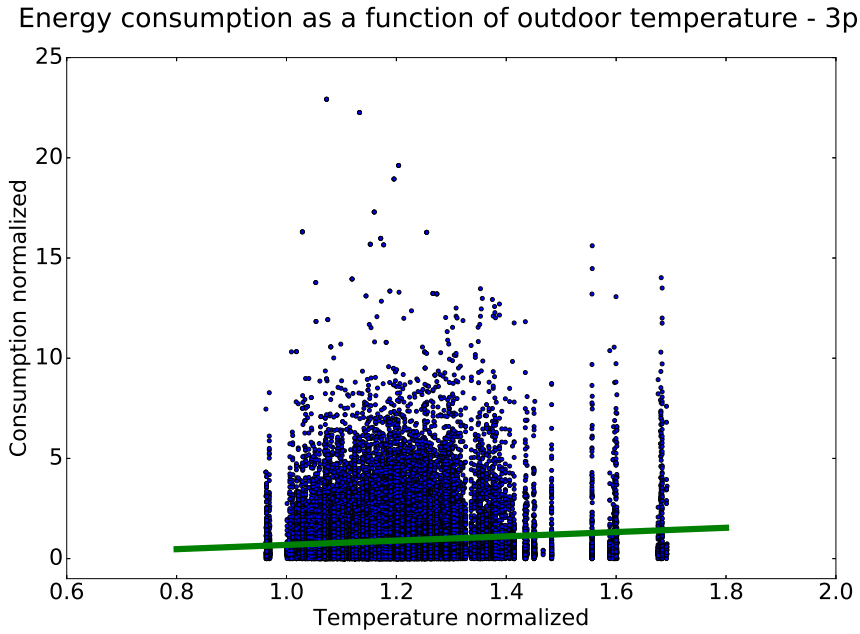

Figure 5.11: Energy consumption as a function of outdoor temperature at time 3pm. The green line shows the linear estimate.

(Mp1), which shows that clustering information improves the quality of the model. This method proves that price sensitivity highly depends on the time of the day, and cannot be defined as a constant characteristic of customers. With model (MP3), we further seek to capture non-constant, non-uniform price sensitivity by studying how it varies across the population.

Figure 5.13 shows (Mp3) results, where one independent regression model is estimated for each cluster. We select the set of customers with no missing consumption data during the entire two year period 03/03/2012 to 03/03/2014. This set does not contain Cluster 0 households, and Fig 5.13 shows the result for clusters 1 to 6. It shows that temperature and price dependence highly varies across clusters. Cluster 3 is very temperature-sensitive, whereas Cluster 1 is temperature-sensitive only during the afternoon, and Cluster 5 and 6 during mornings and evenings. Clusters 5 and 6 offer the best price-response, as higher prices result in lower electricity consumption during several periods of the day. On the contrary, clusters 1, 2 and 4 often tend to increase consumption when the price increases. To conclude, this study shows varied impacts of price on energy. It isolates two groups, clusters 5 and 6, with favorable price dependence. These profiles should be targeted with price-based offers, whereas other solutions should be preferred for other clusters, including information and feedback technologies. For example Fig 5.13 shows that Clusters 1 and 3 are very temperature sensitive, therefore automated and energy-saving HVAC systems would be an effective way to induce electricity consumption reduction among these groups.

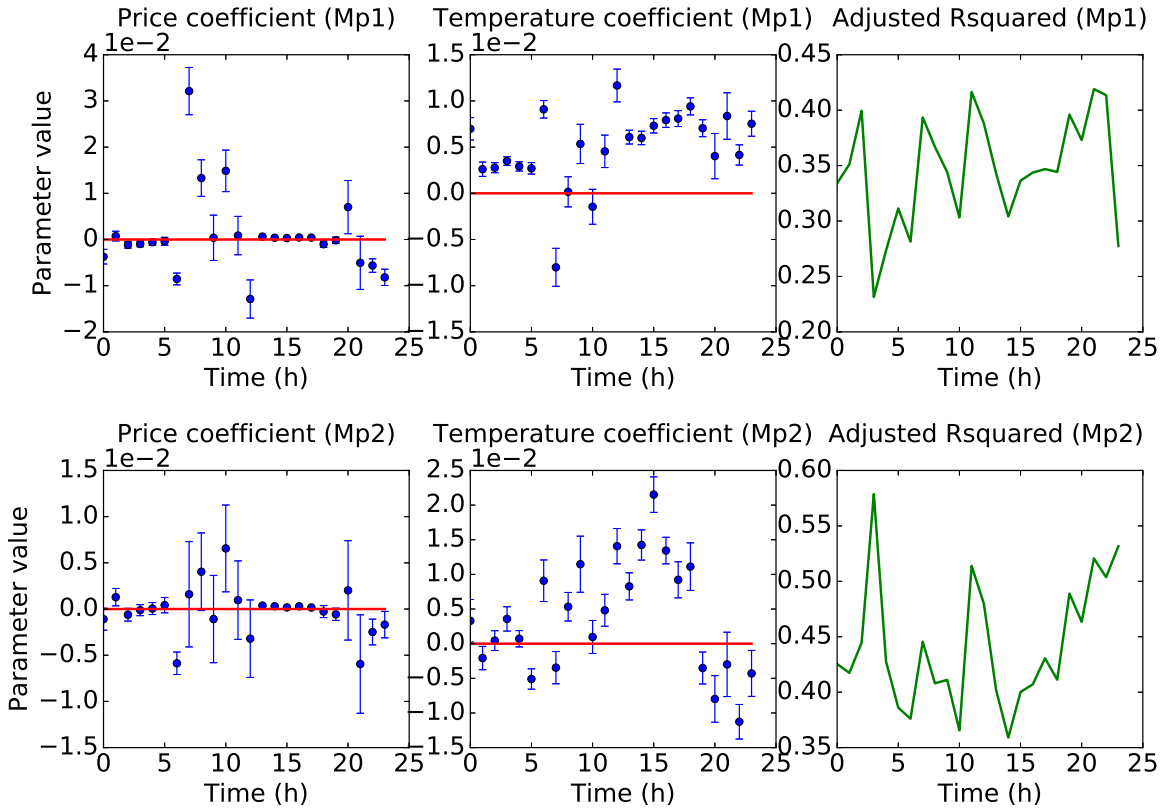

Figure 5.12: Price coefficient and temperature coefficient without cluster-level effect (top line shows Model (Mp1)) and with cluster-level effect (bottom line shows Model (Mp2)). The red line shows the x axis.

5.6.4 Summary

Figure 5.14 summarizes how energy clusters defined in Section 5.4 can inform energy policies and help utilities better target customers with effective DR offers. Section 5.5 shows that low-entropy households are more likely to accept DR offers. Section 5.6.1 shows that the DPP program has positive effects only on clusters 1, 2, 3, 5 and 6. Section 5.6.3 shows that clusters 5 and 6 are price sensitive, and can be targeted with time-of-use rates, whereas clusters 1 and 3, with low price sensitivity and high temperature sensitivity, should be targeted with automated HVAC control.

5.7 Summary

In this chapter, we predict probabilities of reducing energy consumption during a DR event, and quantify the reduction of power consumption in the case of DPP events and price-based programs. More generally, we develop a methodology to study Demand Response behaviors, and apply the method to the Smart Grid Smart City trial data in Australia. First, we use K-means algorithms

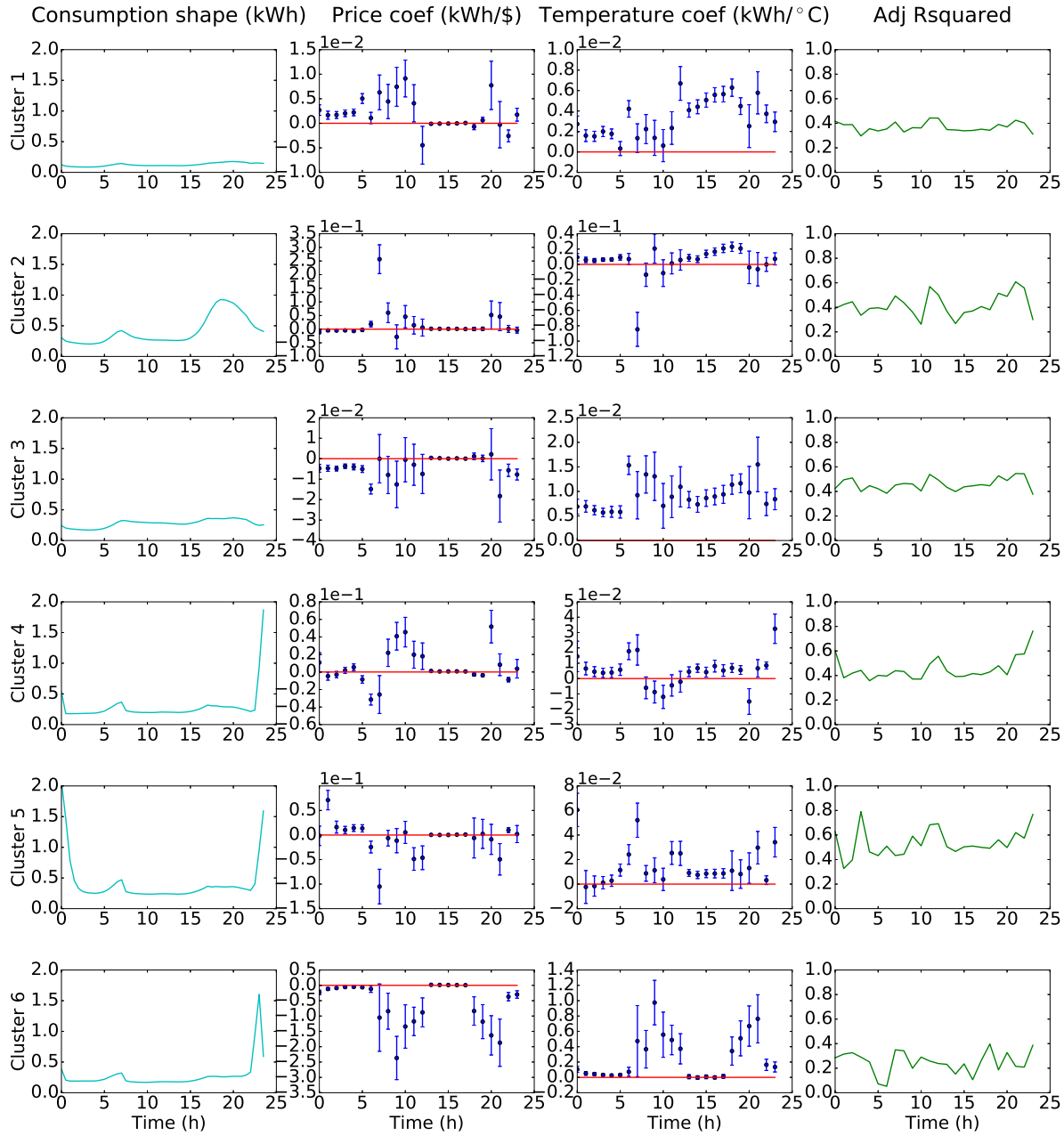

Figure 5.13: Results of model (Mp3). For clusters 1 to 6: (i) consumption shape, (ii) estimated price coefficient with 95% confidence interval, (iii) estimated temperature coefficient with 95% confidence interval and (iv) adjusted R-squared. The red line shows the x axis.

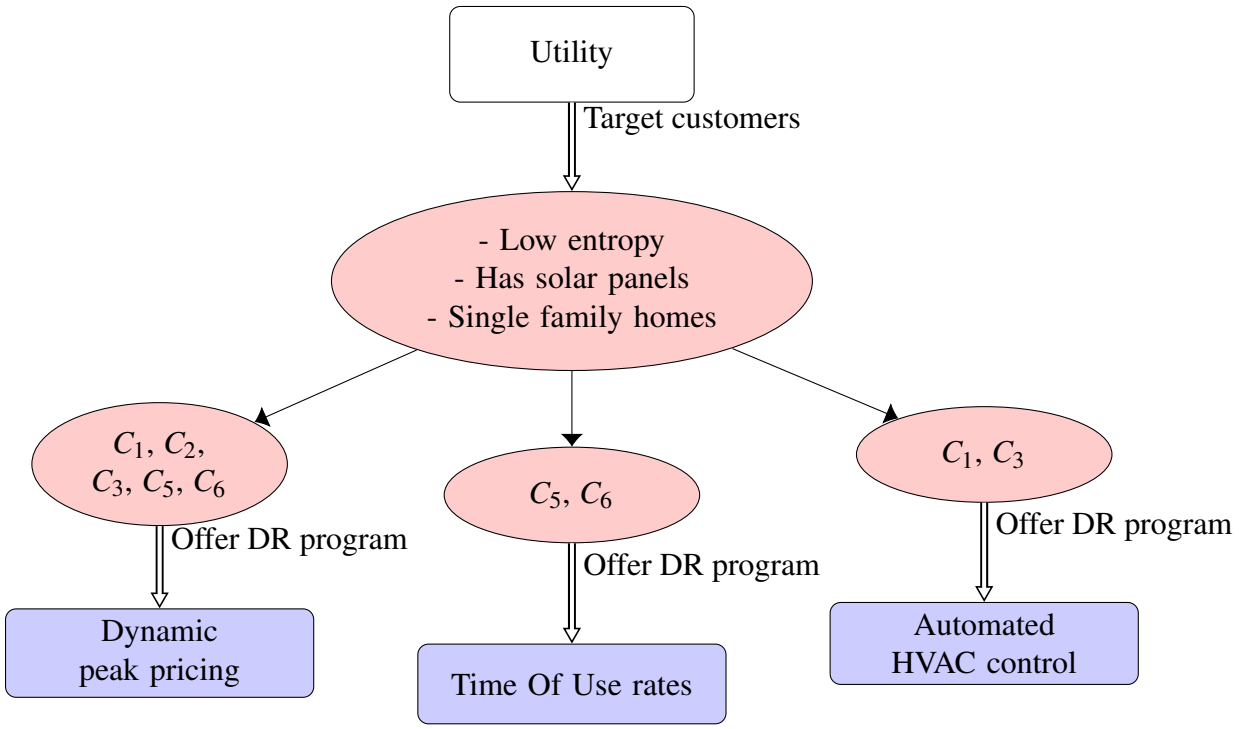

Figure 5.14: Summary of findings, and recommendation for utilities. Red ellipse shows energy consumption characteristics and blue rectangle shows the most effective DR offer, based on the findings of this work.

on smart meter data, and divide the population into seven clusters of energy consumption. Second, this information is used to analyze DR program enrollment and DR energy response, and the numerical results show that the type of energy consumption impacts both DR enrollment and DR electricity response. The logit binary choice model demonstrates that customers with high energy entropy tend to be more reluctant to commit to energy reduction programs, and utilities should target low entropy customers to increase their DR acceptance rate. Several difference-in-differences and regression models are used to measure the impact of DPP events, and capture sensitivity to temperature and electricity price. The results show that clusters have statistically significant differences in how they respond to DR events, along with different price sensitivities and temperature sensitivities.

This information can be very valuable for utilities, as it gives insights on how to segment customers for electricity consumption, and how to target customers with tailored successful DR offers. A tailored offer will be more likely to be accepted by the customer, and induce a beneficial change in energy consumption. Figure 5.14 summarizes the findings and recommendations for utilities in the specific case of Australia.

Chapter 6

Conclusion

6.1 Summary of contributions

This dissertation presents three novel optimization techniques for energy management of large fleets of electric cars. These methods are applicable in three different scenarios, namely (i) a centrally located fleet that can be controlled solely by on/off signals, (ii) a spatially distributed fleet that is controlled by an aggregator to provide load shaping, (iii) a spatially distributed fleet in a stranded distribution grid that is controlled to provide voltage regulation and load shaping services. We show that each problem has different constraints and mathematical properties, and identify techniques to respond to each of them. We further extend this work by studying how human behaviors may affect energy management programs, and study an example of Demand Response trial in Australia.

With the first method, we propose a novel state space modeling framework for large fleets of PEVs with discrete charging rate. First we aggregate PEVs in three different states, namely G2V, idle and V2G. We derive the dynamics of the fleet as a system of three coupled PDEs, with uncontrollable flows coming from drivers. We use a Lax Wendroff discretization to transform the system of PDEs into a state space representation, where the flows between the three different charging categories are controlled. We propose a Linear Quadratic Regulator with the objective to track a power signal, while respecting drivers' mobility constraints. We use Model Predictive Control techniques to solve this problem in real time. We perform various case studies and examine how the performance of the aggregator depends on LQR parameters, drivers' flexibility and capacity bidding strategies. These examples show that the system is particularly adapted to load following, with zero-mean reference signals.

With the second method, we propose distributed load shaping strategies to control PEV charging schedules via dual splitting. We define a global optimization problem, which aims at coordinating PEVs to minimize the load variance. We show that this objective can be distributed and solved in a decentralized framework. In the first step each PEV solves a local optimal program based on a broadcast price signal, and communicates their response to the aggregator. In the second step, the aggregator updates the price signal to reach minimal load variance. We propose three

methods to compute this iterative process and prove their characteristics. First, the gradient ascent method converges in a linear rate but needs an update from every agent at each iteration. Second, the Stochastic Incremental Method with constant step-size converges in a linear rate, needs the update from only one agent at each iteration but converges to an approximate solution. Third, the the Stochastic Incremental Method with decreasing step-size converges to the optimal solution as $\frac{1}{k}$ and needs the update from only one agent at each iteration. Finally, we compute several case studies based on real data, and demonstrate that PEVs provide a compelling opportunity to integrate renewable energy sources in the electricity mix.

With the third method, we propose a predictive controller that is capable of handling Plug & Play requests of flexible and deferrable loads. First, an MPC approach for minimizing the global cost of the system is used to aggregate flexible loads and provide load shaping objectives under distribution grid constraints. Second, we propose a MIP that safely connects loads and minimizes waiting times. We prove that our algorithm achieves recursive feasibility, by appropriately defining the connection conditions and the terminal constraint set. The performance of the proposed method is demonstrated for the control of a radial distribution system with 55 buses.

6.2 Perspective on future extensions

There exists various opportunities to extend the work presented in this dissertation.

6.2.1 PDE modeling and control techniques for heterogeneous fleets of PEVs

Chapter 2 of this dissertation presents a PDE modeling method, and discretization technique for homogeneous fleets of PEVs. This can be extended to heterogeneous fleets (i.e. different battery sizes and charging rates). This will present key challenges for developing adequate numerical discretization schemes, with the right consistency and stability properties.

6.2.2 PEV scheduling through Distributed Plug & Play Model Predictive Control techniques

Chapter 4 proposes a Plug & Play Model Predictive Controller to solve the PEV scheduling problem in an over-loaded power network. If P&P MPC techniques are particularly tractable for large scale systems, each iteration requires solving a centralized optimization problem. As a result, in a case of a very large distribution network, or if lots of loads connect at the same time, the computation time can become very high. In this case, distributed P&P MPC would be more appropriate. Future research can look at distributed versions of the proposed algorithms, which will present a few challenges for integrating fixed load-charging deadlines, as proposed in Chapter 4.

6.2.3 Human-in-the-loop PEV smart charging

Chapters 2, 3 and 4 propose optimal scheduling algorithms by assuming that drivers will mainly respond to a price signal when making decision of when to charge their cars. Chapters 2 and 3 look at extensions where drivers respond to price signals and look at reducing their battery degradation at the same time. However, Chapter 5 shows that human behaviors are much more complex when it comes to making energy choices. Future work can research how to include more realistic behaviors in the optimal scheduling problem. In particular, driver choices should be more realistically modeled by utility functions. This should account for the tradeoffs that one driver makes when he/she chooses when to charge his/her PEV.

6.3 Concluding remark

The future of our electric car fleets will be diverse and heterogeneous, in terms of infrastructure, vehicles and mobility patterns. Behaviors and human choices will play a key role in the success of energy management strategies for fleets of electric cars. In Chapters 2 and 3, this dissertation provides separate solutions for the problem with ON/OFF-type of infrastructure and the problem with continuous range of charging infrastructure. Chapter 4 attempts to combine these two cases by modeling two types of loads and two types of scheduling objectives, i.e. load shaping at the aggregate level and voltage regulation at the node level. In future, it is essential to develop generic solutions that globally coordinate and aggregate electric vehicles, and efficiently account for driver's behaviors. We should research and develop unified frameworks that combines techniques and models, and can adapt to grid constraints, computation requirements, and driver behavioral changes.

Appendix A

Proof of LQR recursive feasibility

This proof refers to Proposition 2. We assume that $X(0) \geq 0$ and that Assumption 1 is verified. Then, we show that the problem is feasible with the control sequence described in Section 2.5.3.2. We consider $k \in \{0,...,N\}$, and apply the control sequence $U_{idle}(k)$ at time k:

$$
\begin{aligned}
& X(k+1) \\
& = \mathbf{A}X(k) + \mathbf{B_u}U_{idle}(k) + \mathbf{B_s}(Dep(k) + Arr(k)) \\
& = \begin{bmatrix} \mathbf{A}_{V2G}u(k) \\ \mathbf{A}_{idle}v(k) \\ \mathbf{A}_{G2V}w(k) \end{bmatrix} + \begin{bmatrix} -\mathbf{A}_{V2G}u(k) \\ \mathbf{A}_{V2G}u(k) + \mathbf{A}_{G2V}w(k) \\ -\mathbf{A}_{G2V}w(k) \end{bmatrix} - \begin{bmatrix} 0 \\ Dep(k) + Arr(k) \\ 0 \end{bmatrix} \\
& = \begin{bmatrix} 0 \\ \mathbf{A}_{V2G}u(k) + \mathbf{A}_{G2V}w(k) + \mathbf{A}_{idle}v(k) - Dep(k) - Arr(k) \\ 0 \end{bmatrix}
\end{aligned}
$$

$$
\begin{aligned}
1^T X(k+1) = \quad & 1^T[\mathbf{A}_{V2G}u(k) + \mathbf{A}_{G2V}w(k) + \mathbf{A}_{idle}v(k)] \\
& -1^T(Dep(k) + Arr(k)) \\
= \quad & 1^T X(k) - d(k) + 1^T|Arr(k)| \qquad \text{(A.1)}
\end{aligned}
$$

The last equality results from the system dynamics properties: the matrices $\mathbf{A}_{V2G}$,$\mathbf{A}_{Idle}$ and A_{G2V} are obtained from the discretization of convection PDEs, which ensure the conservation of loads. Then:

$$
\begin{aligned}
1^T X(k+1) - 1^T X(k) &= 1^T|Arr(k)| - D(k) \\
\text{Then, by induction:} & \\
1^T X(k+1) - 1^T X(0) &= \sum_{l=0}^{k} 1^T|Arr(l)| - D(l) \qquad \text{(A.2)}
\end{aligned}
$$

Assumption 1 and relations (A.1), (A.2) give:

$$\begin{aligned} 1^T X(k+1) &> 0 \\ 1^T X(k) - d(k) + 1^T |Arr(k)| &> 0 \end{aligned} \tag{A.3}$$

We define:

$$\begin{aligned} Dep(k) &= d(k) \frac{\mathbf{A}_{V2G} u(k) + \mathbf{A}_{G2V} w(k) + \mathbf{A}_{idle} v(k) + |Arr(k)|}{1^T [A_{V2G} u(k) + \mathbf{A}_{G2V} w(k) + \mathbf{A}_{idle} v(k) + |Arr(k)|} \\ &= d(k) \frac{\mathbf{A}_{V2G} u(k) + \mathbf{A}_{G2V} w(k) + \mathbf{A}_{idle} v(k) + |Arr(k)|}{1^T [X(k) + |Arr(k)|]} \end{aligned}$$

We conclude:

$$1^T Dep(k) = d(k) \tag{A.4}$$

$$Dep(k) \geq 0 \tag{A.5}$$

$$\begin{aligned} X(k+1) &= \begin{bmatrix} 0 \\ \mathbf{A}_{V2G} u(k) + \mathbf{A}_{G2V} w(k) + \mathbf{A}_{Idle} v(k) + |Arr(k)| \times \mathfrak{G} \\ 0 \end{bmatrix} \\ &\geq 0 \end{aligned} \tag{A.6}$$

where

$$\mathfrak{G} = 1 - \frac{d(k)}{1^T [X(k) + 1^T |Arr(k)|]} \tag{A.7}$$

where the last inequality comes from relation (A.3).
Equations (A.4), (A.5), (A.6) show that the problem is feasible at time k. □

Appendix B

Proof of necessary constraints for capacity bidding

This proof refers to Section 2.6.0.2. We need to solve the following N_t Linear Programs (LP):

$$\min_{y\in\mathbb{R}^{N_t}} \quad -\sum_{j=1}^{N_t} h_{ij}y_j \tag{B.1a}$$

$$\text{st} \quad -c_j \leq y_j \leq c_j \quad \forall j \in \{1,...,N_t\} \tag{B.1b}$$

$$-\varepsilon \leq \sum_{j=1}^{N_t} y_j \leq \varepsilon \tag{B.1c}$$

We dualize the constraint B.1c in the above problem:

$$\min_{y\in\mathbb{R}^{N_t}} \max_{\lambda\geq 0,\mu\geq 0} -\sum_{j=1}^{N_t} h_{ij}y_j + \lambda(\sum_{j=1}^{N_t} y_j - \varepsilon) + \mu(-\sum_{j=1}^{N_t} y_j - \varepsilon)$$

$$\text{st} \quad -c_j \leq y_j \leq c_j \quad \forall j \in \{1,...,N_t\} \tag{B.2}$$

Problem (B.1) is feasible and is linear, therefore strong duality holds. Then, this is equivalent to the following distributed problem:

$$\begin{aligned}
&\max_{\lambda\geq 0,\mu\geq 0} -\varepsilon(\lambda+\mu) + \sum_{j=1}^{N_t} \min_{-c_j\leq y_j\leq c_j} y_j(-h_{ij}+\lambda-\mu) \\
&= \max_{\lambda\geq 0,\mu\geq 0} -\varepsilon(\lambda+\mu) - \sum_{j=1}^{N_t} c_j|-h_{ij}+\lambda-\mu| \\
&= -\min_{\lambda\geq 0,\mu\geq 0} \varepsilon(\lambda+\mu) + \sum_{j=1}^{N_t} c_j|-h_{ij}+\lambda-\mu|
\end{aligned} \tag{B.3}$$

We write the above equation B.3 with ordered h_{ij} such that $h_{i1} \leq h_{i2} \leq ... \leq h_{iN_t}$. We compute iteratively the minimization over λ and μ. To compute the minimization over λ, let define the following function

$$\begin{aligned} \phi_\mu : \mathbb{R}^+ &\to \mathbb{R} \\ \lambda &\to \varepsilon\lambda + \sum_{j=1}^{N_t} c_j|\lambda - (\mu + h_{ij})| \end{aligned} \tag{B.4}$$

ϕ_μ is convex and admits a minimum $p^*(\mu)$ on $\mathbb{R}^+$.

- *Case 1:* $\exists\, \lambda_\mu^*$ s.t. $0 \in \partial\phi_\mu(\lambda_\mu^*)$. Then $p^*(\mu) = \phi_\mu(\lambda_\mu^*)$.
- *Case 2:* $\lambda_\mu^* = 0$, and $p^*(\mu) = \sum_{j=1}^{N_t} c_j|(\mu + h_{ij})|$

We compute the subgradient as follows:

$$\begin{aligned} &\partial\phi_\mu(\lambda) \\ &= \varepsilon + \sum_{j=1}^{N_t} c_j \text{sgn}[\lambda - (\mu + h_{ij})] && \text{if } \lambda \neq h_{ij} + \mu \\ &= \varepsilon + \sum_{j \neq k_0} c_j \text{sgn}[\lambda - (\mu + h_{ij})] + c_{k_0}[-1, 1] && \text{if } \lambda = h_{ik_0} + \mu \end{aligned}$$

If $\varepsilon \geq \sum_{j=1}^{N_t} c_j$, ϕ_μ is always increasing and the minimum is attained at $\lambda_\mu^* = 0$.In our case, we suppose ε number and this condition is not true, then we note m the index such that:

$$\begin{aligned} &\varepsilon + \sum_{j=1}^{m-1} c_j - \sum_{j=m}^{N_t} c_j < 0 \text{ AND } \varepsilon + \sum_{j=1}^{m} c_j - \sum_{j=m+1}^{N_t} c_j \geq 0 \\ &0 \in \partial\phi_\mu(\mu + h_{im}) \end{aligned}$$

We obtain de following cases:

- *Case 1,* $\mu \geq -h_{im}$*:* Then, $\lambda_\mu^* = \mu + h_{im}$ and $p^*(\mu) = \varepsilon(\mu + h_{im}) + \sum_{j=1}^{N_t} c_j|h_{im} - h_{ij}|$.
- *Case 2,* $\mu < -h_{im}$*:* Then, $\lambda_\mu^* = 0$, and $p^*(\mu) = \sum_{j=1}^{N_t} c_j|(\mu + h_{ij})|$

Now, we perform the minimization over $\mu \geq 0$:

$$\begin{aligned} \zeta(\mu) =& p^*(\mu) + \varepsilon\mu \\ =& \begin{cases} \sum_{j=1}^{N_t} c_j|(\mu + h_{ij})| + \varepsilon\mu & \text{on } [-\infty, -h_{im}[\\ 2\varepsilon\mu + \varepsilon h_{im} + \sum_{j=1}^{N_t} c_j|h_{im} - h_{ij}| & \text{on } [-h_{im}, +\infty] \end{cases} \end{aligned}$$

ζ is continuous and

$$\partial\zeta(\mu) = \begin{cases} \varepsilon + \sum_{j=1}^{N_t} c_j \text{sgn}[(\mu + h_{ij})] & \text{on } [-\infty, -h_{im}[\\ \varepsilon + \sum_{j \neq h_{ik_0}} c_j \text{sgn}[(\mu + h_{ij})] + c_{k_0}[-1,1], & \mu = -h_{ik_0} < -h_{im} \\ 2\varepsilon & \text{on } [-h_{im}, +\infty] \end{cases}$$

We note r, the index such that:

$$\varepsilon - \sum_{j=1}^{r-1} c_j + \sum_{j=r}^{N_t} c_j \geq 0 \text{ AND } \varepsilon - \sum_{j=1}^{r} c_j + \sum_{j=r-1}^{N_t} c_j < 0$$
$$0 \in \partial\zeta(-h_{ir}) \text{ if } h_{ir} \geq h_{im}$$

We obtain the following values for the minimum v^*:

- *Case 1:* $h_{im} \geq 0$*:*
  $\mu^* = 0$, $\lambda^* = h_{im}$, $v^* = \varepsilon h_{im} + \sum_{j=1}^{N_t} c_j |h_{im} - h_{ij}|$.
  $y_j^* = \text{sgn}(h_{ij} - h_{im}) c_j$ if $j \neq m$,
  $y_m^* = \varepsilon - \sum_{j=1}^{N_t} \text{sgn}(h_{ij} - h_{im}) c_j$
- *Case 2:* $h_{im} < 0, h_{im} \leq h_{ir} < 0$*:*
  $\mu^* = -h_{ir}$, $\lambda^* = 0$, $v^* = -\varepsilon h_{ir} + \sum_{j=1}^{N_t} c_j |h_{ir} - h_{ij}|$.
  $y_j^* = \text{sgn}(h_{ij} - h_{ir}) c_j$ if $j \neq r$,
  $y_r^* = -\varepsilon - \sum_{j=1}^{N_t} \text{sgn}(h_{ij} - h_{ir}) c_j$
- *Case 3: otherwise:*
  $\mu^* = 0$, $\lambda^* = 0$, $v^* = \sum_{j=1}^{N_t} c_j |h_{ij}|$.
  $y_j^* = \text{sgn}(h_{ij}) c_j$

To summarize, y^* can take $2N_t + 1$ values as follows:

$$y^* = \Gamma c + \beta \text{ where}$$
$$\exists m \text{ st } \begin{cases} \gamma_{jj} = \text{sgn}(h_{ij} - h_{im}), \beta_j = 0 \text{ for } j \neq m, \\ \gamma_{mj} = -\text{sgn}(h_{ij} - h_{im}), \beta_m = \varepsilon \text{ for } j \neq m, \\ \gamma_{lk} = 0 \text{ otherwise} \end{cases}$$
$$\text{or } \exists r \text{ st } \begin{cases} \gamma_{jj} = \text{sgn}(h_{ij} - h_{ir}), \beta_j = 0 \text{ for } j \neq r, \\ \gamma_{rj} = -\text{sgn}(h_{ij} - h_{ir}), \beta_r = -\varepsilon \text{ for } j \neq r, \\ \gamma_{lk} = 0 \text{ otherwise} \end{cases}$$
$$\text{or } \gamma_{jj} = \text{sgn}(h_{ij}),\ \gamma_{lj} = 0,\ \beta_j = 0\ \forall i, j \text{ st } i \neq j$$

The annex shows that the solution to the LP (2.65b) can take $2N_t+1$ different values $y_k^* = \Gamma_k c + \beta_k$, $k \in [1, 2N_t+1]$ where Γ_k, β_k (see the annex).

$$
\begin{aligned}
& y^* = \Gamma c + \beta \text{ where} \\
& \exists m \text{ st } \begin{cases} \gamma_{jj} = \text{sgn}(h_{ij} - h_{im}), \beta_j = 0 \text{ for } j \neq m, \\ \gamma_{mj} = -\text{sgn}(h_{ij} - h_{im}), \beta_m = \varepsilon \text{ for } j \neq m, \\ \gamma_{lk} = 0 \text{ otherwise} \end{cases} \qquad \text{(B.5a)} \\
& \text{OR} \\
& \exists r \text{ st } \begin{cases} \gamma_{jj} = \text{sgn}(h_{ij} - h_{ir}), \beta_j = 0 \text{ for } j \neq r, \\ \gamma_{rj} = -\text{sgn}(h_{ij} - h_{ir}), \beta_r = -\varepsilon \text{ for } j \neq r, \\ \gamma_{lk} = 0 \text{ otherwise} \end{cases} \qquad \text{(B.5b)} \\
& \text{OR} \\
& \gamma_{jj} = \text{sgn}(h_{ij}),\ \gamma_{lj} = 0,\ \beta_j = 0\ \forall i, j \text{ st } i \neq j \qquad \text{(B.5c)}
\end{aligned}
$$

We can derive simplified feasibility conditions for solutions (B.5). We define v_i^*, the maximum of LP (2.65b). If y_k^*, then v_i^* is higher than $\sum_j h_{ij} y_j^*$. This can be summarized as follows:

$$
\begin{aligned}
\text{(B.5a) is feasible} \quad & \Leftrightarrow \begin{cases} \sum_{j=1}^{N_t} \text{sgn}(h_{im} - h_{ij}) c_j - c_m \leq -\varepsilon \\ \sum_{j=1}^{N_t} \text{sgn}(h_{im} - h_{ij}) c_j + c_m \geq -\varepsilon \end{cases} \\
& \Rightarrow v_i^* \geq \varepsilon h_{im} + \sum_{j=1}^{N_t} c_j |h_{im} - h_{ij}| \\
\text{(B.5b) is feasible} \quad & \Leftrightarrow \begin{cases} \sum_{j=1}^{N_t} \text{sgn}(h_{ir} - h_{ij}) c_j - c_r \leq \varepsilon \\ \sum_{j=1}^{N_t} \text{sgn}(h_{ir} - h_{ij}) c_j + c_r \geq \varepsilon \end{cases} \\
& \Rightarrow v_i^* \geq -\varepsilon h_{ir} + \sum_{j=1}^{N_t} c_j |h_{ir} - h_{ij}| \\
\text{(B.5c) is feasible} \quad & \Leftrightarrow \begin{cases} \sum_{j=1}^{N_t} \text{sgn}(h_{ij}) c_j \leq \varepsilon \\ \sum_{j=1}^{N_t} \text{sgn}(h_{ij}) c_j \geq -\varepsilon \end{cases} \\
& \Rightarrow v_i^* \geq \sum_{j=1}^{N_t} c_j |h_{ij}|
\end{aligned}
$$

The above statements form a set of conditional constraints, which can be modeled by introducing

integer variables [17]. δ is a small deviation and L is a large number.

$$\begin{cases} \sum_{j=1}^{N_t} \text{sgn}(h_{ij}) c_j \leq \varepsilon \\ \sum_{j=1}^{N_t} \text{sgn}(h_{ij}) c_j \geq -\varepsilon \end{cases} \Rightarrow v_i^* \geq \sum_{j=1}^{N_t} c_j |h_{ij}|$$

$$\Leftrightarrow \begin{cases} \sum_{j=1}^{N_t} \text{sgn}(h_{ij}) c_j \leq \varepsilon \\ \sum_{j=1}^{N_t} \text{sgn}(h_{ij}) c_j \geq -\varepsilon \end{cases} \text{false} \quad \text{OR} \quad v_i^* \geq \sum_{j=1}^{N_t} c_j |h_{ij}|$$

$$\Leftrightarrow \begin{cases} \sum_{j=1}^{N_t} \text{sgn}(h_{ij}) c_j > \varepsilon + \delta - Lx \\ \sum_{j=1}^{N_t} \text{sgn}(h_{ij}) c_j < -\varepsilon - \delta + Lz \\ v_i^* \geq \sum_{j=1}^{N_t} c_j |h_{ij}| - L(2-(x+z)) \\ x, z \in \{0,1\};\ x+z \geq 1 \end{cases}$$

Finally, the problem can be written as a Mixed Integer Linear Program:

$$\max_{C, v^*, z, x} \quad \lambda^T C \tag{B.6a}$$

$$\text{st} \quad \forall i \in \{1, ..., N_t\}, k \in \{1, ..., 2N_t + 1\} \tag{B.6b}$$

$$\sum_{j=1}^{N_t} \overline{\alpha_{ij}^k} c_j > \overline{\theta_i^k} + \delta - L_i^k x_i^k \tag{B.6c}$$

$$\sum_{j=1}^{N_t} \underline{\alpha_{ij}^k} c_j < \underline{\theta_i^k} - \delta + L_i^k z_i^k \tag{B.6d}$$

$$v_i^* \geq v_i^k - L(2 - (x_i^k + z_i^k)) \tag{B.6e}$$

$$x_i^k, z_i^k \in \{0,1\};\ x_i^k + z_i^k \geq 1 \tag{B.6f}$$

$$v_i^* \leq b_i \tag{B.6g}$$

Appendix C

Proof of Plug & Play recursive feasibility

Assume that the problem is feasible at time k, with the optimal control sequence $U^*(k) = \{u^*(k), u^*(k+1), ..., u^*(k$ and the predicted state trajectory $X^*(k) = \{x^*(k+1), ..., x^*(k+N-1), x^*(k+N)\}$. Then, at time $k+1$, we show that the control sequence $U^*(k+1) = \{u^*(k+1), u^*(k+2), ..., u^*(k+N-1), v(k+N)\}$ is feasible where $v(k+N)$ is defined by Equations (4.25), (4.26), (4.27). The state trajectory at time $k+1$ is $X^*(k+1) = \{x^*(k+2), ..., x^*(k+N), x(k+N+1)\}$, where $x(k+N+1)$ is derived in the next sections. With the notations in Section 4.2.5:

$$\begin{aligned} x^*(k+N) &= \left[x_1(k+N), x_2(k+N)\right]^T \\ &= \left[(e_1^{shp}, \ldots, e_{M^{shp}}^{shp}), (e_1^{bat} \ldots, e_n^{bat})\right]^T (N) \\ x(k{+}N{+}1) &= \left[x_1(k{+}N{+}1), x_2(k{+}N{+}1)\right]^T \\ v(k+N) &= \left[q^g(k+N)\ u^{shp}(k+N)\ p^{bat}(k+N)\right]^T \end{aligned}$$

And $v(k+N)$ is defined by the following control values:

$$c_j^{shp}(k{+}N) = \frac{e_{des,j}^{shp} - e_j^{shp}(k+N)}{(k_j^{out} - (k+N))\eta\Delta T} 1_{(k+N)<k_j^{out}}$$

$$j \in \{1, ..., M^{shp}\}$$

$$q_i(k{+}N) = \hat{q}_i(k{+}N) \quad i \in \{1, ..., n\}$$

$$p_i^{bat}(k{+}N) = [\hat{p}_i{}^{bat}(k{+}N) - p_i^{def}(k{+}N) - p_i^{shp}(k{+}N)]$$

In the remainder of this section, we derive $x(k+N+1)$ and prove that the solution is feasible.

C.0.1 Shapeable loads state of charge

Let consider $j \in \{1,...,M^{shp}\}$:

$$\begin{aligned} e_j^{shp}(k+N+1) &= e_j^{shp}(k+N) + \eta \Delta T c_j^{shp}(k+N) \\ &= e_j^{shp}(k+N) \\ &\quad + \eta \Delta T \frac{e_{des,j}^{shp} - e_j^{shp}(k+N)}{(k_j^{out} - (k+N))\eta \Delta T} 1_{(k+N) \leq k_j^{out}} \end{aligned}$$

At time $k+N$:

$$\begin{aligned} e_j^{shp}(k+N) &\geq e_{des,j}^{shp} \text{ - } \max(0, \eta \Delta T (k_j^{out} \text{ - } (k+N) c_{max,j}^{shp}) \\ e_j^{shp}(k+N) &\geq e_{min,j}^{shp} \end{aligned}$$

Thus, we obtain the following condition at time $k+N+1$, which ensures recursive feasibility of the terminal constraint for shapeable loads e_j^{shp}:

$$e_j^{shp}(k+N+1) \geq e_j^{shp}(k+N) \geq e_{min,j}^{shp} \tag{C.1}$$

If $N < k_j^{out}$

$$\begin{aligned} & e_{des,j}^{shp} - e_j^{shp}(k+N+1) \\ & = e_{des,j}^{shp} - (e_j^{shp}(k+N) + \frac{e_{des,j}^{shp} - e_j^{shp}(k+N)}{(k_j^{out} - (k+N))} \\ & = \Big(e_{des,j}^{shp} - e_j^{shp}(k+N)\Big)(1 - \frac{1}{k_j^{out} - k - N}) \\ & \leq \eta \Delta T (k^{out} - k - N) c_{max,j}^{shp} \frac{k_j^{out} - (k+N+1)}{k^{out} - N} \\ & \leq \eta \Delta T \Big(k^{out} - (k+N+1)\Big) c_{max,j}^{shp} \end{aligned} \tag{C.2}$$

Moreover:

$$e_{des,j}^{shp} - e_j^{shp}(k+N+1) \geq 0 \text{ since } k_j^{out} - (k+N) \geq 1$$

If $N \geq k^{out}$

$$e_j^{shp}(k+N+1) = e_j^{shp}(k+N) \geq e_{des,j}^{shp} \tag{C.3}$$

$$\leq e_{des,j}^{shp} \tag{C.4}$$

C.0.2 Network constraints

Consider a node $i \in \{1,...,n\}$. Equations (4.26), (4.27) give:
$\begin{cases} q_i(k+N) = \hat{q}_i(k+N) \\ p_i^{bat}(k+N) = \hat{p}_i{}^{bat}(k+N) - p_i^{def}(k+N) - p_i^{shp}(k+N) \end{cases}$
Equation (4.7a) gives:

$$\begin{aligned} P_{ij}(k+N) &= p_j^l(k+N) + \hat{p}_j{}^{bat}(k+N) + r_{ij} l_{ij}(k+N) \\ &+ \sum_{m:(j,m)\in\mathscr{L}} P_{jm}(k+N) \end{aligned}$$

Equation (4.7b), (4.7c) and (4.8) give:

$$\begin{aligned} Q_{ij}(k+N) &= q_j^l(k+N) - \hat{q}_j^g(k+N) + x_{ij} l_{ij}(k+N) \\ &+ \sum_{k:(j,m)\in\mathscr{L}} Q_{jm}(k+N) \\ v_j(k+N) &= v_i(k+N) + (r_{ij}^2 + x_{ij}^2) l_{ij} \\ &- 2(r_{ij} P_{ij}(k+N) + x_{ij} Q_{ij}) \\ l_{ij}(k+N) &\geq \frac{P_{ij}^2(k+N) + Q_{ij}^2(k+N)}{v_i(k+N)} \end{aligned}$$

This is the system of power flow equations for $(p,q) = (\hat{p},\hat{q})$. Thus it is feasible and the voltage bounds are satisfied:

$$v_{min} \leq v(k+N) \leq v_{max}$$

C.0.3 Battery banks

The power constraint and terminal constraint for the SOC of battery banks must be satisfied. By induction, we show that $\forall l \in [k+N, k_{max}^{out}]$:

$$e_i^{bat}(l) = \hat{e}_i^{bat}(l) + \sum_{m=l}^{k_{max}^{out}} \Delta T [p_i^{def} + \tilde{p}_i^{shp}](m) \tag{C.5}$$

By definition of the terminal set, this is true at time $k+N$. Now, suppose it is true at time $l \in [k+N, k_{max}^{out}]$, then:

$$\begin{aligned} e_i^{bat}(l+1) &= e_i^{bat}(l) + \Delta T\, p_i^{bat}(l) \\ &= e_i^{bat}(l) + \Delta T [\hat{p}_i{}^{bat}(l) - p_i^{def}(l) - \tilde{p}_i^{shp}(l)] \\ &= \hat{e}_i^{bat}(l) + \sum_{m=l}^{k_{max}^{out}} \Delta T [p_i^{def}(m) + \tilde{p}_i^{shp}(m)] \end{aligned}$$

$$
\begin{aligned}
&+\Delta T[\hat{p}_i^{bat}(l)\text{- } p^{def}(l)\text{- } \tilde{p}^{shp}(l)] \\
&= \hat{e}_i^{bat}(l+1) + \sum_{m=l+1}^{k_{max}^{out}} \Delta T[p_i^{def}(m) + \tilde{p}_i^{shp}(m)]
\end{aligned}
$$

This is Eq. (C.5) at time $l+1$, proving that (C.5) holds by induction. Now, Eq. (C.5) at time $k+N+1$ gives:

$$
\begin{aligned}
e_i^{bat}(k+N+1) &= \hat{e}_i^{bat}(k+N+1) \\
&\quad + \sum_{l=k+N+1}^{k_{max}^{out}} \Delta T[p_i^{def}(l) + \tilde{p}_i^{shp}(l)]
\end{aligned}
$$

Thus $e_i^{bat}(k+N+1) \geq \hat{e}_i^{bat}(k+N+1) \geq e_{i,min}^{bat}$ and Assumption (4.23) gives $e_i^{bat}(k+N+1) \leq e_{i,max}^{bat}$. Moreover,

$$
\begin{aligned}
p_i^{bat}(k+N) &= [\hat{p}_i^{bat}(k+N)\text{- } p_i^{def}(k+N)\text{- } p_i^{shp}(k+N)] \\
&\leq p_i^{bat}(k+N) \leq p_{i,max}^{bat}
\end{aligned}
$$

and condition (4.24) gives $p_i^{bat}(k+N) \geq p_{i,min}^{bat}$.
This concludes the proof of recursive feasibility.

Bibliography

[1] Mar. 2017. URL: https://energy.gov/oe/services/technology-development/smart-grid.

[2] COMPETES Act. "The American Recovery and Reinvestment Act of 2009". In: (2011).

[3] Anna Alberini, Will Gans, and Daniel Velez-Lopez. "Residential consumption of gas and electricity in the US: The role of prices and income". In: *Energy Economics* 33.5 (2011), pp. 870–881.

[4] Adrian Albert and Mehdi Maasoumy. "Predictive segmentation of energy consumers". In: *Applied Energy* 177 (2016), pp. 435–448.

[5] Adrian Albert and Ram Rajagopal. "Smart meter driven segmentation: What your consumption says about you". In: *IEEE Transactions on Power Systems* 28.4 (2013), pp. 4019–4030.

[6] Susan Athey and Guido W Imbens. "Identification and inference in nonlinear difference-in-differences models". In: *Econometrica* 74.2 (2006), pp. 431–497.

[7] Somil Bansal, Melanie N Zeilinger, and Claire J Tomlin. "Plug-and-play model predictive control for electric vehicle charging and voltage control in smart grids". In: *Conference on Decision and Control*. 2014.

[8] M. E. Baran and F. F. Wu. "Optimal capacitor placement on radial distribution systems". In: *IEEE Trans. on Power Delivery* 4.1 (1989), pp. 725–734.

[9] M. E. Baran and F. F. Wu. "Optimal sizing of capacitors placed on a radial distribution system". In: *IEEE Trans. on Power Delivery* 4.1 (1989), pp. 735–743.

[10] Philip P Barker and Robert W De Mello. "Determining the impact of distributed generation on power systems. I. Radial distribution systems". In: *Power Engineering Society Summer Meeting, 2000. IEEE*. Vol. 3. IEEE. 2000, pp. 1645–1656.

[11] S. Bashash and H.K. Fathy. "Modeling and control insights into demand-side energy management through setpoint control of thermostatic loads". In: *American Control Conference (ACC), 2011*. June 2011, pp. 4546–4553. DOI: 10.1109/ACC.2011.5990939.

[12] S. Bashash and H.K. Fathy. "Transport-Based Load Modeling and Sliding Mode Control of Plug-In Electric Vehicles for Robust Renewable Power Tracking". In: *IEEE Transactions on Smart Grid* 3.1 (Mar. 2012), pp. 526–534. ISSN: 1949-3053. DOI: 10.1109/TSG.2011.2167526.

[13] Moshe E Ben-Akiva and Steven R Lerman. *Discrete choice analysis: theory and application to travel demand*. Vol. 9. MIT press, 1985.

[14] Dimitri P Bertsekas. *Nonlinear programming*.

[15] R.J. Bessa et al. "Optimized Bidding of a EV Aggregation Agent in the Electricity Market". In: *Smart Grid, IEEE Transactions on* 3.1 (Mar. 2012), pp. 443–452. ISSN: 1949-3053. DOI: 10.1109/TSG.2011.2159632.

[16] Michel Bierlaire. "BIOGEME: a free package for the estimation of discrete choice models". In: *Swiss Transport Research Conference*. TRANSP-OR-CONF-2006-048. 2003.

[17] Johannes Bisschop. *AIMMS optimization modeling*. Lulu. com, 2006.

[18] Andrew Blake, Pushmeet Kohli, and Carsten Rother. *Markov random fields for vision and image processing*. Mit Press, 2011.

[19] Stephen Boyd and Lieven Vandenberghe. *Convex optimization*. Cambridge university press, 2004.

[20] Edmund G. Brown. *ZEV action plan*. Tech. rep. Feb. 2013.

[21] CAISO. *Day-Ahead Daily Market Watch Aug 22 2014*. URL: http://www.caiso.com/Documents/Day-AheadDailyMarketWatchAug222014.pdf.

[22] CAISO. *What the Duck Curve tells us about managing a green grid*. URL: http://www.caiso.com.

[23] D.S. Callaway and I.A. Hiskens. "Achieving Controllability of Electric Loads". In: *Proceedings of the IEEE* 99.1 (Jan. 2011), pp. 184–199. DOI: 10.1109/JPROC.2010.2081652.

[24] Yijia Cao et al. "An optimized EV charging model considering TOU price and SOC curve". In: *IEEE Transactions on Smart Grid* 3.1 (2012), pp. 388–393.

[25] Tsung-Hui Chang, Angelia Nedic, and Anna Scaglione. "Distributed constrained optimization by consensus-based primal-dual perturbation method". In: *Automatic Control, IEEE Transactions on* 59.6 (2014), pp. 1524–1538.

[26] Niangjun Chen, Chee Wei Tan, and Tony QS Quek. "Electric vehicle charging in smart grid: Optimality and valley-filling algorithms". In: *Selected Topics in Signal Processing, IEEE Journal of* 8.6 (2014), pp. 1073–1083.

[27] Gianfranco Chicco et al. "Load pattern-based classification of electricity customers". In: *IEEE Transactions on Power Systems* 19.2 (2004), pp. 1232–1239.

[28] Steven Chu and Arun Majumdar. "Opportunities and challenges for a sustainable energy future". In: *nature* 488.7411 (2012), pp. 294–303.

[29] K. Clement, E. Haesen, and J. Driesen. "Coordinated charging of multiple plug-in hybrid electric vehicles in residential distribution grids". In: *Power Systems Conference and Exposition, 2009. PSCE '09. IEEE/PES*. Mar. 2009, pp. 1–7. DOI: 10.1109/PSCE.2009.4839973.

[30] Patrick L Combettes and Jean-Christophe Pesquet. "Proximal splitting methods in signal processing". In: *Fixed-point algorithms for inverse problems in science and engineering*. Springer, 2011, pp. 185–212.

[31] Litos Strategic Communication. *The SMART GRID: an introduction.* US Department Of Energy.

[32] Andrew R Conn, Nicholas IM Gould, and Philippe L Toint. *Trust region methods*. SIAM, 2000.

[33] Sara Deilami et al. "Real-time coordination of plug-in electric vehicle charging in smart grids to minimize power losses and improve voltage profile". In: *IEEE Transactions on Smart Grid* 2.3 (2011), pp. 456–467.

[34] F Delfino et al. "A multilevel approach for the optimal control of distributed energy resources and storage". In: *IEEE Transactions on Smart Grid* 5.4 (2014), pp. 2155–2162.

[35] Stephan Dempe. *Foundations of bilevel programming*. Springer Science & Business Media, 2002.

[36] Ming Dong et al. "Non-intrusive signature extraction for major residential loads". In: *IEEE Transactions on Smart Grid* 4.3 (2013), pp. 1421–1430.

[37] PG & E. *http://www.pge.com/en/mybusiness/rates/tvp/toupricing.page*.

[38] Erik Ela, Michael Milligan, and Brendan Kirby. "Operating reserves and variable generation". In: *Contract* 303 (2011), pp. 275–3000.

[39] Omar Ellabban, Haitham Abu-Rub, and Frede Blaabjerg. "Renewable energy resources: Current status, future prospects and their enabling technology". In: *Renewable and Sustainable Energy Reviews* 39 (2014), pp. 748–764.

[40] M. Farivar, L. Chen, and S. Low. "Equilibrium and dynamics of local voltage control in distribution systems". In: *52nd IEEE Annual Conference on Decision and Control (CDC), 2013*, pp. 4329–4334.

[41] Masoud Farivar and Steven H Low. "Branch flow model: Relaxations and convexification—Part I". In: *IEEE Transactions on Power Systems* 28.3 (2013), pp. 2554–2564.

[42] M. Farivar et al. "Inverter VAR control for distribution systems with renewables". In: *IEEE International Conference on Smart Grid Communications, 2011*, pp. 457–462.

[43] Ahmad Faruqui and Sanem Sergici. "Dynamic pricing of electricity in the mid-Atlantic region: econometric results from the Baltimore gas and electric company experiment". In: *Journal of regulatory economics* 40.1 (2011), pp. 82–109.

[44] Ahmad Faruqui and Sanem Sergici. "Household response to dynamic pricing of electricity: a survey of 15 experiments". In: *Journal of regulatory Economics* 38.2 (2010), pp. 193–225.

[45] Ahmad Faruqui, Sanem Sergici, and Ahmed Sharif. "The impact of informational feedback on energy consumption—A survey of the experimental evidence". In: *Energy* 35.4 (2010), pp. 1598–1608.

[46] Vera Figueiredo et al. "An electric energy consumer characterization framework based on data mining techniques". In: *IEEE Transactions on power systems* 20.2 (2005), pp. 596–602.

[47] Lingwen Gan, Ufuk Topcu, and Steven H Low. "Optimal decentralized protocol for electric vehicle charging". In: *IEEE Transactions on Power Systems* 28.2 (2013), pp. 940–951.

[48] Lingwen Gan, Ufuk Topcu, and Steven H Low. "Stochastic distributed protocol for electric vehicle charging with discrete charging rate". In: *Power and Energy Society General Meeting, 2012 IEEE*. IEEE. 2012, pp. 1–8.

[49] James Newcomb Garrett Fitzgerald Chris Nelder. *ELECTRIC VEHICLES AS DISTRIBUTED ENERGY RESOURCES*. Rocky Mountain Institute. 2016.

[50] C. W. Gellings. *The smart grid: enabling energy efficiency and demand response*. The Fairmont Press, Inc., 2009.

[51] Alessandro Di Giorgio, Francesco Liberati, and Silvia Canale. "Electric vehicles charging control in a smart grid: A model predictive control approach". In: *Control Engineering Practice* 22 (2014), pp. 147–162. ISSN: 0967-0661. DOI: http://dx.doi.org/10.1016/j.conengprac.2013.10.005. URL: http://www.sciencedirect.com/science/article/pii/S0967066113001871.

[52] M. Gonzalez Vaya and G. Andersson. "Optimal Bidding Strategy of a Plug-In Electric Vehicle Aggregator in Day-Ahead Electricity Markets Under Uncertainty". In: *Power Systems, IEEE Transactions on* 30.5 (Sept. 2015), pp. 2375–2385. ISSN: 0885-8950. DOI: 10.1109/TPWRS.2014.2363159.

[53] João Pedro Gouveia and Júlia Seixas. "Unraveling electricity consumption profiles in households through clusters: Combining smart meters and door-to-door surveys". In: *Energy and Buildings* 116 (2016), pp. 666–676.

[54] Sekyung Han, Soohee Han, and Kaoru Sezaki. "Estimation of achievable power capacity from plug-in electric vehicles for V2G frequency regulation: Case studies for market participation". In: *IEEE Transactions on Smart Grid* 2.4 (2011), pp. 632–641.

[55] Yifeng He, Bala Venkatesh, and Ling Guan. "Optimal scheduling for charging and discharging of electric vehicles". In: *IEEE Transactions on Smart Grid* 3.3 (2012), pp. 1095–1105.

[56] Jing Hu et al. "On the global solution of linear programs with linear complementarity constraints". In: *SIAM Journal on Optimization* 19.1 (2008), pp. 445–471.

[57] Junjie Hu et al. “Coordinated Charging of Electric Vehicles for Congestion Prevention in the Distribution Grid”. In: *IEEE Transactions on Smart Grid* 5.2 (2014), pp. 703–711. ISSN: 1949-3053. DOI: 10.1109/TSG.2013.2279007.

[58] Sikai Huang and David Infield. “The impact of domestic Plug-in Hybrid Electric Vehicles on power distribution system loads”. In: *Power System Technology (POWERCON), 2010 International Conference on*. IEEE. 2010, pp. 1–7.

[59] Katrina Jessoe and David Rapson. “Commercial and Industrial Demand Response Under Mandatory Time-of-Use Electricity Pricing”. In: *The Journal of Industrial Economics* 63.3 (2015), pp. 397–421.

[60] Katrina Jessoe, David Rapson, and Jeremy B Smith. “Towards understanding the role of price in residential electricity choices: Evidence from a natural experiment”. In: *Journal of Economic Behavior & Organization* 107 (2014), pp. 191–208.

[61] Emre C. Kara et al. “Estimating the benefits of electric vehicle smart charging at non-residential locations: A data-driven approach”. In: *Applied Energy* 155 (2015), pp. 515–525. ISSN: 0306-2619. DOI: http://dx.doi.org/10.1016/j.apenergy.2015.05.072.

[62] Willett Kempton and Jasna Tomić. “Vehicle-to-grid power fundamentals: Calculating capacity and net revenue”. In: *Journal of power sources* 144.1 (2005), pp. 268–279.

[63] Willett Kempton and Jasna Tomić. “Vehicle-to-grid power implementation: From stabilizing the grid to supporting large-scale renewable energy”. In: *Journal of Power Sources* 144.1 (2005), pp. 280–294.

[64] Willett Kempton et al. “A test of vehicle-to-grid (V2G) for energy storage and frequency regulation in the PJM system”. In: *Results from an Industry-University Research Partnership* (2008), p. 32.

[65] Michael Kintner-Meyer, Kevin Schneider, and Robert Pratt. “Impacts assessment of plug-in hybrid vehicles on electric utilities and regional US power grids, Part 1: Technical analysis”. In: *Pacific Northwest National Laboratory* (2007), pp. 1–20.

[66] J Zico Kolter and Matthew J Johnson. “REDD: A public data set for energy disaggregation research”. In: *Workshop on Data Mining Applications in Sustainability (SIGKDD), San Diego, CA*. Vol. 25. Citeseer. 2011, pp. 59–62.

[67] Jungsuk Kwac, June Flora, and Ram Rajagopal. “Household energy consumption segmentation using hourly data”. In: *IEEE Transactions on Smart Grid* 5.1 (2014), pp. 420–430.

[68] Jungsuk Kwac, June Flora, and Ram Rajagopal. “Lifestyle segmentation based on energy consumption data”. In: *IEEE Transactions on Smart Grid* ().

[69] A. Langton and N. Crisostomo. *Vehicle-Grid Integration: A Vision for Zero-Emission Transportation Interconnected throughout California’s Electricity System*. Tech. rep. California Public Utilities Commission.

[70] Caroline Le Floch, Francois Belletti, and Scott Moura. "Optimal Charging of Electric Vehicles for Load Shaping: a Dual Splitting Framework with Explicit Convergence Bounds". In: *IEEE Transactions on Transportation Electrification* (2016).

[71] Caroline Le Floch, Florent Di Meglio, and Scott Moura. "Optimal Charging of Vehicle-to-Grid Fleets via PDE Aggregation Techniques". In: *American Control Conference* (2015).

[72] Caroline Le Floch et al. "Distributed Optimal Charging of Electric Vehicles for Demand Response and Load Shaping". In: *54th Annual Conference on Decision and Control*. 2015.

[73] Caroline Le Floch et al. "Distributed optimal charging of electric vehicles for demand response and load shaping". In: *2015 54th IEEE Conference on Decision and Control (CDC)*. IEEE. 2015, pp. 6570–6576.

[74] Rong-Ceng Leou, Chun-Lien Su, and Chan-Nan Lu. "Stochastic analyses of electric vehicle charging impacts on distribution network". In: *IEEE Transactions on Power Systems* 29.3 (2014), pp. 1055–1063.

[75] Randall J LeVeque. *Finite volume methods for hyperbolic problems*. Vol. 31. Cambridge university press, 2002.

[76] Chiao-Ting Li et al. "Synergistic control of plug-in vehicle charging and wind power scheduling". In: *IEEE Transactions on Power Systems* 28.2 (May 2013), pp. 1113–1121. ISSN: 0885-8950. DOI: 10.1109/TPWRS.2012.2211900.

[77] Zhengshuo Li et al. "Storage-like devices in load leveling: Complementarity constraints and a new and exact relaxation method". In: *Applied Energy* 151 (2015), pp. 13–22.

[78] Tim Futing Liao. *Interpreting probability models: Logit, probit, and other generalized linear models*. 101. Sage, 1994.

[79] Y Liu et al. "Distribution system voltage performance analysis for high-penetration PV". In: *Energy 2030 Conference, 2008. ENERGY 2008. IEEE*. IEEE. 2008, pp. 1–8.

[80] JA Pecas Lopes et al. "Integrating distributed generation into electric power systems: A review of drivers, challenges and opportunities". In: *Electric power systems research* 77.9 (2007), pp. 1189–1203.

[81] João A Peças Lopes, Filipe Joel Soares, and Pedro M Rocha Almeida. "Integration of electric vehicles in the electric power system". In: *Proceedings of the IEEE* 99.1 (2011), pp. 168–183.

[82] H. Lund and W. Kempton. "Integration of renewable energy into the transport and electricity sectors through V2G". In: *Energy policy* 36.9 (2008), pp. 3578–3587.

[83] Zhi-Quan Luo, Jong-Shi Pang, and Daniel Ralph. *Mathematical programs with equilibrium constraints*. Cambridge University Press, 1996.

[84] Wann-Jiun Ma, Vijay Gupta, and Ufuk Topcu. "On distributed charging control of electric vehicles with power network capacity constraints". In: *American Control Conference (ACC), 2014*. IEEE. 2014, pp. 4306–4311.

[85] Wann-Jiun Ma, Vijay Gupta, and Ufuk Topcu. "On distributed charging control of electric vehicles with power network capacity constraints". In: *2014 American Control Conference*. IEEE. 2014, pp. 4306–4311.

[86] Zhongjing Ma, Duncan S Callaway, and Ian A Hiskens. "Decentralized charging control of large populations of plug-in electric vehicles". In: *IEEE Transactions on Control Systems Technology* 21.1 (2013), pp. 67–78.

[87] Zhongjing Ma, Duncan Callaway, and Ian Hiskens. "Decentralized charging control for large populations of plug-in electric vehicles". In: *49th IEEE conference on decision and control (CDC)*. IEEE. 2010, pp. 206–212.

[88] Johanna L Mathieu, Stephan Koch, and Duncan S Callaway. "State estimation and control of electric loads to manage real-time energy imbalance". In: *IEEE Transactions on Power Systems* 28.1 (2013), pp. 430–440.

[89] Omid Motlagh, Greg Foliente, and George Grozev. "Knowledge-mining the Australian smart grid smart city data: A statistical-neural approach to demand-response analysis". In: *Planning Support Systems and Smart Cities*. Springer, 2015, pp. 189–207.

[90] Yuting Mou et al. "Decentralized Optimal Demand-Side Management for PHEV Charging in a Smart Grid". In: *IEEE Transactions on Smart Grid,* 6.2 (2015), pp. 726–736.

[91] Scott J Moura, Jeffrey L Stein, and Hosam K Fathy. "Battery-health conscious power management in plug-in hybrid electric vehicles via electrochemical modeling and stochastic control". In: *IEEE Transactions on Control Systems Technology* 21.3 (2013), pp. 679–694.

[92] Scott Moura, Jan Bendtsen, and Victor Ruiz. "Parameter identification of aggregated thermostatically controlled loads for smart grids using PDE techniques". In: *International Journal of Control* 87.7 (2014), pp. 1373–1386. DOI: 10.1080/00207179.2014.915083.

[93] Arkadi Nemirovski et al. "Robust stochastic approximation approach to stochastic programming". In: *SIAM Journal on Optimization* 19.4 (2009), pp. 1574–1609.

[94] *NERC operating manual*. URL: http://www.nerc.com.

[95] Yurii Nesterov et al. *Gradient methods for minimizing composite objective function*. 2007.

[96] Sheila Nolan and Mark O'Malley. "Challenges and barriers to demand response deployment and evaluation". In: *Applied Energy* 152 (2015), pp. 1–10.

[97] Peter Palensky and Dietmar Dietrich. "Demand side management: Demand response, intelligent energy systems, and smart loads". In: *IEEE Transactions on Industrial Informatics* 7.3 (2011), pp. 381–388.

[98] Michael Angelo A Pedrasa, Ted D Spooner, and Iain F MacGill. "Coordinated scheduling of residential distributed energy resources to optimize smart home energy services". In: *IEEE Transactions on Smart Grid* 1.2 (2010), pp. 134–143.

[99] Fabian Pedregosa et al. "Scikit-learn: Machine learning in Python". In: *Journal of Machine Learning Research* 12.Oct (2011), pp. 2825–2830.

[100] Scott B Peterson, Jay Apt, and JF Whitacre. "Lithium-ion battery cell degradation resulting from realistic vehicle and vehicle-to-grid utilization". In: *Journal of Power Sources* 195.8 (2010), pp. 2385–2392.

[101] Marine Gorner Pierpaolo Cazzola. *Global EV Outlook 2016 - beyond one million electric cars*. Tech. rep. International Energy Agency, 2016.

[102] Manisa Pipattanasomporn, Murat Kuzlu, and Saifur Rahman. "An algorithm for intelligent home energy management and demand response analysis". In: *IEEE Transactions on Smart Grid* 3.4 (2012), pp. 2166–2173.

[103] PJM. *Manual 12: Balancing Operations*. 2014. URL: http://www.pjm.com/~/media/documents/manuals/m12.ashx.

[104] Franklin L Quilumba et al. "Using smart meter data to improve the accuracy of intraday load forecasting considering customer behavior similarities". In: *IEEE Transactions on Smart Grid* 6.2 (2015), pp. 911–918.

[105] David B Richardson. "Electric vehicles and the electric grid: A review of modeling approaches, Impacts, and renewable energy integration". In: *Renewable and Sustainable Energy Reviews* 19 (2013), pp. 247–254.

[106] P. Richardson, D. Flynn, and A. Keane. "Local Versus Centralized Charging Strategies for Electric Vehicles in Low Voltage Distribution Systems". In: *Smart Grid, IEEE Transactions on* 3.2 (June 2012), pp. 1020–1028. ISSN: 1949-3053. DOI: 10.1109/TSG.2012.2185523.

[107] J. Rivera et al. "Alternating Direction Method of Multipliers for decentralized electric vehicle charging control". In: *2013 IEEE 52nd Annual Conference on Decision and Control (CDC)*. Dec. 2013, pp. 6960–6965. DOI: 10.1109/CDC.2013.6760992.

[108] S. Riverso, M. Farina, and G. Ferrari-Trecate. "Plug-and-play decentralized model predictive control for linear systems". In: *IEEE Trans. on Automatic Control* 58.10 (2013), pp. 2608–2614.

[109] Stefano Riverso, Fabio Sarzo, and Giancarlo Ferrari-Trecate. "Plug-and-play voltage and frequency control of islanded microgrids with meshed topology". In: *IEEE Transactions on Smart Grid* 6.3 (2015), pp. 1176–1184.

[110] N. Rotering and M. Ilic. "Optimal Charge Control of Plug-In Hybrid Electric Vehicles in Deregulated Electricity Markets". In: *IEEE Transactions on Power Systems* 26.3 (Aug. 2011), pp. 1021–1029. ISSN: 0885-8950. DOI: 10.1109/TPWRS.2010.2086083.

[111] Peter J Rousseeuw. "Silhouettes: a graphical aid to the interpretation and validation of cluster analysis". In: *Journal of computational and applied mathematics* 20 (1987), pp. 53–65.

[112] Ahmed Yousuf Saber and Ganesh Kumar Venayagamoorthy. "Intelligent unit commitment with vehicle-to-grid—A cost-emission optimization". In: *Journal of Power Sources* 195.3 (2010), pp. 898–911.

[113] Samveg Saxena et al. “Quantifying EV Battery End-of-Life through Analysis of Travel Needs with Vehicle Powertrain Models”. In: *Journal of Power Sources* (2015).

[114] Mostafa F Shaaban et al. “Real-time PEV charging/discharging coordination in smart distribution systems”. In: *IEEE Transactions on Smart Grid* 5.4 (2014), pp. 1797–1807.

[115] Shengnan Shao, Manisa Pipattanasomporn, and Saifur Rahman. “Demand response as a load shaping tool in an intelligent grid with electric vehicles”. In: *Smart Grid, IEEE Transactions on* 2.4 (2011), pp. 624–631.

[116] Pierluigi Siano. “Demand response and smart grids—A survey”. In: *Renewable and Sustainable Energy Reviews* 30 (2014), pp. 461–478.

[117] João Soares et al. “A multi-objective model for the day-ahead energy resource scheduling of a smart grid with high penetration of sensitive loads”. In: *Applied Energy* 162 (2016), pp. 1074–1088.

[118] Shuang Song, Kamalika Chaudhuri, and Anand D Sarwate. “Stochastic gradient descent with differentially private updates”. In: *IEEE Global Conference on Signal and Information Processing*. 2013.

[119] E. Sortomme et al. “Coordinated Charging of Plug-In Hybrid Electric Vehicles to Minimize Distribution System Losses”. In: *IEEE Transactions on Smart Grid* 2.1 (Mar. 2011), pp. 198–205. ISSN: 1949-3053. DOI: 10.1109/TSG.2010.2090913.

[120] Peter Spellucci. “An SQP method for general nonlinear programs using only equality constrained subproblems”. In: *Mathematical programming* 82.3 (1998), pp. 413–448.

[121] Suvrit Sra, Sebastian Nowozin, and Stephen J Wright. *Optimization for machine learning*. Mit Press, 2012.

[122] *Standard J1772-201210*. Standard. SAE International. 2012.

[123] J. Stoustrup. “Plug & play control: Control technology towards new challenges”. In: *European Journal of Control* 15.3 (2009).

[124] John C Strikwerda. *Finite difference schemes and partial differential equations*. Siam, 2004.

[125] Olle Sundström and Carl Binding. “Flexible charging optimization for electric vehicles considering distribution grid constraints”. In: *Smart Grid, IEEE Transactions on* 3.1 (2012), pp. 26–37.

[126] Kang Miao Tan, Vigna K Ramachandaramurthy, and Jia Ying Yong. “Integration of electric vehicles in smart grid: A review on vehicle to grid technologies and optimization techniques”. In: *Renewable and Sustainable Energy Reviews* 53 (2016), pp. 720–732.

[127] Zhao Tan, Peng Yang, and A. Nehorai. “An Optimal and Distributed Demand Response Strategy With Electric Vehicles in the Smart Grid”. In: *IEEE Transactions on Smart Grid* 5.2 (Mar. 2014), pp. 861–869. ISSN: 1949-3053. DOI: 10.1109/TSG.2013.2291330.

[128] J. Taylor et al. “Evaluations of plug-in electric vehicle distribution system impacts”. In: *Power and Energy Society General Meeting, 2010 IEEE*. July 2010, pp. 1–6. DOI: 10.1109/PES.2010.5589538.

[129] Lloyd N Trefethen and David Bau III. *Numerical linear algebra*. Vol. 50. Siam, 1997.

[130] John Twidell and Tony Weir. *Renewable energy resources*. Routledge, 2015.

[131] USDOT-FHWA. *National Household Travel Survey*. Tech. rep. http://nhts.ornl.gov/index.shtml. U.S. Department of Transportation, Federal Highway Administration, 2009.

[132] *V2G-Sim*. URL: http://v2gsim.lbl.gov.

[133] S.I. Vagropoulos and A.G. Bakirtzis. “Optimal Bidding Strategy for Electric Vehicle Aggregators in Electricity Markets”. In: *Power Systems, IEEE Transactions on* 28.4 (Nov. 2013), pp. 4031–4041. ISSN: 0885-8950. DOI: 10.1109/TPWRS.2013.2274673.

[134] Stijn Vandael et al. “Decentralized demand side management of plug-in hybrid vehicles in a smart grid”. In: *Proceedings of the First International Workshop on Agent Technologies for Energy Systems (ATES 2010)*. 2010, pp. 67–74.

[135] Wenye Wang, Yi Xu, and Mohit Khanna. “A survey on the communication architectures in smart grid”. In: *Computer Networks* 55.15 (2011), pp. 3604–3629.

[136] Young-Min Wi, Jong-Uk Lee, and Sung-Kwan Joo. “Electric vehicle charging method for smart homes/buildings with a photovoltaic system”. In: *IEEE Transactions on Consumer Electronics* 59.2 (2013), pp. 323–328.

[137] Zhe Yu et al. “Modeling and stochastic control for home energy management”. In: *IEEE Transactions on Smart Grid* 4.4 (2013), pp. 2244–2255.

[138] M. N. Zeilinger et al. “Plug and play distributed model predictive control based on distributed invariance and optimization”. In: *52nd IEEE Annual Conference on Decision and Control, 2013*, pp. 5770–5776.

[139] Minghui Zhu and Sonia Martınez. “On distributed convex optimization under inequality and equality constraints”. In: *Automatic Control, IEEE Transactions on* 57.1 (2012), pp. 151–164.

[140] Ziming Zhu et al. “An integer linear programming based optimization for home demand-side management in smart grid”. In: *Innovative Smart Grid Technologies (ISGT), 2012 IEEE PES*. IEEE. 2012, pp. 1–5.